

JUACEP Program 2018

**at University of Michigan,
UCLA & University of Toronto**



Japan-US-Canada Advanced Collaborative Education Program

Nagoya University

Table of Contents

<1> About the Program.....	1
(a) Overview.....	2
(b) Participants.....	3
(c) Schedule.....	4
<2> Research Reports.....	5
<3> Research Presentations.....	53
● For 2018 Short-term course.....	54
● For 2018 Medium-term course.....	67
<4> Findings through JUACEP.....	75
● Students' reviews	76
● Questionnaires (in Japanese).....	87

<1> About the Program

- (a) Overview ...2
- (b) Participants ...3
- (c) Schedule ...4

(a) Overview

JUACEP provides three program courses for students of the Graduate School of Engineering at Nagoya University to study abroad: a short-term (two months) course; a medium-term (six months) course; a long-term (eight months) course. Choosing one of those courses the selected students are offered an opportunity to work together with faculty and other researchers or students from all over the world at the world's top universities.

Each student works on a research project related to his own master's thesis topic while belonging to a specialized research group of the University of Michigan (UM), UCLA or University of Toronto (UT). In addition to research implementation, the students are expected to attend the group seminars, the group discussions and other events. At the end of each course, the students are required to submit research reports to their mentors at the host institution, and after returning to Nagoya, give research presentations based on their achievements in front of the faculty and peer students at JUACEP Workshop held in Nagoya University. The report and the presentation are primary requisites for course credits of the program.

This publication is compiling the activities of the following students.

- [a] One students of short-term course from August to September and another from November to December 2018 at UM
- [b] Two students of short-term course from August to September 2018 at UT
- [c] Two students of medium-term course from August 2018 to February 2019 at UM
- [d] Two students of medium-term course from August 2018 to January 2019 at UCLA
- [e] Two students of Long-term course from August 2018 to March 2019 at UM
- [f] One student of long-term course from August 2018 to March 2019 at UCLA

JUACEP 2018 Short-, Medium- and Long-term Courses Flowchart

	Short-term course	Medium-term course	Long-term course
January 2018	Public announcement and accepting application (Jan. - Mar.)		
February			
March			
April	Screening candidates		
May	Selected students approach UM/UCLA/UT faculty to get post of 'Visiting Scholar' (called *VGR at UCLA). After acceptance by faculty, visa procedure starts including examination of CV, English proficiency and other qualification.		
June			
July	J-1 Visa application		
August	[a,b] Short-term course study at UM/UT Aug. - Sep. 2018	[c,d] Medium-term course study at UM/UCLA Aug. 2018 - Feb. 2019	[e,f] Long-term course study at UM/UCLA Aug. 2018 - Mar. 2019
September			
October	23 rd Workshop, Oct. 9, 2018		
November	[a] Short-term course study at UM Nov. - Dec. 2018		
December			
January 2019			
February			
March		24 th Workshop, Mar. 28, 2019	

*VGR: Visiting Graduate Researcher for UCLA

(b) 2018 Participants

★Short-term course at University of Michigan

#	Name	Yr.	Advisor at Nagoya University	Advisor at Visiting University
August 1, 2018 - September 30, 2018				
1	Motoki Yamada 山田 基生	M1	Prof. Motonobu Goto Materials Process Engineering	Prof. Richard Laine Materials Science and Engineering
November 5, 2018 - December 21, 2018				
2	Keiichi Okubo 大久保 慶一	M2	Prof. Atsushi Satsuma Molecular Design and Engineering	Prof. Levi Thompson Chemical Engineering

★Short-term course at University of Toronto

August 3, 2018 - September 25, 2018				
3	Kotaro Takamura 高牟礼 光太郎	D3	Prof. Yasuhiko Sakai Mechanical Systems Engineering	Prof. Phippe Lavoie Inst. Aerospace Studies
August 2, 2018 - September 26, 2018				
4	Shuichi Higaki 檜垣 秀一	M2	Prof. Yasuhiko Sakai Mechanical Systems Engineering	Prof. Pierre Sullivan Mechanical and Industrial Engineering

★Medium-term course at University of Michigan

August 20, 2018 - January 31, 2019				
5	Takahiko Kosegaki 小瀬垣 貴彦	M1	Prof. Kazuo Shiokawa Electrical Engineering	Prof. Mark Moldwin Climate and Space Science and Engineering
August 20, 2018 - February 19, 2019				
6	Kotaro Hotta 堀田 貢太郎	M1	Prof. Jiro Kasahara Aerospace Engineering	Prof. Mirko Gamba Aerospace Engineering

★Medium-term course at UCLA

August 6, 2018 - January 31, 2019				
7	Koki Hojo 北條 孝樹	M1	Prof. Noritsugu Umehara Micro-Nano Mechanical Science and	Prof. Suneel Kodambaka Materials Science and Engineering
August 6, 2018 - January 31, 2019				
8	Hiroki Kogure 木暮 大貴	M1	Prof. Tsuyoshi Inoue Mechanical Systems Engineering	Prof. Tsu-Chin Tsao Mechanical and Aerospace Engineering

★Long-term course at University of Michigan

August 6, 2018 - March 22, 2019				
9	Ryo Tsunoda 角田 涼	M1	Prof. Takeo Matsumoto Mechanical Systems Engineering	Prof. Krishna Garikipati Mechanical Engineering
August 22, 2018 - May 19, 2019				
10	Kimihiko Sugiura 杉浦 公彦	M1	Prof. Seiichi Hata Micro-Nano Mechanical Science and	Prof. Gregory Hulbert Mechanical Engineering

★Long-term course at UCLA

August 6, 2018 - March 22, 2019				
11	Yuta Ujiie 氏家 雄太	M1	Prof. Koji Nagata Aerospace Engineering	Prof. Chang-Jin Kim Mechanical and Aerospace Engineering

Coordinators at Partner Universities

Prof. Katsuo Kurabayashi	Mechanical Engineering
Prof. Jenn-Ming Yang	Materials Science and Engineering
Prof. Shaker Meguid	Mechanical and Industrial Engineering

JUACEP Members

Prof. Yang Ju	Micro-Nano Mechanical Science and Engineering
Prof. Noritsugu Umehara	Micro-Nano Mechanical Science and Engineering
Prof. Toshiro Matsumoto	Mechanical Systems Engineering
Assoc. Prof. Yasumasa Ito	Mechanical Systems Engineering
Assoc. Prof. Takayuki Tokoroyama	Micro-Nano Mechanical Science and Engineering
Tomoko Kato, Administrative staff	JUACEP Office

JUACEP Office Room #341, Engineering Building 2, Nagoya University
Furo-cho, Chikusa-ku, Nagoya 4648603 Tel/Fax +81 (0)52 789 2799

(c) JUACEP Research Abroad 2018 Schedule

Period	Short-term course	Medium-term course	Long-term course
2018/07/30~2018/08/20	Departure from Japan and starting of JUACEP research activity at Univ. Michigan, UCLA and Univ. Toronto		
~2018/09	Research activity at each lab	Research activity at each lab	Research activity at each lab
2018/09/25~2018/10/03	Departure from US/Canada and arrival at Nagoya. Submission of Research report, JUACEP report, JASSO questionnaire and evaluation sheet to JUACEP Office.		
2018/10/09	The 23rd Workshop for Short-term course	Departure from US and arrival at Nagoya. Submission of Research report, JUACEP report, JASSO questionnaire and evaluation sheet to JUACEP Office.	Departure from US and arrival at Nagoya. Submission of Research report, JUACEP report, JASSO questionnaire and evaluation sheet to JUACEP Office.
2018/10			
2018/11	Departure from Japan and starting of JUACEP	Departure from US and arrival at Nagoya. Submission of Research report, JUACEP report, JASSO questionnaire and evaluation sheet to JUACEP Office.	Departure from US and arrival at Nagoya. Submission of Research report, JUACEP report, JASSO questionnaire and evaluation sheet to JUACEP Office.
2018/12	Research activity at each lab		
2019/01	Departure from US and arrival at Nagoya. Submission of Research report, JUACEP report, JASSO questionnaire and evaluation sheet to JUACEP Office.	The 24th Workshop for Medium/Long-term course	The 24th Workshop for Medium/Long-term course
2019/01/31~2019/02/22			
2019/03/25			
2019/03/28			

<2> Research Reports

Studies at University of Michigan

- [S] Motoki Yamada, *mentored by Prof. Richard M. Laine* (P.6)
“Synthesis of MZPF_e Nanopowders to Thin Films as Solid Electrolytes by Processing Liquid-Feed Flame Spray Pyrolysis”
- [S] Keiichi Okubo, *mentored by Prof. Levi Thompson and Dr. Saemin Choi* (P.11)
“Synthesis of MO₂C Supported Metal Catalysis”
- [M] Takahiko Kosegaki, *mentored by Prof. Mark B. Moldwin* (P.14)
“Thermal Testing of the New Small Magnetic Sensor for SmallSAT”
- [M] Kotaro Hotta, *mentored by Prof. Mirko Gamba* (P.20)
“Experimental Investigation of Primary Breakup Induced by High Mach Number Shock Wave”
- [L] Ryo Tsunoda, *mentored by Prof. Krishna Garikipati* (P.24)
“A Computational Study of Cell Growth and Division as an Energy-Based Soft Packing Problem Using a Diffuse Interface Framework”
- [L] Kimihiko Sugiura, *mentored by Prof. Gregory M. Hulbert* (P.33)
“Sensitivity Analysis of Five-Link Suspension” *(Undisclosed)*

Studies at UCLA

- [M] Koki Hojo, *mentored by Prof. Suneel Kodambaka* (P.34)
“Reactive DC Magnetron Sputtering of MoS₂ and MoS₂/HBN Layers” *(Undisclosed)*
- [M] Hiroki Kogure, *mentored by Prof. Tsu-Chin Tsao* (P.35)
“Stabilize and Repetitive Controller Design for an Active Magnetic Bearing”
- [L] Yuta Ujii, *mentored by Prof. Chang-Jin Kim* (P.43)
“Evaluation of the UCLA Low-Profile Direct Shear Sensor for Air Flows in Wind Tunnel” *(Undisclosed)*

Studies at University of Toronto

- [S] Kotaro Takamura, *mentored by Prof. Philippe Lavoie* (P.44)
“Synthetic Jet Characterization for Differences in Nozzle Size and Thickness of Gasket”
- [S] Shuichi Higaki, *mentored by Prof. Pierre Sullivan* (P.48)
“Analytical and Numerical Modeling of High-Temperature Pressure Transducer”

[S] Short-term course; [M] Medium-term course; [L] Long-term course

Synthesis of MZPFe nanopowders to thin films as solid electrolytes by Processing Liquid-Feed Flame Spray Pyrolysis

Motoki Yamada

Department of Materials Process Engineering, Graduate School of Engineering, Nagoya University
yamada.motoki@h.mbox.nagoya-u.ac.jp

Eleni Temeche, Richard Laine

Department of Materials Science and Engineering, Graduate School of Engineering, University of Michigan
elenite@umich.edu, talsdad@umich.edu

ABSTRACT

Although there are increasing demands on lithium-ion batteries, development of alternatives that are lower cost or are easier to assemble is under way. Here we target developing thin film Mg^{2+} conducting electrolytes for all-solid-state Mg batteries. Initially, we made $\text{Mg}_{0.9}(\text{Zr}_{0.6}\text{Fe}_{0.4})_2(\text{PO}_4)_3$ nanopowders (MZPFe NPs) as a route to thin films of the same ceramic. In this work, NPs synthesized by liquid-feed flame spray pyrolysis (LF-FSP) were used as the starting material for fabricating thin films. A suspension of MZP was made by mixing powders, plasticizer, binder, dispersant, and solvent. After the suspension was ball-milled for 24 h, suspensions were cast on mylar and dried to obtain green films. The green films were sintered at selected temperatures. The microstructures of the sintered thin films were characterized using SEM and XRD. We report characterization data here.

1. INTRODUCTION

There is no doubt that the one of challenging issues in electrochemistry is the development of rechargeable batteries with multiple performance capabilities including sufficient energy density, appropriate voltage and current capabilities, and low safety requirements. Conventional lithium batteries containing liquid electrolytes based on highly volatile and flammable organic solvents suffer significantly from the potential to fail catastrophically via electrolyte leakage, boiling, freezing, combustion or even explosion, of particular importance for in vivo applications [1-3]. There is considerable need to develop batteries with much higher safety and greater energy densities to satisfy growing market demands. Under such circumstance, all-solid-state batteries (ASBs) have been proposed as a fundamental solution [4]. They do not require liquid cell electrolytes relieving this avenue for catastrophic failure. They are also capable of operating over both wide

temperature and electrochemical potential ranges. Especially, for the most widely implemented Li ASBs batteries [5]. Replacement of liquid electrolytes with solid-state electrolytes should offer great advantages in terms of ease of fabrication, flexibility in dimensions, battery geometries, and safety features. However, the limited accessibility of Li (e.g. low natural abundance in the earth's crust 0.04-1.16% in brine ponds) goes against its sustainability. High and probably rising costs also limit future use of lithium ion batteries for large-scale applications [6-8].

Alternately, magnesium is an excellent candidate for batteries. It is an active metal, easily obtained in the earth's crust (5th most abundant element, approximately 10^4 times that of Li), and has high volumetric capacities of 3830 mAh/cc (vs. 2050 mAh/cc for Li). Additionally, Mg provides greater atmospheric stability and melting point than Li making it safer for handling compared [9].

In spite of these preferred attributes, the development of Mg-based ASBs has been limited compared to Li batteries. One critical issue blocking its progress is the lower availability of stable Mg^{2+} -conducting solid electrolytes that enable reversible release of Mg^{2+} ions from a magnesium metal anode. This is because the interaction of Mg ion is strong, it hardly diffuses in the solid phase, and the electrode reaction is extremely slow. To date, there exist only limited reports on Mg^{2+} -conducting solid electrolytes. Recently, R. Laine groups reported that Ce-doped MZP thin films (45 μm) sintering at 1200°C has offered values of $1.9 \times 10^{-4} \text{ mS}\cdot\text{cm}^{-1}$ at 200°C . Introduction of Ce allows sintering to full density at temperatures where Ce free films do not densify completely [9].

In this study, we develop Fe-doped MZP thin film electrolytes. MZPFe nanopowders were first studied to optimize compositions, and then thin films were processed and analyzed on the morphology.

2. EXPERIMENTAL

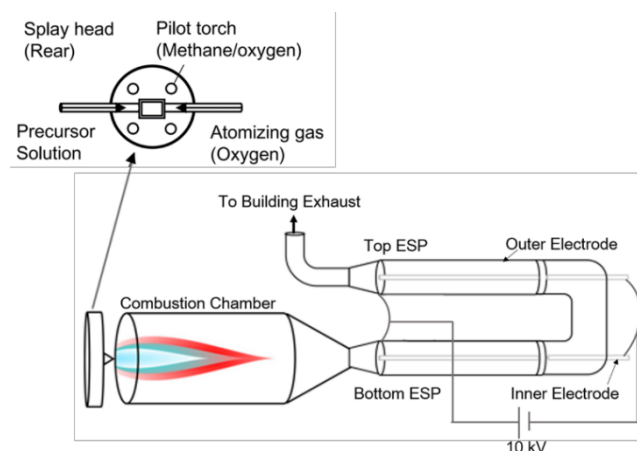


Fig. 1. Schematic of Liquid Feed Flame Spray Pyrolysis [11]

2.1 Precursors synthesis

Triethyl phosphate, $(C_2H_5)_3PO_4$, was used directly as the phosphorus source. The three other precursors were synthesized as sources of Mg, Zr, and Fe, respectively.

Magnesium propionate, $Mg(O_2CCH_2CH_3)_2$, was synthesized by reacting $Mg(OH)_2$ (157 g, 2.7 mole) with excess $CH_3CH_2CO_2H$ (500 ml, 6.8 mole) in a round-bottom flask equipped with a still head. The mixture was heated at 130 °C for 2 h with magnetic stirring until it became transparent. On cooling to room temperature, magnesium propionate crystallized, then was filtered off, dried naturally, ground into powder for use [9].

Zirconium isobutyrate, $Zr[O_2CCH(CH_3)_2]_2(OH)_2$, was synthesized by reacting zirconium basic carbonate (160 g, 0.52 mole) with isobutyric acid (390 g, 4.4 mole) and isobutyric anhydride (350 g, 2.2 mole) in a flask equipped with a still head in N_2 atmosphere. The reactants were heated at 110°C until they became transparent. Zirconium isobutyrate crystallized on cooling, then was filtered off, dried, ground into powder for use [9].

Iron propionate [$Fe(O_2CCH_2CH_3)_3$] was synthesized by reacting Iron hydroxide with excess propionic acid in a flask.

2.2 Liquid-Feed Flame Spray Pyrolysis (LF-FSP)

The MZPFe nanopowders were prepared by liquid-feed flame spray pyrolysis (LF-FSP) developed at University of Michigan [10-18]. The LF-FSP apparatus consists of a precursor reservoir, an ultrasonic atomizer, a combustion chamber, and electrostatic precipitators (ESPs) as shown in Figure 1.

All the precursors for Mg, Zr, Fe, P, respectively magnesium propionate (15.7 g), zirconium isobutyrate (35.6 g), iron propionate (48.7 g), triethyl phosphate (84.1 g) were mixed and dissolved in ethanol (1400 mL), providing a solution with 3 wt% ceramic yield. As-obtained precursor solution was aerosolized with oxygen into a 1.5 m long combustion chamber and ignited using methane/ O_2 pilot torches. After combustion and cooling, NPs were collected downstream in wire-in-tube electrostatic precipitators operated at 10 kV. Collected NPs and 1.0 wt% of bicine as dispersant were dispersed into ethanol with an ultrasonic horn. After sufficient sedimentation, the supernatant suspension was decanted into a container, the recovered powder dried in an oven at 80 °C for 12 hours.

2.3 Film processing

As-synthesized MZPFe NPs were mixed with binder, plasticizer and solvents in designated ratios (Table 1), put into a 20 mL vial. The suspension was ball-milled with 3.0 mm diameter spherical 99% zirconia beads (6.0 g) for 12-24 h to homogenize the suspension. A ball mill (Rotary Tumbler Model B, Tru-Square Metal Products, Auburn, WA, UK) was used for ball-milling.

The suspension was cast using a wire-wound rod coater (Automatic Film Applicator-1137, Sheen Instrument, Ltd., UK) producing thin NP filled polymeric films. The gap between the rod and the Mylar substrate was adjusted by using spacers, therefore easily film thicknesses were controlled.

After solvent evaporation, dried green films were cut into small pieces, two were uniaxially pressed at 50MPa/100°C/5min between stainless steel dies using a heated bench-top press (Carver, Inc), then manually peeled off the Mylar substrate and cut to selected sizes.

Table 1. Starting chemical components for film casting

Components	Roles	Mass (g)	Wt.%	Vol%
MZPFe	Powder	1.00	32	10
Polyvinyl butyral (PVB)	Binder	0.10	3	4
Benzyl butyl Phthalate(BBP)	Plasticizer	0.10	3	4
Acetone	Solvent	0.95	31	41
Ethanol	Solvent	0.95	31	41

2.4 Film sintering

Green films were placed between Al_2O_3 plates and sintered in air at selected temperatures and times with a ramp rate of 3 °C/min in a furnace. The plates were used to prevent films from warping through all the process.

2.5 Characterization

2.5.1 Fourier- transform infrared spectroscopy (FTIR)

Infrared spectra were obtained using a FTIR spectrometer (Nicolet 6700 FT-IR, Thermo Fisher Scientific, Inc., Madison, WI). Optical grade KBr was ground with 1.2 wt% of the as-shot powders. The ground powder was packed into a sample holder and leveled off with a glass plate to give a smooth surface. The FTIR sample chamber was purged continuously with N₂ prior to data acquisition. Scans were carried out in the range of 4000-400 cm⁻¹.

2.5.2 Thermal gravimetric analysis (TG-DTA)

Mass loss events during heating of as-produced NPs were characterized using a TGA-DTA (TA Instruments, Inc., New Castle, DE). As-prepared MZPF₂ powders of 17-20 mg were hand pressed in a 3 mm dual-action die, placed inside alumina sample pans, and heated at ramp rates of 10°C/min from ambient to 1000°C. A Nitrogen gas flow of 60 mL/min was maintained during all SDT experiments.

2.5.3 Ionic conductivity measurements

BioLogic SP-300 potentiostat (Bio Logic Science Claix, France) was used to evaluate the ionic conductivity of as-sintered MZPF₂ films. All film surfaces were coated with gold coatings using an SPI sputter coater (SPI Supplies Inc., West Chester, PA). Gold electrode with a diameter of 3.0 mm was deposited on both sides of film surfaces. Ionic conductivity measurements were operated at 30-150 °C.

Nyquist plots were fitted using EIS spectrum analyzer software to get total resistance of samples. Conductivities (σ_t) were calculated from formula.

$$\sigma_t = d/(A_e \times R) \quad (1)$$

where d , A_e , R denote film thickness, electrode area and total resistance, respectively.

2.5.4 X-ray diffraction (XRD)

X-ray diffraction patterns were collected using a Rigaku Miniflex XRD system. The scans were collected from 10 to 80 in 2 θ with a step of 0.01° with Cu K α radiation (1.541 Å) as the X-ray source. The Jade program was used to determine the presence of crystallographic phases, wt. fraction, and to refine lattice constants.

2.5.5 Scanning electron microscopy (SEM)

Micrographs were taken using JEOL IT500 SEM. Samples were sputter coated with gold.

2.5.6 Energy Dispersive X-ray spectrometry (EDX)

A JEOL JEM-2100F (JOEL, Japan) aberration corrected STEM operated at 200 kV with a SDD EDAX's energy dispersive spectroscopy (EDX) detector attached was used to study the microstructure and chemistry of the nanoparticles. TEM specimens were prepared by simply dusting some dry powder on holey carbon film coated Cu grids. STEM images were taken using both high-angle annular dark-field (HAADF) and bright-field detectors.

Element mapping was performed using Mg, Zr, Fe, P and O X-ray signals.

3. RESULTS AND DISCUSSION

3.1 As-produced NPs

As seen in the Fig. 2, TG-DTA analysis of as-shot NPs reveals mass losses of 10 wt% from adsorbed water and carbonate species on heating to 400 °C, as expected from other oxide NPs systems [18]. At the same time, exotherm could be seen up to 200 °C accompanied by mass losses from decomposition of adsorbed species. Unfortunately, the crystallization points of as-produced powders were not confirmed because crystallization exotherm was not observed.

FTIR spectra of as obtained powders are presented in Fig. 3.

Metal oxide stretches appeared as a broad band between 400 and 700 cm⁻¹. Also, a broad and intense phosphate peaks at around 1150 cm⁻¹ and weak OH peak at around 3400 cm⁻¹ from stretching bands could be seen.

Fig. 4. XRD patterns reveal as-produced NPs tend to be amorphous contrary to expectations. This might be because the atoms were quenched rapidly before crystallization.

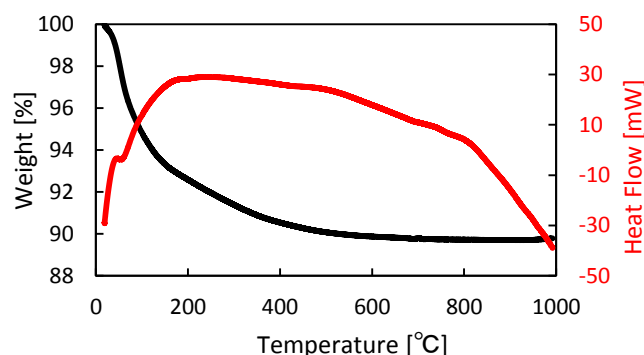


Fig. 2. TG-DTA analysis of as-shot NPs

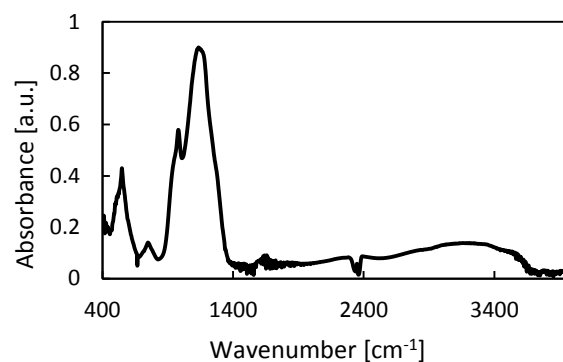


Fig. 3. FTIR analysis of as-shot NPs

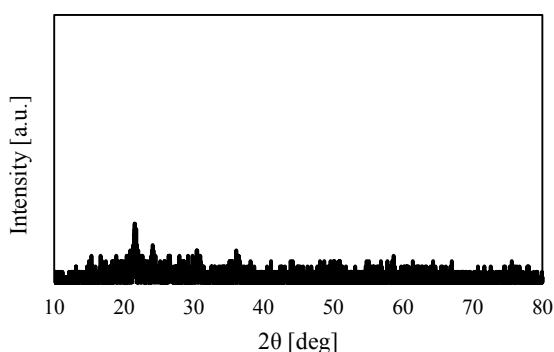


Fig. 4. XRD pattern of as-produced NPs

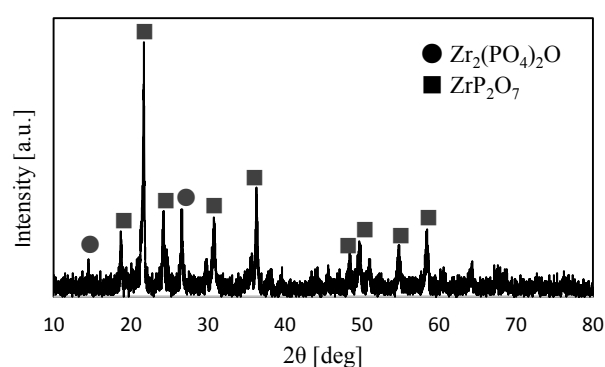


Fig.7. XRD patterns of films after sintering at 750 °C/3h/air

3.2 Sintered films

Firstly, pressed green films were sintered at 750 °C for 3 hours, aiming to obtain dense films at temperatures as low as possible. Fig. 5, EDX mapping shows that all elements are distributed well except for iron. This might be ascribed to the fact that the iron precursor did not solidify during the synthesis. Fig. 6, SEMs show fracture morphologies for sintered films. At 750 °C, processed film exhibited some microporous structures, which means the film did not have enough density. The Fig. 7. XRD patterns reveal phase compositions of the as-sintered films. Unfortunately, sintered film was composed of only Zr₂(PO₄)₂O and ZrP₂O₇ without Mg phase. Relative contents of phases in sintered films were 74 wt% of ZrP₂O₇ and 26 wt% of Zr₂(PO₄)₂O. Therefore, higher temperature in furnace process was examined as a next step.

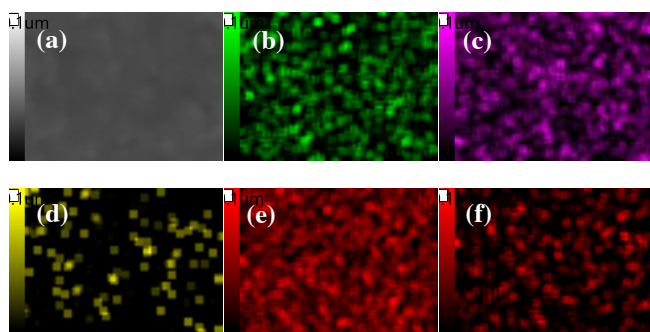


Fig. 5. EDX mapping of films after sintering at 750 °C/3h/air
(a) HAADF, (b) Mg, (c) Zr, (d) Fe, (e) P, (f) O

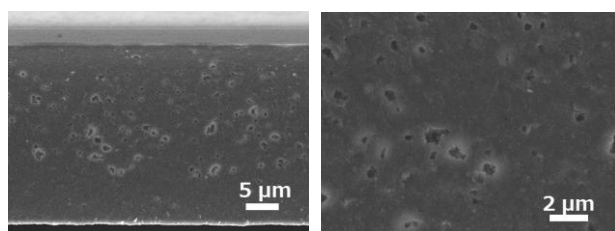


Fig. 6. SEMs of fracture surfaces of films after sintering at 750 °C/3 h/air

Next, pressed green films were sintered at 900 °C for 3 hours. Fig. 8. SEMs show fracture morphologies for sintered films. Contrary to the expectation, obtained fracture surfaces did not look dense. On the contrary, much microporous structures could be seen. Usually, higher sintering temperature is examined in, denser structures can be obtained. So, this results are needed to be examined again. The Fig. 9. XRD patterns reveal phase compositions of the as-sintered films. Unfortunately, sintered film was composed of only Mg₂P₂O₇ and ZrP₂O₇ without MZP phase. Relative contents of phases in sintered films were 56 wt% of ZrP₂O₇ and 44 wt% of Mg₂P₂O₇. Also, EIS spectrum of the sintered films did not lead the ionic conductivity. One of the reasons why this happened is the measurement was conducted at room temperature and the frequency ranges were not proper.

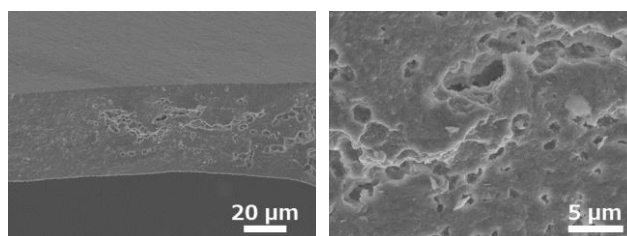


Fig. 8. SEMs of fracture surfaces of films after sintering at 900 °C/3 h/air

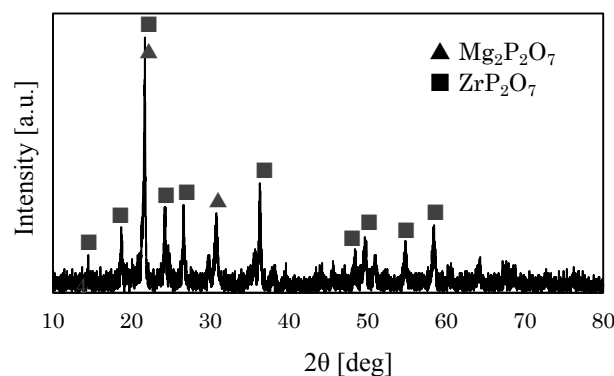


Fig.9. XRD patterns of films after sintering at 900 °C/3h/air

4. CONCLUSIONS

In this work, we aimed to synthesize MZPFe nanopowders to thin films via LF-FSP. The SEMs showed that the sintered thin films had pores structures, not so dense. Although EDX mapping of sintered films showed that all elements were distributed, unfortunately MZP phase could not be seen by XRD analysis. This might be ascribed to the fact that the obtained powders were amorphous, not crystallized. So, we have just started preparing the precursors again to get powders containing MZP phase.

ACKNOWLEDGEMENTS

I would like to thank Professor Richard M. Laine for giving me such a valuable opportunity to study at University of Michigan. I would like to thank Eleni Temeche for giving me a lot of advice. I have given her much trouble, so I feel so sorry about that. Moreover, I would like to thank the administrators of equipment which I used for helping me to master those devices. Finally, this work was supported by Japan-US-Canada Advanced Collaborative Education Program. I would like to thank all office workers for processing my studying abroad.

REFERENCES

- [1] L. Baggetto, R. A. H. Niessen, F. Roozeboom and P. H. L. Notten, *Adv. Funct. Mater.*, (2008), 18, 1057-1066.
- [2] M. Ogawa, K. Yoshida and K. Harada, *SEI Tech. Rev.*, (2012), 74, 89.
- [3] F. Du, N. Zhao, Y. Li, C. Chen, Z. Liu and X. Guo, *J. Power Sources*, (2015), 300, 24-28.
- [4] A. Hooper and B. C. Tofield, *J. Power Sources*, (1984), 11, 33-41.
- [5] D. Linden, *Handbook of Batteries* (Ed: D. Linden), McGraw-Hill, NewYork (1994), Ch. 33.
- [6] M. M. Huie, D. C. Bock, E. S. Takeuchi, A. C. Marschilok and K. J. Takeuchi, *Coord. Chem. Rev.*, (2015), 287, 15-27.
- [7] P. Novak, R. Imhof and O. Haas, *Electrochimica Acta*, (1999), 45, 351-367.
- [8] H. D. Yoo, I. Shterenberg, Y. Gofer, G. Gershinsky, N. Pour and D. Aurbach, *Energy Environ. Sci.*, (2013), 6, 2265.
- [9] Liang, B. Processing liquid-feed flame spray pyrolysis synthesized $Mg_{0.5}Ce_{0.2}Zr_{1.8}(PO_4)_3$ nanopowders to free standing thin films and pellets as potential electrolytes in all-solid-state Mg batteries. *Electrochimica Acta* (2018), 272, 144-153
- [10] Kim, M., Hinklin, T. R. and Laine, R. M., Core-shell nanostructured nanopowders along $(CeO_x)_x(Al_2O_3)_{1-x}$ tieline by Liquid-Feed Flame Spray Pyrolysis (LF-FSP), *Chem. Mater.*, (2008), 20, 5154-5162
- [11] Bickmore, C. R., Waldner, K. F., Baranwal, R., Hinklin, T. and Laine, R. M., Ultrafine titania by Flame Spray Pyrolysis of a titanatran complex, *JECS*, (1998), 18, 287-296
- [12] Marchal, J., Johns, T., Baranwal, R., Hinklin, T. and Laine, R. M., Yttrium aluminium garnet nanopowders produced by Liquid-Feed Flame Spray Pyrolysis (LFFSP) of metalloorganic precursors, *Chem. Mater.*, (2004), 16, 822-831
- [13] Kim, S., Gislason, J. J., Morton, R. W., Pan, X. Q. and Laine, R. M., Liquid-Feed Flame Spray Pyrolysis of nanopowders in the alumina-titania system., *Chem. Mater.* (2004), 26, 2336-2343
- [14] Azurdia, J., Marchal, J. and Laine, R. M., Synthesis and characterization of mixed-metal oxide nanopowders along the $CoO_x-Al_2O_3$ tie line using Liquid-Feed Flame Spray Pyrolysis., *JACM*, (2006), 89, 2336-2343
- [15] Kim, M. and Laine, R. M., One-step synthesis of coreshell $(Ce_{0.7}Zr_{0.3}O_2)_x(Al_2O_3)_{1-x}$ [$(Ce_{0.7}Zr_{0.3}O_2)_{12}O_3$] nanopowders via Liquid-Feed Flame Spray Pyrolysis (LF-FSP)., *JACS*, (2007), 8, 9920-9929
- [16] Laine, R. M., Hinklin, T., Williams, G. and Rand, S. C., Low-cost nanopowders for phosphor and laser applications by Flame Spray Pyrolysis., *Materials Science Forum*, (2000), 343-346, 500-510
- [17] Hinklin, T., Toury, B., Gervais, C., Babonneau, F., Gislason, J. J., Morton, R. W. and Laine, R. M., LiquidFeed Flame Spray Pyrolysis of metalloorganic and inorganic alumina sources in the production of nanoalumina powders, *Chem. Mater.*, (2004), 16, 21-30
- [18] Azurdia, J. A., Marchal, J., Shea, P., Sun, H., Pan, X. Q. and Laine, R. M., Liquid-Feed Flame Spray Pyrolysis as a method of producing mixed-metal oxide nanopowders of potential interest as catalytic materials. Nanopowders along $NiO-Al_2O_3$ tie line including $(NiO)_{0.22}(Al_2O_3)_{0.78}$, a new inverse spinel composition, *Chem. Mater.*, (2006), 18, 731-739
- [19] A.S. Bondarenko, G.A. Ragoisha, in: A.L. Pomerantsev (Ed.), *Progress in Chemometrics Research*, Nova Science Publishers, New York, (2005), 89-102
- [20] Adnan, S. B. R. S., and N. S. Mohamed. Characterization of novel $Li_4Zr_{0.06}Si_{0.94}O_4$ and $Li_{3.94}Cr_{0.02}Zr_{0.06}Si_{0.94}O_4$ ceramic electrolytes for lithium cells. *Ceramics International*. (2014), 6373-6379.

SYNTHESIS OF MO₂C SUPPORTED METAL CATALYSTS

Keiichi Okubo

(Affiliation) Graduate School of Engineering, Nagoya University
ookubo.keiichi@nagoya-u.ac.jp

Supervisor: Saemin Choi

(Affiliation) Department of Chemical Engineering, Michigan University
saeminc@umich.edu

ABSTRACT

Molybdenum carbides supported metal has been reported to be a useful catalysts for ammonia synthesis and low temperature CO₂ hydrogenation^{1,2,3}. High surface area molybdenum carbide (α -Mo₂C and β -Mo₂C were mixed) were prepared by the temperature programmed reaction with CH₄ + H₂ mixed gas. To prepare molybdenum carbide, the precursor (NH₄)₆Mo₇O₂₄•4H₂O was heated up to 863K and held for 2 h under CH₄ + 4H₂ flow. The surface areas of Mo₂C were about 145 m² g⁻¹. Molybdenum carbides supported metal (Co, Ni, Ru) were prepared by the incipient wetness impregnation method, and then were reduced at 723K under H₂ flow. After the reduction, Mo₂C supported metal catalysts were confirmed that they have the appropriate crystal structure by XRD (X-ray diffraction analysis).

1 INTRODUCTION

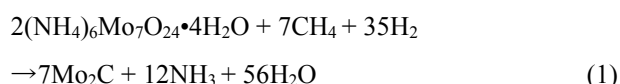
Molybdenum carbides supported metal has been reported to be a useful catalysts for various reactions. For example, these are ammonia synthesis and low temperature CO₂ hydrogenation and so on¹⁻⁷. In particular, ammonia synthesis is a very important reaction for our lives. More than 180 million tons of NH₃ are produced annual via the Haber-Bosch process which converts N₂ and H₂ at high temperatures (400-500°C) and pressures (150-300 bars). Ammonia synthesis also accounts for 1-2% of global energy consumption. The development of higher activity catalysts that can operate under less severe conditions would enhance the economics associated with and sustainability of NH₃ synthesis⁸. Previously, Mo₂C and Mo₂N have been reported to be more active than Ru-based catalysts, but slightly less active than the doubly-promoted Fe catalyst typically used in industrial processes. Moreover Mo₂C and Mo₂N have the unique property depending on the crystal structure. β -Mo₂C showed the higher activity for ammonia synthesis than α -MoC_{1-x}^{8,9}. To enhance the performance of the bulk carbides, we introduced metals including Co and Ni, Ru. And we investigate the interaction between the metal and carbides. First, we focused on the synthesis of the high surface area molybdenum carbide (α -Mo₂C and β -Mo₂C were mixed)

and molybdenum carbides supported various metals in this study.

2 EXPERIMENT SECTION

2.1 Preparation of high surface area molybdenum carbide (HSA-Mo₂C)

HSA-Mo₂C was prepared using a temperature programmed reaction technique starting from an ammonium molybdate (AM) precursor, (NH₄)₆Mo₇O₂₄•4H₂O (Alfa Aesar). 1.7g of AM was sieved to 60-120 μ m and then loaded into a quartz tube reactor (Fig. 1). The AM was treated in H₂ flowing at 400 mL/min for 70 min, as the temperature was increased from 298 to 623 K and held at 623 K for 12 h. The reaction gas was then switched to 15% CH₄/H₂ (400 mL/min) while the temperature was increased to 863 K in 1.5 h and maintained at 863 K for 2 h. The reactor was then immediately quenched to room temperature. (Condition A) The reaction is showed by the following formula (1)



For comparison, molybdenum carbide was prepared under another experimental conditions. In the condition B, the AM was treated in H₂ flowing at 400 mL/min at 373 K. In the condition C, molybdenum carbide was synthesized in the reactor containing oxygen by condition B (Table 1).

Table 1 Preparation condition of HSA-Mo₂C

Condition (Step)	Gas	T _{initial}	T _{final}	t _{tramp}	t _{soak}
A(1)	(H ₂)	298 K	623 K	70 min	12 hrs
A(2)	(CH ₄ /H ₂)	623 K	863 K	90 min	2 hrs
B(1)	(H ₂)	373 K	623 K	70 min	12 hrs
B(2)	(CH ₄ /H ₂)	623 K	863 K	90 min	2 hrs

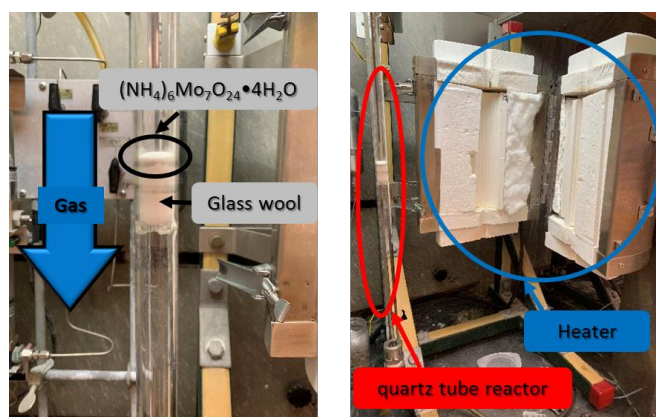


Fig. 1 A pattern of the preparation for HSA-Mo₂C

2.2 Metal deposition on HSA-Mo₂C

Co/HSA-Mo₂C, Ni/HSA-Mo₂C, Ru/HSA-Mo₂C were synthesized by incipient wetness impregnation of HSA-Mo₂C (0.144 cm³/g pore volume measured by N₂ physisorption) with aqueous solutions of Co(NO₃)₂·6H₂O (Alfa Aesar), Ni(NO₃)₂·6H₂O (Alfa Aesar), RuCl₆·nH₂O (Alfa Aesar) (5 wt% loading). The amount of solution corresponds to the pore volume of HSA-Mo₂C. The freshly synthesized Mo₂C was transferred under Argon to a H₂O-tolerant, oxygen free glovebox filled with N₂ to avoid any bulk or surface oxidation of Mo₂C. The resulting catalysts were dried in the glovebox on a heating plate at 373 K for 1 h and then transferred under Argon into a quartz reactor where they were reduced in flowing H₂ (400 ml/min) for 4 h at 723 K.

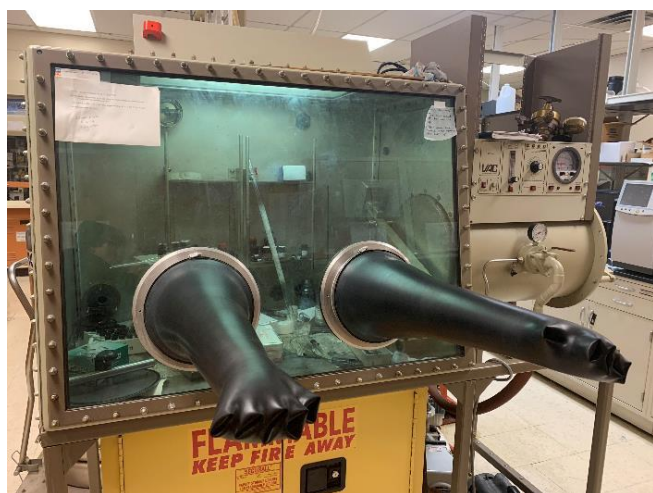


Fig.2 The picture of the globe box filled with inert gas.

2.3 Characterization method

Surface areas of the materials were measured using a Micromeritics ASAP 2010 analyzer based on N₂ physisorption. All of the Mo₂C-based catalysts were degassed (< 5mm Hg) at 623 K for 4 h prior to the surface area measurements. The bulk crystalline structures were characterized using X-ray diffraction (Rigaku Miniflex 600) with 2θ ranging from 10° to 90° and a scan rate of 5 °/min.

3 RESULT AND DISCUSSION

3.1 Preparation of HSA-Mo₂C

Fig. 3 showed that the color of the molybdenum carbides was changed from white to grey after flowing CH₄/H₂ gas.

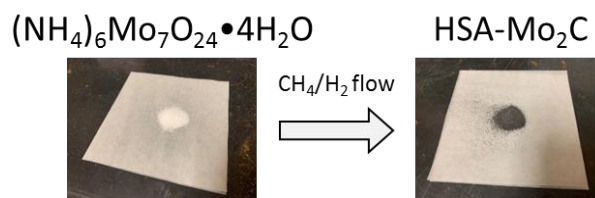


Fig.3 Synthesis of HSA-Mo₂C.

3.2 Crystal structure of HSA-Mo₂C

The crystal structure of the molybdenum carbides were investigated by XRD (Fig. 4). In condition A, the molybdenum carbides mixed with α-Mo₂C and β-Mo₂C were synthesized (the target product). However, condition B and condition C didn't make them. In case of condition B, β-Mo₂C was generated as most stable phase³ because the reaction temperature is higher than that in condition A. In case of condition C, Mo₂O and α-Mo₂C and β-Mo₂C were mixed. It means that oxides are formed due to the slight contamination of oxygen.

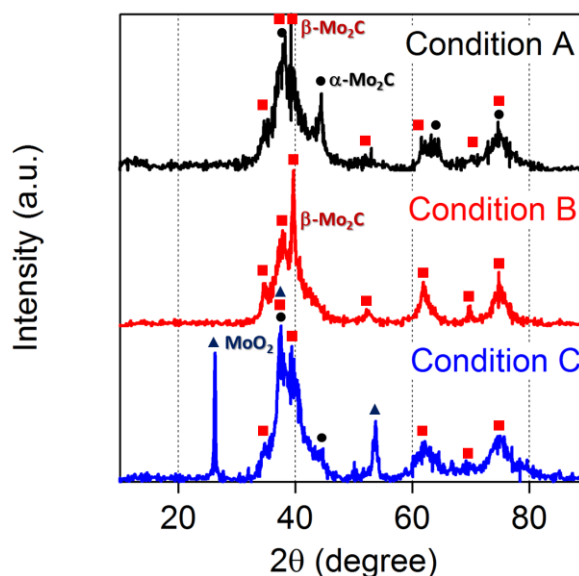


Fig. 4 The XRD patterns of HSA-Mo₂C.

3.3 Mo₂C supported metal catalysts (Co/HSA-Mo₂C, Ni/HSA-Mo₂C, Ru/HSA-Mo₂C)

The XRD patterns of the Mo₂C supported metal catalysts after reduction were showed in Fig. 5. The crystal phase of the Mo₂C were not changed after metal loading. It was expected that supporting metal were dispersed on HSA-Mo₂C by incipient impregnation method because the peaks of supporting metal were not emerged or slightly emerged.

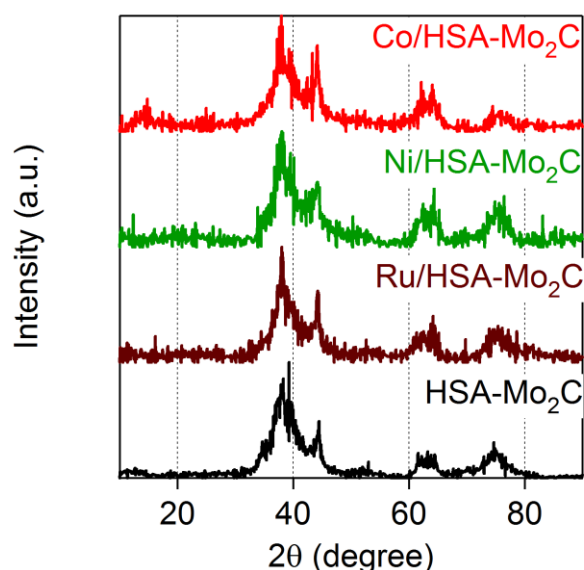


Fig. 5 The XRD patterns of Mo₂C supported metal catalysts.

4 CONCLUSION

High surface area molybdenum carbides were prepared using a temperature programmed reaction technique starting from an ammonium molybdate precursor. They have both α -phase and β -phase. And Mo₂C supported metal catalysts (Co/HSA-Mo₂C, Ni/HSA-Mo₂C, Ru/HSA-Mo₂C) synthesized by incipient wetness impregnation method. After metal loading, the crystal structure of the molybdenum carbides were not changed.

FUTURE WORK

In this study, molybdenum carbides supported metal were synthesized. By using them, the catalytic performance test should be done. For example, ammonia synthesis. It also would be nice to change the amount of deposition of supporting metals and test them in order to investigate the interaction between the metal and mixed phase molybdenum carbides.

ACKNOWLEDGEMENTS

I would like to thank Professor. Levi Thompson, and Dr. Saemin Choi as supervisors for accepting me. Thanks to you, I enjoyed studying in the USA. I am grateful to **Dr.** Wei-Chung Wen for assistance with the experiment when you are busy. I congratulate you on your degree acquisition. I was also supported by Japan-US Advanced Collaborative Education Program. Thank you all I have met in U.S. I want to see you again someday.

REFERENCES

- (1) Ryoichi Kojima, Ken-ichi Aika *Applied Catalysis A: General* 2001, 219, 141-147.
- (2) Weiqing Zheng, Thomas P. Cotter, Payam Kaghazchi, Timo Jacob, Benjamin Frank, Klaus Schlichte, Wei

- Zhang, Dang Sheng Su, Ferdi Schüth, and Robert Schlög *J. Am. Chem. Soc.* 2013, 135, 3458–3464.
- (3) Yuan Chen, Saemin Choi, Levi T. Thompson *Journal of Catalysis* 2016, 343, 147–156.
- (4) Claus J. H. Jacobsen, Søren Dahl, Bjerne S. Clausen, Sune Bahn, Ashildur Logadottir, and Jens K. Nørskov *J. Am. Chem. Soc.* 2001, 123, 8404-8405.
- (5) D. Mckay, J.S.J. Hargreaves, J.L. Rico, J.L. River, X.-L. Sun *Journal of Solid State Chemistry* 2008, 181, 325–333.
- (6) Leo Volpe and M. Boudart *J. Phys. Chem.* 1986, 90, 4874-4877. (9) Brian M. Wyvratt, Jason R. Gaudet, Daniel B. Pardue, Andrea Marton, Svemir Rudić, Elizabeth A. Mader, Thomas R. Cundari, James M. Mayer, and Levi T. Thompson *ACS Catal.* 2016, 6, 5797–5806.
- (7) Brian M. Wyvratt, Jason R. Gaudet, Daniel B. Pardue, Andrea Marton, Svemir Rudić, Elizabeth A. Mader, Thomas R. Cundari, James M. Mayer, and Levi T. Thompson *ACS Catal.* 2016, 6, 5797–5806.
- (8) Huazhang Liu *Chinese Journal of Catalysis* 2014, 35, 1619–1640.
- (9) Ryoichi Kojima, Ken-ichi Aika *Applied Catalysis A: General* 2001, 215, 149–160.

Thermal Testing of the New Small Magnetic Sensor for SmallSAT

Takahiko Kosegaki

Department of Climate and Space Science and Engineering,
University of Michigan
kosegaki@umich.edu

Supervisors: Mark. B. Moldwin, Leonardo Regoli

Department of Climate and Space Science and Engineering,
University of Michigan
mmoldwin@umich.edu
lregili@umich.edu

Abstract.

Magnetic field sensors are getting smaller and use less electric consumption. Thus, the researchers are interested in multiple point observations using a number of small spacecraft in the magnetosphere. RM3100, which made by PNI sensor corporation, is one of the candidates of the small (20 mm x 20 mm) L/R magnetic sensor for small spacecraft. This paper examines the temperature dependence of this sensor using a dry ice and a magnetic shield can. The sensor's slope coefficient was $3.1 \text{ nT}/^\circ\text{C}$ in linear fitting in maximum. It is too large to be negligible with respect to the sensor's resolution. Moreover, once the temperature of sensor go to below $-42 \text{ }^\circ\text{C}$, it generates relatively large spike noise unless the temperature is higher than $-40 \text{ }^\circ\text{C}$ (the lower limit of the sensor).

1. INTRODUCTION

1.1 GEOMAGNETIC FIELD

There are magnetic fields surrounding the Earth, called the magnetosphere. The magnetosphere has a distorted shape, unlike the magnetic field of a bar magnet,

due to the solar wind (see Fig. 1). The solar wind is a cloud of ionized gas and transport the magnetic field of the Sun as the Interplanetary Magnetic Field (IMF) [1]. The IMF reaching the Earth's geomagnetic fields (magnetopause) combine with the geomagnetic field. Afterwards, it passes the Earth and the geomagnetic field re-connects at the opposite side of the Earth at the back of night side (geomagnetic tail). Then, the energy of the magnetic field is converted into the kinetic energy of particles [2] [3]. As a result, it constructs ring currents and radiation belts that contain the highest energy in the magnetosphere. That region contains the possibility of killing the astronauts and damaging electronics on spacecraft [2].

1.2 MAGNETIC DISTURBANCE

When the energy transfers from IMF into magnetosphere, enhancement of ring current is observed. Then, a rapid decrease in the Disturbed Storm Time (Dst) index is also observed (see Fig. 2). The substorms are also a phenomenon of magnetic disturbance in the magnetosphere. It differs from the geomagnetic storm in the time and space scales. Its timescale is shorter and

more localized than the storm's. It should be noted that all storms are accompanied by substorms, but not all substorms are associated with a storm [2]. Understanding these behavior of the magnetic field is one of the most important objectives for a space weather forecast.

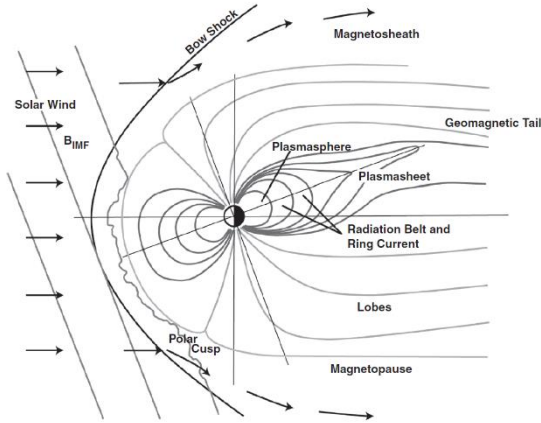


Fig. 1 The schematic of the geomagnetic field and IMF. (from Moldwin, 2008)

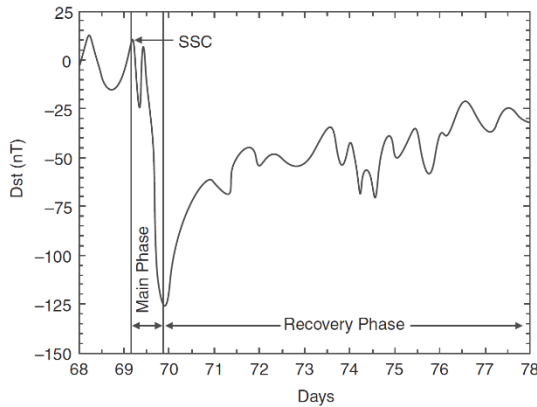


Fig. 2 When the geomagnetic storm occurred, the Dst decreases suddenly. (from Moldwin, 2008)

1.3 MEASUREMENTS

Traditionally, it is difficult to observe different points in the magnetosphere simultaneously. However, the significant progress of sensor and electronic technologies enable the magnetic field measurements at low electrical consumption and manufacturing costs. Therefore, researchers are interested in small satellites to investigate

the multiple points in the magnetosphere simultaneously (e.g. [4]). Therefore, the commercial off the shelf (COTS) instruments (e.g. [5] [6] [7]) attract researchers because of manufacturing time and cost savings.

1.4 MAGNETIC-INDUCTIVE (MI) SENSOR

The RM3100 is a COTS 3-axis magneto-inductive (MI) sensor that lacks an analog-digital (A/D) converter, as shown in Fig. 3. It is small and low powered, which enable to be used in SmallSATS. The basic circuit is shown in Fig 4. H_E and I represent the external magnetic field parallel to MI sensor and the current running through the circuit. The total magnetic field that the sensor experience is represented as:

$$H = k_0 I + H_E \quad (1)$$

k_0 represents the constant that depends on physical parameters of the sensor. The Schmitt trigger generate a signal oscillating between 0 V (logical "0") and Vs (logical "1"), using the feedback through the coil. The core of solenoidal coil in MI Sensor has a magnetic permeability that depends on the magnetic field through itself. If there is external field, the difference of permeability can be measured by observing the difference of the frequency of oscillation. Counting the frequency of the oscillation using the internal clock of the RM3100 provides the magnetic field value. According to past research, this sensor has a resolution of 8.73 nT [5]. However, the question remaining is whether the sensors have a temperature dependence. In general, such a low noise sensor is made of the materials should have a stable temperature dependence. However, there is the possibility that the solenoid is stressed a little which affects the value of the measured magnetic field. Therefore, this paper studies the temperature dependence of the sensor.

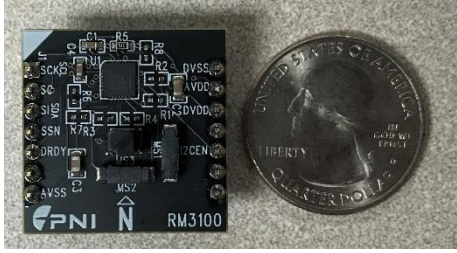


Fig. 3 RM3100 is as small as US quarter coin.

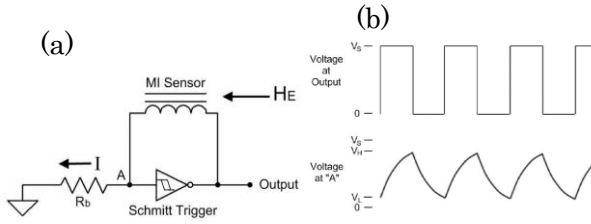


Fig. 4 The basic circuit of the MI sensor (a) includes the Schmitt trigger which oscillate like (b).

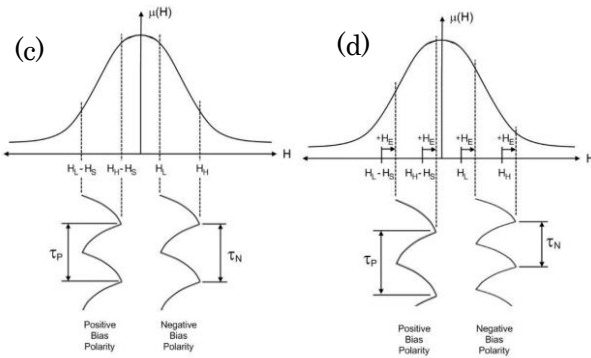


Fig. 5 The cycle times of oscillation are set same value without external magnetic field in negative and positive biased (c) When the external magnetic field are applied, the difference between the cycle times derives the magnitude of magnetic field.(from Leuzinger and Taylor, 2010)

2. METHOD

The thermal test procedure requires the minimization of noise to get an accurate temperature dependence curve. Ideally, the test should be held in a noise free space with the same sensor, however, another method was chosen in this paper. We used two RM3100 magnetic-sensors to get simultaneously both of the magnetic field values with the temperature changing and not. The procedure of the thermal test is:

1. To characterize two of RM3100 magnetic field sensors, both sensors were placed next to each other. The system was left running for 60 h (see Fig. 5-a).

2. To measure the difference of the magnetic field inside and outside of the shield can, one sensor was placed in the shield can, the other one was placed outside the shield can. The system was also left running for 60 h (see Fig. 5-b).

3. A similar system to 2. but the dry ice was added inside the shield can and was left running for 60 h to test for the temperature dependence (see Fig. 5-c).

4. Finally, to test if there was permanent damage to the sensor due to temperature change, experiment 2 was run again for 60 h.

Arduino uno, which made by Arduino, was used to run the RM3100 magnetic sensors. It offers the operation of four devices in same time with ASIC communications. This control board has five analog ports and 14 digital ports. The analog ports were used to communicate with TMP36 temperature sensor, which made by Analog Devices, Inc. Note that the wires connected to the SD card reader generate huge noise on the measurements of TMP36. Therefore, TMP36 should be separated away from wires connected to SD card reader.

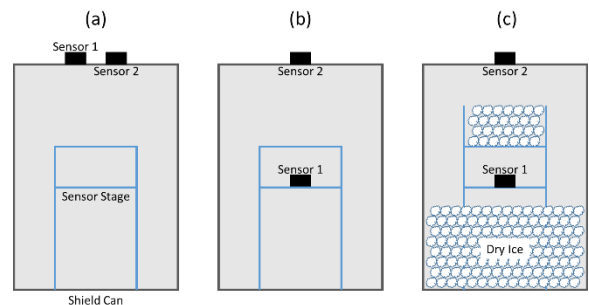


Fig. 6 (a) The test to reveal the difference of sensor characters (b) The test to reveal the difference of the inside and outside the shield can. (c) The main thermal test with the dry ice

3. RESULTS AND DISCUSSION

3.1 SPIKES AND TEMPERATURE GRADIENT

Fig. 7 shows the three measurements gathered with the RM3100 and the temperature in the shield can. The measurements of RM3100 was calculated into the magnetic field(B_x , B_y , B_z). There is a flat period in the measurements of temperature because the temperature was outside the sensor's measurement range of $-50 \sim +150$ degrees. In Fig.7, the three groups of noise spikes (labeled I, II, III) can be seen. Because the two separate chunks of dry ice melted at different times, the temperature graph had two sections of temperature rises. The notable point is that there are few noise spikes between I. and II. even though the temperature was below -50 degrees. It indicates the possibility that spike noise occurs when the temperature suddenly changes causing a problem in the electrical circuits.

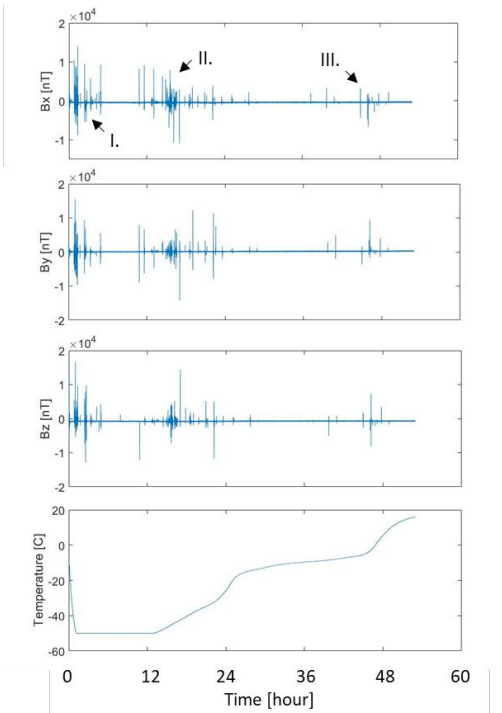


Fig. 7 The measurements of magnetic field becomes noisy when the temperature is changing.

3.2 TEMPERATURE DEPENDENCY

Fig. 2 shows the graph of the magnetic field versus temperature. To see the trend of the graph, the measurements was taken the moving mean of 1000 samples with Matlab(Mathworks, Inc). You can see the gradual rise of the magnetic field value depends on the temperature on B_x and B_y . Furthermore, the shapes of the first 20 minutes(cooling) and heating curve (Fig. 9) are similar. It indicates that temperature dependency is an inherent characteristic of each sensor.

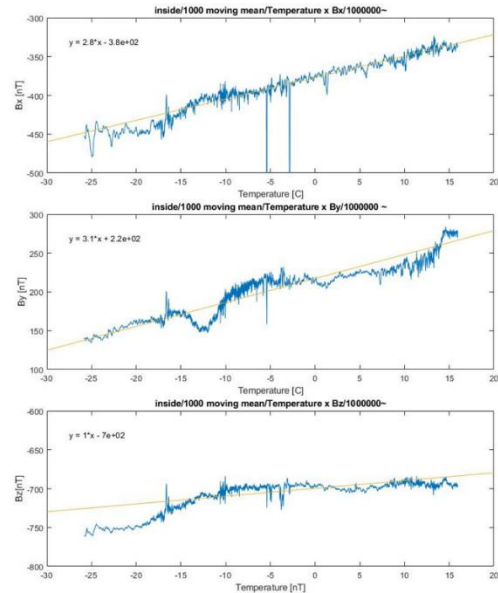


Fig. 8 The measurements of magnetic fields versus time while the temperature rising (These results were the moving mean of 1000 samples)

Table 1 Trend coefficients of magnetic field to temperature

axis	Trend coefficients (nT /°C)
X	2.8
Y	3.1
Z	1.0

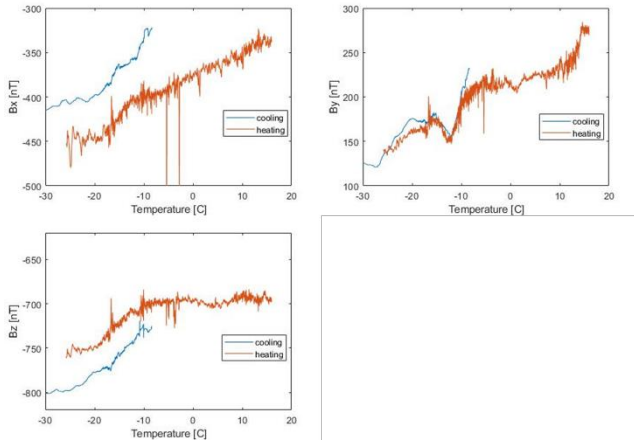


Fig. 9 The comparison between the temperature dependency of cooling(first 20 minutes) and heating

3.3 NO PERMANENT DAMAGE

The testing was carried out beyond the temperature range specified by the manufacturer, hence the sensors might have been damaged. Fig. 10 shows the measurements five days after and before thermal testing. The resolution does not get worse and there is not any additional spike noise in the measurements after thermal testing. The effects of thermal test did not remain more than five days after testing.

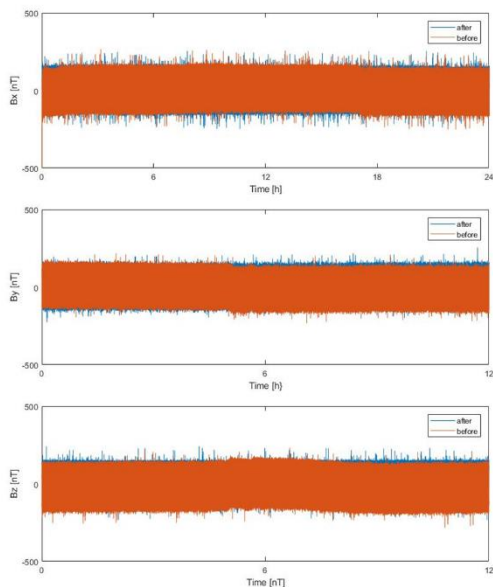


Fig. 10 The measurements of magnetic field five days after thermal testing

CONCLUSION.

This test showed the significant temperature dependence of the magnetic sensors, however each axis behaves differently. Basically, the measured magnetic field rises with the temperatures (Fig 8). Their coefficients of trend are shown in Table 1.

After temperature drops below $-40\text{ }^{\circ}\text{C}$, a spike noise tended to appear when the temperature was changing.

It is recommended to do the thermal testing at temperatures above -40 degrees again. Using the thermal chamber, the chamber is made cooled below -40 degrees. When the thermal chamber will be -40 degrees, the sensors will be put in it. By doing so, the real temperature dependency of each sensors will be revealed. Furthermore, whether the increase in the noise spikes below -40 degrees is caused by the sensor's temperature limits or sharp temperature changes is still to be investigated.

REFERENCE

- [1] A. J. Hundhausen, Coronal Expansion and Solar Wind, Springer Science & Business Media, 2012
- [2] M. Moldwin, An introduction to space weather, Cambridge University Press, 2008
- [3] R. L. McPherron, Magnetic Pulsations: Their Sources and Relation to Solar Wind and Geomagnetic Activity, Surveys in Geophysics, vol. 26, No. 5, pp. 545-592, 2005
- [4] J. C. Springmann, A. J. Sloboda, A. T. Klesh, M. W. Bennett, J. W. Cutler, The attitude determination system of the RAX satellite, Acta Astronautica, 75, pp. 120-135, 2012
- [5] L. H. Legoli, M. B. Moldwin, M. Pellioni, B. Bronner, K. Hite, A. Sheinker, B.M. Pnder, Investigation of a low-cost magneto-inductive magnetometer for

space science applications, Geoscientific Instrumentation Method and Data Systems, 7, pp. 129-142, 2018

[6] M. Diaz-Michlana, R. Sanz, M. F. Cerdan, A.B. Fernandez, Calibration of QM-MOURA three-axis magnetometer and gradiometer, Geoscientific Instrumentation Methods and data Systems, 4, 1-18, 2015

[7] E. Matandirotya, R. R. Van Zyl, D. J. Gouws, E. F. Saunderson, Evaluation of a Commercial-Off-the-Shelf Fluxgate Magnetometer for CubeSat Space Magnetometry, Journal of Small Satellites, Vol. 2, No. 1 pp. 133-146, 2013

[8] A. Leuzinger, A. Taylor, Magneto-Inductive Technology Overview, Tech. rep, PNI Sensor Corporation, 2010

Experimental Investigation of Primary Breakup Induced by High Mach Number Shock Wave

Kotaro Hotta

Department of Aerospace Engineering, Nagoya University
hotta@prop2.nuae.nagoya-u.ac.jp

Supervisor: Mirko Gamba

Department of Aerospace Engineering, University of Michigan
mirkog@umich.edu

Abstract

This work investigates the primary breakup process in the supersonic crossflow. The flow is generated in a shock tube facility and the breakup process is captured by a high speed camera using the schlieren technique. Break up caused by an incident shock wave with Mach number of 3.5, which induces a Weber number of 9003, is investigated. Instabilities are observed on the windward side of the water column, and it is presumed to be the growth stage of the Rayleigh-Taylor instability, ultimately causing the breakup.

Nomenclature

- ρ_∞ = density of ambient flow
 ρ_l = density of liquid
 u_∞ = velocity of ambient flow
 d_0 = diameter of water column
 σ_1 = surface tension of water column
 μ_1 = dynamic viscosity of liquid
 p_{driver} = pressure at the driver section
 p_{driven} = pressure at the driven section
 We = Weber number
 Oh = Ohnesorge number
 Ms = incident shock Mach number
 M_1 = flow Mach number behind incident shock wave
 M_2 = flow Mach number behind reflected shock wave

1. Introduction

The primary breakup processes of a liquid column in a gaseous crossflow was studied

experimentally and numerically, motivated by applications to spray break up in crossflow in air-breathing propulsion systems, liquid rocket engines, diesel engines and agricultural sprays. Classically, the primary breakup processes in the subsonic crossflow are characterized by the Weber number (We) and Ohnesorge number (Oh). For a liquid column, they are defined as:

$$We = \frac{\rho_\infty u_\infty^2 d_0}{\sigma_1} \quad (1)$$

$$Oh = \frac{\mu_1}{\sqrt{\rho_l \sigma_1 d_0}} \quad (2)$$

At low Ohnesorge number ($Oh < 0.1$), the mode of primary breakup is classified into four regions. They are expressed column, bag, multimode and shear breakup, and the corresponding Weber numbers are $We < 4$, $4 < We < 30$, $30 < We < 110$, $110 < We$, respectively. [1] The primary breakup process of a liquid column in supersonic crossflow was also studied experimentally and numerically, [2][3] which is aimed for the application of supersonic combustion of scramjet engines and transpiration cooling of re-entry vehicles. In the experimental study, [3] they are varying the injector shape and reveal the correlation of injector shape and the penetration height of liquid which is critical for a combustor. However, we lacked the physical understanding of breakup process in the supersonic cross-flow. The objective of this investigation is to further investigate the process of primary breakup in supersonic cross-flow generated by a high Mach number incident shock wave over a range of Weber numbers.

2. Apparatus and Instrumentation

The experimental equipment is composed of two main components: the facility used to generate an incident shock wave and the water column generator. The incident shock wave and the flow is generated in the Hypersonic Expansion Tube facility [4] at the Gas Dynamics Imaging Laboratory at the University of Michigan. It is composed of a 2.9 m long driver section, a 8 m long driven section and a 3 m expansion section. At the end of the driven section and at the end of the expansion section it has a group of four equidistantly spaced pressure sensors. These sensors are operated at a sampling rate of 2 MHz and are used to measure the velocity of the incident shock wave. This facility was operated in incident shock mode, with the 2.9 m long driver section and the 11 m long driven section. The test section is connected at the end of expansion section. The test section has a dimension of 457 mm × 483 mm × 343 mm. It has parallel UV-grade quartz windows at the both sides of the test section that provide us optical access to the end of the shock tube exit. The

water column generator is connected on the top of the test section, and it generates a stable water column with a speed of 2.8 m/s and a diameter of 1.2 mm. A schlieren system is used to record the primary breakup process. Although several conditions were investigated, here we only consider one specific operating condition, which is summarized in table 1.

3. Experimental Results and Considerations

A. Test conditions

We conducted tests and their conditions are summarized in Table 1. High speed images of tests are recorded with a Phantom v711 camera at a resolution of 128 × 32 pixels. The field of view of about 40 mm × 10 mm is kept. The frame rate is set to 600,000 frames per second. We used a pulsed LED light source that generates pulses with a 650 ns width as the light source of the schlieren system.

Table 1, Test conditions

Test case	Gases	p_{driver}	p_{driven}	M_1	Ms	We
	driver/driven	[MPa]	[kPa]	[-]	[-]	[-]
1	He/Air	1.35	12.6	1.5	3.5	9003

B. Results and Discussion

The breakup sequence at test case 1 is shown in figure 1 as a typical result (incident shock is from left to right), and the trajectory of the reflected shock wave and windward (left) edge of the water column is shown figure 2. The origin of the x-axis corresponds to left edge of initial water column position. The time for each image is given with respect to the arrival of the incident shock wave at the water column. Time steps between images are not of equal interval. In figure 2, the

position of the water column is normalized by the diameter of the water column, and time is normalized by the breakup time of a liquid column scale with the liquid phase time, t^* , from [6], which is defined by Eq. 3. The field of view consists of a 38.01 mm × 9.50 mm rectangular window. As the resolution is 0.297 mm per pixel, the 1.22 mm water column is resolved by four pixels.

$$t^* = \left(\frac{\rho_l}{\rho_g} \right)^{0.5} \frac{d_0}{u_\infty} \quad (3)$$

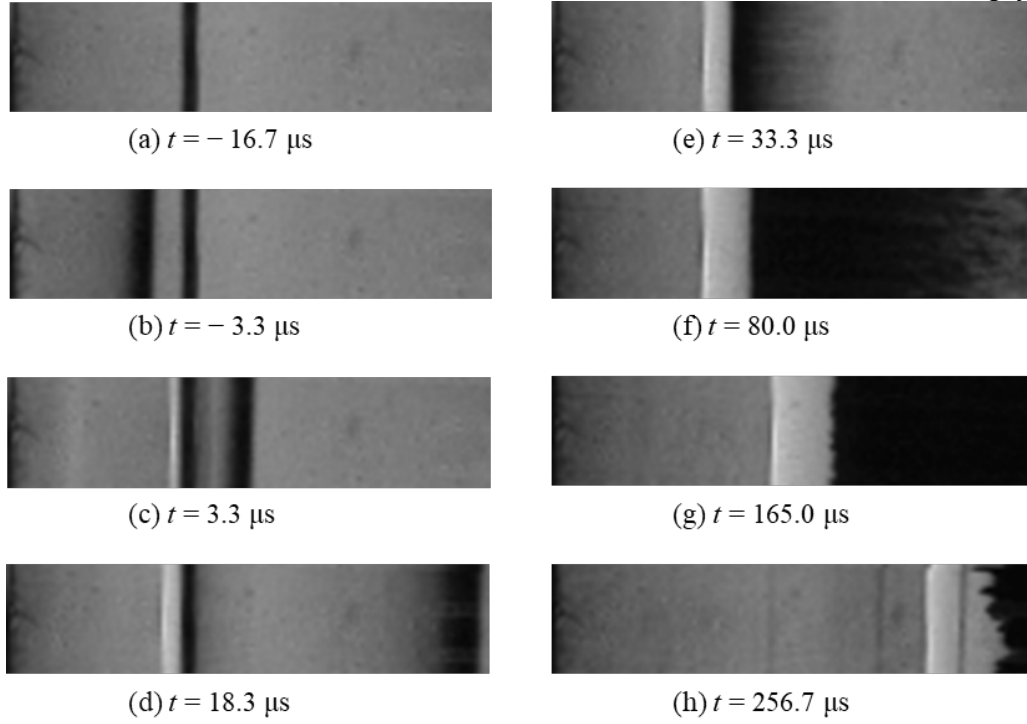


Figure 1 Breakup sequence for test case 1

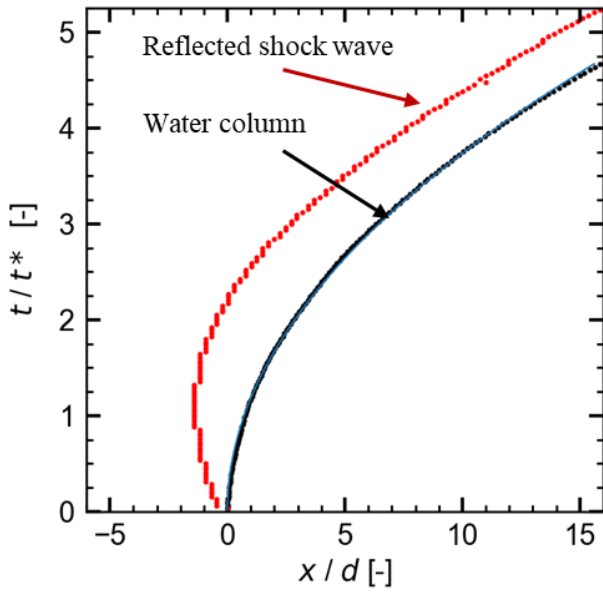


Figure 2 The trajectory of water column and reflected shock wave.

The water is injected at a speed of 2.8 m/s and forms a straight and smooth column (figure 1 (a)). An approximately 1.5 mm of low light intensity region on the left-hand side in figure 1 (b) indicates the incident shock wave entering the test section. The reflected wave can clearly be

identified as it propagates upstream on the left-hand side of the water column (figure 2 (c), (d)). Since an intensity increase corresponds to a positive density gradient to the direction of the positive x-axis, the recorded wave is identified as a reflected shock wave.

The second sequence starts with the stripping of droplets and ligaments from the water column. Both sheared off ligaments and a fine mist can be seen the leeward side of the water column (figure 1 (e), (f)). The instability starts to form in the windward side of the water column (figure 1 (g)). As the lower density fluid (air) goes to the higher density fluid (water), these instabilities are supposed to be associated with a Rayleigh-Taylor instability. The fastest growing wavelength of the Rayleigh-Taylor instability at the initial stage is computed by[6]

$$\lambda_M = \sqrt{\frac{3\sigma_1}{a(\rho_1 - \rho_\infty)}} \quad (4)$$

where λ_M is the fastest growing wavelength and a is the acceleration in a direction normal to the interface. We can write the fitting curve of the trajectory of water column by $x = 312440 t^2$, and R^2 value is 0.9996. The properties of water at an

ambient temperature, $\sigma_1 = 72$ mN/m and $\rho_1 = 996.5$ are chosen. When we assume the density of air is much lower than the density of water, that is $(\rho_1 - \rho_\infty) \approx \rho_1$, the wavelength is computed as $\lambda_M = \sqrt{\frac{3\sigma_1}{a\rho_1}} = 26.3$ μm . The wave length of the instability which is observed was approximately 1mm, and that corresponds to three pixels. As this is the minimum wavelength which can be recorded in this camera setting, the initial wavelength could be smaller than 1 mm.

Conclusion

We investigated the primary breakup process of the water column in supersonic crossflow. We observed instabilities on the windward side of the water column, and it is presumed to be the growth stage of the Rayleigh-Taylor instability.

ACKNOWLEDGEMENT

I would like to express my gratitude to my supervisor Professor Mirko Gamba of my research. The weekly meeting helps me to think of next steps of my research. I would like to thank my laboratory members for helping me with the experiments. I would like to thank my supervisor at Nagoya university, Professor Jiro Kasahara, for letting me do research abroad. This work was supported by Japan-US-Canada Advanced Collaborative Education Program (JUACEP).

Reference

- [1] Sallam, K., Aalburg, C., Faeth, G., "Breakup of round nontubulent liquid jets in gaseous crossflow," *AIAA*, Vol.42, No.12, 2004, pp. 2529–2540.
- [2] Xiao, F., Wang, Z. G., Sun, M. B., Liang, J.H., Liu, N., "Large eddy simulation of liquid jet primary breakup in supersonic air crossflow," *international Journal of Multiphase Flow*, Vol. 87, 2016, pp. 229-240.
- [3] Beloki Perurena, J., Asma, C., O., Theunissen, R., Chazot, O., "Experimental investigation of liquid jet injection into Mach 6 hypersonic crossflow," *Experiments in Fluids*, Vol. 46, 2009, Issue 3, pp. 403-417.
- [4] Abul-Huda, Y.M., and Gamba, M., "Design and characterization of the Michigan

hypersonic expansion tube facility," *AIAA Paper*, 2015, pp.1–13.

- [5] Nicholls, J. and Ranger, A. Aerodynamic "shattering of liquid drops." *AIAA Journal*, Vol. 7, No. 2, 1969, pp. 285–290.
- [6] Sharp, D. H., "An overview of Rayleigh-Taylor instability," *Physica D: Nonlinear Phenomena*, Vol. 12, 1984, Issues 1-3, pp. 3-10.

A computational study of cell growth and division as an energy-based soft packing problem using a diffuse interface framework

Ryo Tsunoda, S. Rudraraju, J. Jiang & K. Garikipati

Abstract

We present computational studies on the dynamics of cell aggregation including cell growth, division and packing. The underlying models were established in previous research but computational results were shown only up to the twelve-cell stage. In this research, we studied the energy of soft packing as the cells divide and grow to fill a volume. The challenge lay in treating interface contact by allowing several equilibration phases in the dynamics, without which unphysical solutions are obtained to the dynamics of growth and division. Also included are the dynamic change in total free energy, which is our measure of packing efficiency.

1. Introduction

Cell aggregation can be described by observing molecular architecture of the cell surface, the mechanisms which controls how dispersed cells are repelled, and the force which causes dispersed cell to aggregate and switch to aggregation [1]. Switching to the aggregation permit correlation of cell-cell interactions with cell differentiation, viability and migration, as well as subsequent tissue formation [2]. Therefore, cell aggregation can be considered to be a basic process behind many process in life, tissue engineering [3], tumor hyperplasia and migration [4], cell healing [5] and embryogenesis [6]. Therefore, it is necessary to understand the underlying process and mechanism of tissue aggregation to better understand these phenomena. Cell aggregation is consisted from the single cells or the multi-cells activation such as cell division, differentiation, migration and packing. It is commonly accepted that the growth of the cell cluster is controlled by the signal path way, influenced by the chemical environment and the mechanical interaction but the research of their affection according to spatial and time variation is primary. In order to further study these mechanisms, we will explore the application of computer simulation.

In previous research effort, lattice models have been used by researchers to study cell aggregation model. In this model, the cell is represented as a square or hexagonal lattice site in the field filled with either lattice [15]. The cells are considered to involve through free energy minimizing cell pair exchanging. This simplified model gave the insight to represent cell aggregation, but it failed to model the cells dynamics generally observed in real cells. One limitation is the single lattice representation of cells, which can't represent the cell shape with the exception of the square or hexagonal shape. To improve the model representation, sub-cellular lattice models were developed, using high-Q Pott model [11]. Cells represented by this model were represented with a cluster of the lattices instead of a single lattice, making the model cell shapes more real. Additionally, although cell migration was represented by the exchange of cell pair in lattice model, more realistic cell migration was realized by the lattices at boundary of the cell switching the parent cell. This switching allowed the cell to approach the length of a lattice to the neighbor cell. Sub-lattice models allow better representation of complex cell shape than lattice model but the cell boundary is still jagged and the shape of the cell is unrealistic.

As a more realistic model, cell-centric/center dynamics models [14] and vertex dynamics models [8,16] were used to model the cell aggregation problem. Cell-centric/center dynamics model represents the cells through Voronoi tessellation which divide the plane to the specific subsets of the plane based on the distance from point and evolution of the boundaries is achieved by a free energy minimization movement of the forming points. Vertex models describe the cell as an approximated polygon. The vertexes are set on the point on the interface shared by over three cells and the area surrounded by vertex and the line connecting neighbor vertexes are considered as the cell. The cell dynamics are driven by the free energy minimizing pair through movement of vertices that conserve cell volume and the internal virtual work is assumed from the variation of the vertexes. Vertex models express the cell dynamics including cell-cell interaction, cell extrusions and cell divisions in 2D and 3D models but the boundaries of cells are still polygon different from real cells.

The models mentioned above have succeeded at representing cell aggregations in high or low quality, however, still lack the ability to describe the smooth and anisotropic cell shape evolution and the mechanism of cell surface evolution due to cell-cell contact as seen in real cells. We call this problem focusing on the process of growth and evolution of multi-cell aggregates the soft packing problem.

Previous research succeeds at solve the soft packing problem with a finite element methods based on phase field method [13,17]. The phase field methods are useful to model diffuse interface kinetic. The evolution of a species concentration and/or phase is represented with a set of conserved or non-conserved order parameter and the relationship between order parameters and interface kinetic is determined according to the parabolic partial differential equations, which are referred to Cahn-Hilliard formulation (for conserved order parameters) [11] and Allen-Cahn formulation (for non-conserved order parameters) [7]. The model succeeded to represent cell division, migration and growth likewise older models. Additionally, it allows for high fidelity representation of smooth, anisotropic cell geometries, cell-cell contact evolution and the resulting mechanical compaction.

The model in previous research succeeded to fill the entire domain with 12 cells shown in fig.1d but 2, 4 and 8 cells could not fill within the membrane. Therefore, we give the model filled entire domain with fewer cells and compare the energy of 2, 4 and 8 cells to understand and help improving soft packing model.

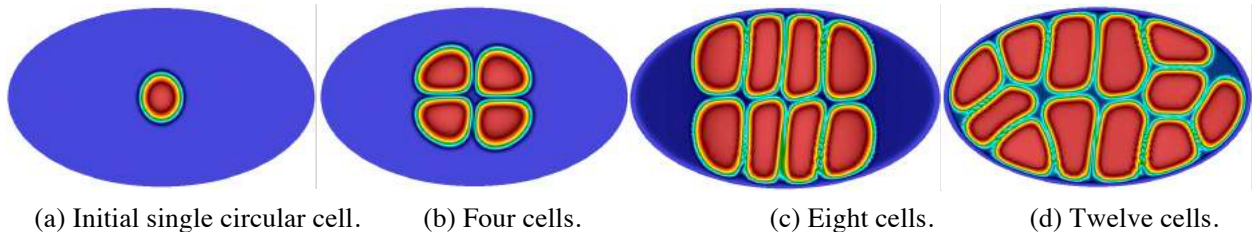


Fig.1 A demonstration of the progression of cell division from one cell into twelve cells. Cell interiors are shown in red and the cell membrane in cyan- yellow, refer from J. Jang 2018

2. Materials and Methods

2.1. A phase field formulation

Let Ω be $\Omega \in \mathbb{R}^2$ and $\partial\Omega$ be a smooth boundary of Ω . The scalar field is written as $c_k \in [0,1]$, where $k=1, \dots, N$ distinguishes the interior and exterior of the cell. The interior of cell k is $\omega_k \in \Omega$, where $\omega_k = \{X \in \Omega \mid c_k(X) = 1\}$ and the exterior of cell k is $\Omega \setminus \omega_k$. The free energy density function of the cell k is the following form:

$$\psi_1(c_k) = \alpha c_k^2 (c_k - 1)^2 + \frac{\kappa}{2} |\nabla c_k|^2 \quad (1)$$

The first term $f(c_k) = \alpha c_k^2 (c_k - 1)^2$ distinguish ω_k and $\Omega \setminus \omega_k$. The second term determine a diffuse cell-matrix interface of finite thickness, where κ control the interface thickness.

The summation of free energy for N cells in Ω is expressed with the following term by adding a cell-cell repulsion term and the principal moments of inertia term

$$\begin{aligned} \Pi[\mathbf{c}] &:= \int_{\Omega} \psi(\mathbf{c}, \nabla \mathbf{c}) dV + \sum_{k=1}^N \sum_{i=1}^{\dim} \delta_k^i (I_k^{i\text{ref}} - I_k^i)^2 \\ &= \int_{\Omega} \left(\sum_{k=1}^N f(c_k) + \sum_{k=1}^N \frac{\kappa}{2} |\nabla c_k|^2 + \sum_{l \neq k} \sum_{k=1}^N \lambda c_k^2 c_l^2 \right) dV + \sum_{k=1}^N \sum_{i=1}^{\dim} \delta_k^i (I_k^{i\text{ref}} - I_k^i)^2 \end{aligned} \quad (2)$$

Here λ is a penalty coefficient that enforces repulsion between any two cells. δ_k^i is a mechanical modulus penalizing variation of I^i , principal moment of inertia of i^{th} cell from $I^{i\text{ref}}$, the i^{th} principal moment of inertia when i^{th} cell birth. Therefore, we can describe anisotropic mechanical character such as elasticity. The moment of inertia tensor through the center of mass is described as following.

$$I[\mathbf{c}] = \begin{bmatrix} I_{11}[\mathbf{c}] & I_{12}[\mathbf{c}] \\ I_{21}[\mathbf{c}] & I_{22}[\mathbf{c}] \end{bmatrix} = \begin{bmatrix} \int_{\Omega} c \bar{X}_1^2 dV & \int_{\Omega} c \bar{X}_1 \bar{X}_2 dV \\ \int_{\Omega} c \bar{X}_1 \bar{X}_2 dV & \int_{\Omega} c \bar{X}_2^2 dV \end{bmatrix} \quad (3)$$

Where, with the center of mass and the difference between the optional position and center of cell mass with respect to the Cartesian coordinates

$$X_i^c = \frac{\int_{\Omega} c X_i dV}{\int_{\Omega} c dV} \quad (4)$$

$$\bar{X}_i = X_i - X_i^c \quad (5)$$

I_k which denotes a principal value of the moment of inertia tensor of the k th cell are calculated through Cayley-Hamilton theory

$$I_k^2 - I_k \text{tr} I_k + \det I_k = 0 \quad (6)$$

The deliberative of (2) with respect to c_k is described as following formulation

$$\begin{aligned} \delta \Pi_k[\mathbf{c}; \omega] &= \frac{d}{d\epsilon} \int_{\Omega} \sum_{k=1}^N \left(f(c_k + \epsilon\omega) + \frac{\kappa}{2} |\nabla(c_k + \epsilon\omega)|^2 + \sum_{l \neq k} \lambda (c_k + \epsilon\omega)^2 c_l^2 \right) dV \\ &\quad + \frac{d}{d\epsilon} \sum_{k=1}^N \sum_{i=1}^{\dim} \delta_k^i (I_k^{i\text{ref}} - I_k^i[c_k + \epsilon\omega])^2 \Big|_{\epsilon=0} \\ &= \int_{\Omega} \omega \left(f'(c_k) - \kappa \Delta c_k + \sum_{l \neq k} 2\lambda c_k c_l^2 \right) dV - \sum_{k=1}^N \sum_{i=1}^{\dim} 2\delta_k^i (I_k^{i\text{ref}} - I_k^i[c_k]) \tilde{I}_k^i[c_k] \\ &\quad + \int_{\delta\Omega} \omega \kappa \nabla c_k \cdot \mathbf{n} dS \end{aligned} \quad (7)$$

where \tilde{I}_k^i is

$$\tilde{I}_k^i = \frac{\int_{\Omega} \omega (I_k^i \text{tr} \bar{\mathbf{I}} - \bar{X}_1^2 \int c \bar{X}_2^2 dV - \bar{X}_2^2 \int c \bar{X}_1^2 dV + 2\bar{X}_1 \bar{X}_2 \int c \bar{X}_1 \bar{X}_2 dV) dV}{2I_k^i - \text{tr} \mathbf{I}} \quad (8)$$

with the tensor

$$\bar{\mathbf{I}} = \begin{bmatrix} \bar{X}_1^2 & \bar{X}_1 \bar{X}_2 \\ \bar{X}_1 \bar{X}_2 & \bar{X}_2^2 \end{bmatrix} \quad (9)$$

Then, chemical potential μ_k is defined as

$$\mu_k = f'(c_k) - \kappa \Delta c_k + \sum_{l \neq k} 2\lambda c_k c_l^2 - \sum_{i=1}^{\dim} 2\delta_k^i (I_k^{i \text{ref}} - I_k^i) \hat{I}_k^i \quad (10)$$

where \hat{I}_k^i is

$$\hat{I}_k^i = \frac{I_k^i \text{tr} \bar{\mathbf{I}} - \bar{X}_1^2 \int c \bar{X}_2^2 dV - \bar{X}_2^2 \int c \bar{X}_1^2 dV + 2\bar{X}_1 \bar{X}_2 \int c \bar{X}_1 \bar{X}_2 dV}{2I_k^i - \text{tr} \mathbf{I}} \quad (11)$$

At equilibrium, $\delta \Pi_k[\mathbf{c}, \omega] = 0$ for the k th cell, yielding $\mu_k = 0$ in Ω , and $\kappa \nabla c_k \cdot \mathbf{n} = 0$ on $\partial \Omega$.

Scalar field c_k is denoted in the following parabolic partial differential equation, generally known Cahn-Hilliard equation, considering the delineation, growth of the N-cell aggregate and repulsion between cell pairs

$$\frac{\partial c_k}{\partial t} = -\nabla \cdot (-M \nabla \mu_k) + s_k \quad (12)$$

where the source term s_k and the mobility M . The dynamics of the cells in soft packing problem is governed by Equation (12) with the thermos dynamics denoted by Equation (10) and the boundary conditions $\kappa \nabla c_k \cdot \mathbf{n} = 0$, $c_k = 0$ on $\partial \Omega$ for $k = 1, \dots, N$.

We use explicit-implicit methods in order to discretize c_k and μ_k depending on time. Let the time step $\Delta t = t^{n+1} - t^n$. Then, the simulation start from the initial conditions which are given as $\{c_k^0, \mu_k^0\}$ and the conditions at n^{th} time step are denoted as $\{c_k^n, \mu_k^n\}$.

$$\begin{aligned} c_k^{n+1} &= c_k^n + \Delta t (M \nabla \cdot (\nabla \mu_k^{n+1}) + s_k) \\ \mu_k^{n+1} &= f'^{n+1}(c_k) - \kappa \Delta c_k^{n+1} + \sum_{l \neq k} 2\lambda c_k^{n+1} c_l^{n+1^2} - \sum_{i=1}^{\dim} 2\delta_k^i (I_k^{i \text{ref}} - I_k^i) \hat{I}_k^i \end{aligned} \quad (13)$$

The weak form follows: Find $c_k^{n+1} \in \mathcal{S} = \{c \in \mathcal{H}^1(\Omega) | c = 0 \text{ and } \nabla c \cdot \mathbf{n} = 0 \text{ on } \partial \Omega\}$ such that for any arbitrary variation $\omega \in \mathcal{V} = \{\omega \in \mathcal{H}^1(\Omega) | \omega = 0 \text{ and } \nabla \omega \cdot \mathbf{n} = 0 \text{ on } \partial \Omega\}$ on c_k the following residual are satisfied:

$$\begin{aligned}
\int_{\Omega} \omega c_k^{n+1} dV &= \int_{\Omega} \omega c_k^n - \nabla \omega \cdot \Delta t M \nabla \mu_k^{n+1} + \omega s_k dV \\
\int_{\Omega} \omega \mu_k^{n+1} dV &= \int_{\Omega} \omega f^{n+1}(c_k) + \nabla \omega \cdot \kappa \nabla c_k^{n+1} dV + \int_{\Omega} \omega \sum_{l \neq k} 2\lambda c_k^{n+1} c_l^{n+1} dV \\
&\quad - \sum_{i=1}^{\dim} 2\delta_k^i (I_k^{i \text{ref}} - I_k^i[c_k]) \int_{\Omega} \omega \hat{I}_k^i dV
\end{aligned} \tag{14}$$

Spatial time discretization is calculated with a standard finite element frame work and use bilinear quadrilateral elements.

2.2. Cell division

The cell mass of k^{th} cell at n^{th} time step is described as $m_k^n = \int_{\Omega} c_k^n dV$. When the tolerance of the cell mass at current time and the twice cell mass at initial time $\varepsilon_1 = m_k^n - 2m_k^0$ become larger than zero, the cell start to divide. Then the number of cell increase from N to $N+1$ and the new scalar field is described as c_{N+1}^0 at initial condition. The cell division axis is corresponding to the direction of major principal axis of moment of inertia through the center of the parent cell just before division. Thus, the new interface dividing the cells is along to major principal axis of moment of inertia of k^{th} cell at time t^n . When the cell mass of k^{th} cell reach to twice larger than initial cell mass at n^{th} time step, ω_k^n divided to ω_k^{n+1} and ω_{N+1}^{n+1} at $n+1^{\text{th}}$ time step. Setting the measure of ω_k as $\text{meas}(\omega_k)$, $\text{meas}(\omega_k^{n+1})$ and $\text{meas}(\omega_{N+1}^{n+1})$ are equal to $0.5\text{meas}(\omega_k^n)$. Though Δt is basically determined such that it ensure the stability and convergence of the Cahn-Hilliard dynamics, we introduce the adaptive time step to ensure the cell dividing convergence and stability. During cell dividing, Δt is decreased by a factor of 1.0×10^{-m} where m is less than 7 for a few time steps less than 5. After that term, the time step is back to regular value till next cell division start.

2.3. Controlling the mass of cells

Here I explain the way to fill the entire field with the cells, the number of which is less than 12. The area of the cells at final step is set as the area of entire domain divided by the number of cells to fill the entire domain with the cells. But there are the things that the cell grows skipping the neighbor cell since the interface of the cells reach to the boundary before the entire domain filled with the cells as shown in fig.2 and the cell was collapsed since there are no space to expand at interface of the cells and could not be converged. The reason why it happens is the cells grow too rapid to repel each cell enough by repulsion term. We put a couple of period to stop growing at certain volume and to repel the cells enough before starting to grow again. The algorithm is shown below.

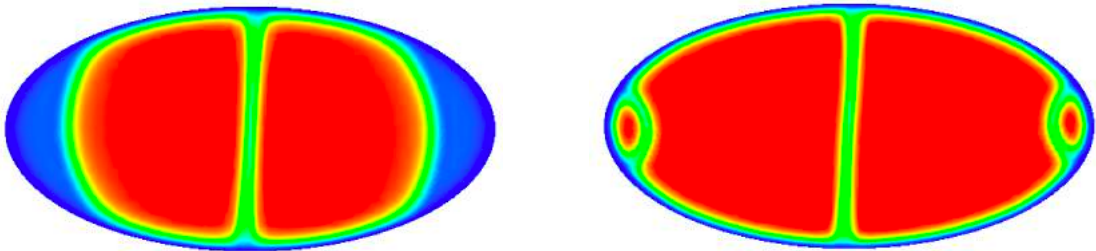


Fig.2 The interface reach to the boundary (left) and the cell skip the neighbor cell to expand (right)

Algorithm

```

for N=1 to N=3
   $v_k^n = m_k^n / m_k^0$ 
   $s_k^n = \text{source term}$ 
  if timeForEquilibrium N < current time < timeForEquilibrium N+1
    if  $v_k^n < \text{CertainValue } N$ 
       $s_k^n *= 1.0$ 
    end
    if  $v_k^n > \text{CertainValue } N$ 
       $s_k^n *= 0.0$ 
    end
  end
  if timeForEquilibrium 4 < current time
     $s_k^n *= 1.0$ 
    if  $v_k^n > \text{Field area} / \text{the number of cell}$ 
       $s_k^n *= 0.0$ 
    end
  end
end
end

```

2.4. The value of each parameter

The values of each parameter are according to the previous research. It was set from numerical experiment.

Table1: Numerical values of parameters

Parameters	α	κ	λ	M	s	$\overline{\Delta t}$
Value	4	1.0e-3	100	1	5.0e2	2.0e-4

2.5. Framework

The model shown here has been implemented in the **C++** based **deal.II** open source finite element library. We use the **superLU** to solve equation (14). The linearization itself is obtained using the Sacado algorithmic differentiation library of the open source Trilinos project.

3. Result

3.1. Full volume packing with the equilibrium term

The result of the simulation according to 2.1 ~ 2.3 is shown in fig.3. At first, the model was simulated with setting the mechanical moduli $\{\delta^1, \delta^2\} = \{0, 0\}$. We succeeded to fill the entire domain of the field with the certain number of cells by taking time for equilibrium to repel the cells before the cell-cell interface configure and it will skip the neighbor cell or will be collapsed. When we consider one section to the term which cell grow up certain volume then stop to grow and repel each other, three sections were set as the terms for equilibrium after cell division. The maximum volume each cell growing up is chosen to ensure that cell grow equally in each term. Each time for equilibrium is determined to disturb the interface generated incorrectly.

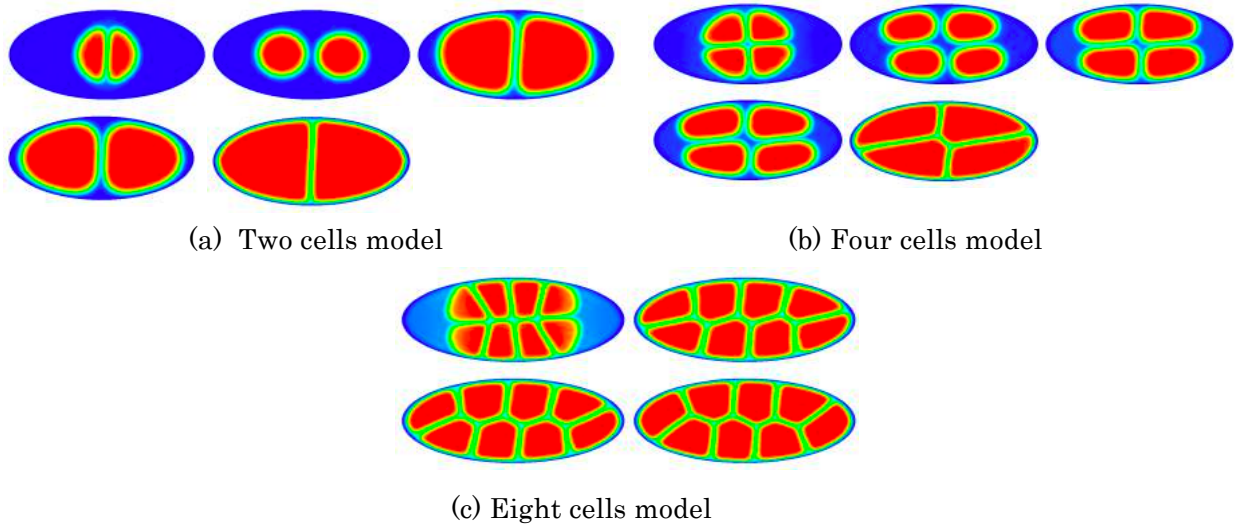


Fig.3 Full volume packing with the equilibrium term of two, four and eight cells.

We show the process of the packing with 5 pictures for two and four cells and 4 pictures for eight cells.

3.2. Full volume packing with the moment of inertia

In order to mention the mechanical property of soft packing problem, we need to turn on the moment of inertia term. The effective value of the mechanical moduli δ_k^i which impose control on cell shape is observed by numerical experiments in the previous study and it is within the range $\delta_k^i \in [1 \times 10^4, 2 \times 10^5]$. The result of the simulation with inertia term is shown in fig.4 with the same parameters as 3.1. except δ_k^i , which is set $\{\delta^1, \delta^2\} = \{0, 1 \times 10^4\}$. We only succeeded with the model divided into 2 cells and the models divided into 4 and 8 cells were not converged.

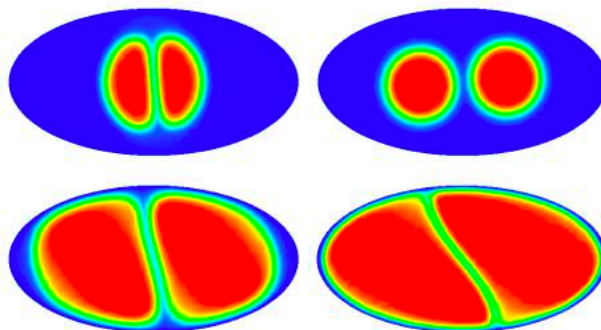


Fig.4 Full volume packing with the equilibrium term and the moment of the inertia term

4. Conclusion

In this research, we succeeded to fill the entire domain of the model with the certain number of the cell under stability by controlling the cell mass and adding equilibrium term after cell grow up to certain volume. We found out that if the cells expand under stability or not depend on how we treat the cell interface. For instance, in two cells model, since the interface between the cells reach to the boundary of the domain before the cells fill the entire domain and the cell mass at the interface lose the area to expand. Then, the cell mass skip the neighbor cell to expand at the empty area. In four cells model, the interfaces of the four cells contact and lose the area to expand likewise two cells model and then the cells are exploded. But, when the number of cell is over 8, the cells could fill the entire domain without time for equilibrium because the cell volume after cell division are not so different from the cell volume filling the entire domain.

The energy plotting of each model is shown in fig.5. We can see the three steps in the two and four cells model including equilibrium term. Third step is significantly larger than the first and second step because the interfaces between cells is closer and much than the other two steps. In the model added inertia term, the spike at the second and third steps which occur at between expanding term and equilibrium term decrease slowly. It is because the cells are penalized to change the shape by inertia term so cannot change it rapidly.

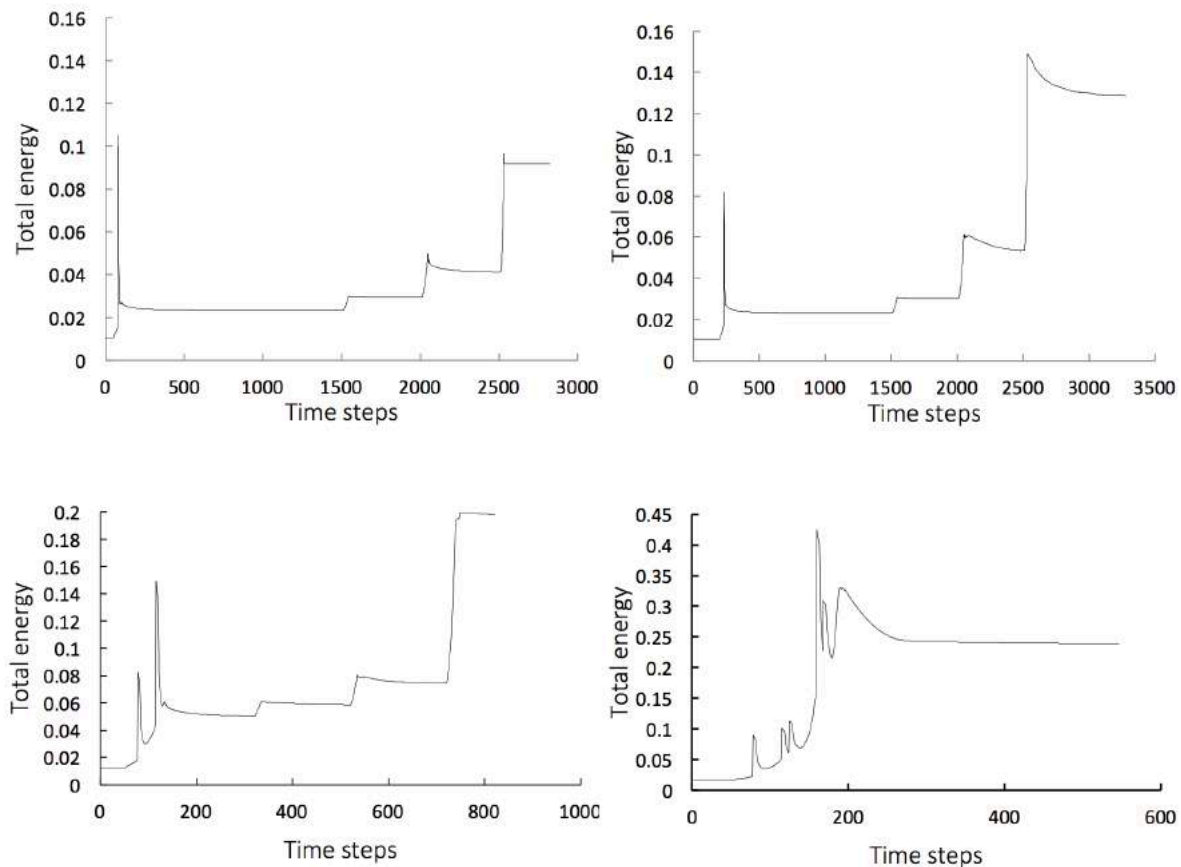


Fig.5 Evolution of total free energy with time steps. All of four energy plotting include the equilibrium term and only upper-right model include the moment of inertia term.

Both of upper plotting is two cells model, bottom-left is four cells model and bottom-right is eight cells model.

References

- [1] Jakob Benedict Seidelin, Mehmet Coskun, Ole Haagen Nielsen, *Advances in Clinical Chemistry Chapter4*, 2013
- [2] W. Mark Saltzman, Themis R. Kyriakides, in *Principles of Tissue Engineering (Fourth Edition) Chapter20*, 2014
- [3] M.J. Mahoney, W.M. Saltzman *Transplantation of brain cells assembled around a programmable synthetic microenvironment*, *Nat Biotechnol*, 19 (2001), pp. 934-939
- [4] Jamie A. Davies, in *Mechanisms of Morphogenesis (Second Edition) Chapter7*, 2013
- [5] Angela J. Wyatt, Klaus J. Busam, in *Dermatopathology Chapter10*, 2010
- [6] A. H. Rose, *Physiology of Cell Aggregation: Flocculation by Saccharomyces cerevisiae As a Model System*, *Microbial Adhesion and Aggregation* pp 323-335
- [7] Samuel M. Allen and John W. Cahn. A microscopic theory for antiphase boundary motion and its application to antiphase domain coarsening. *Acta Metallurgica*, 27(6):1085 – 1095, 1979.
- [8] Silvanus Alt, Poulami Ganguly, and Guillaume Salbreux. Vertex models: from cell mechanics to tissue morphogenesis. *Philosophical Transactions of the Royal Society of London B: Biological Sciences*, 372(1720), 2017.
- [9] W. Bangerth, R. Hartmann, and G. Kanschat. deal.II – a general purpose object oriented finite element library. *ACM Trans. Math. Softw.*, 33(4):24/1–24/27, 2007.
- [10] G. W. Brodland. *Computational modeling of cell sorting, tissue engulfment, and related phenomena: A review*, volume 57. 2004.
- [11] James A. Glazier and Francois Graner. Simulation of the differential adhesion driven rearrangement of biological cells. *Phys. Rev. E*, 47:2128–2154, Mar 1993.
- [12] Francois Graner. Can surface adhesion drive cell-rearrangement? part i: Biological cell-sorting. *Journal of Theoretical Biology*, 164(4):455 – 476, 1993.
- [13] Michael Heroux, Roscoe Bartlett, Vicki Howle Robert Hoekstra, Jonathan Hu, Tamara Kolda, Richard Lehoucq, Kevin Long, Roger Pawlowski, Eric Phipps, Andrew Salinger, Heidi Thornquist, Ray Tuminaro, James Wilenbring, and Alan Williams. *An Overview of Trilinos*. Technical Report SAND2003-2927, Sandia National Laboratories, 2003. 16
- [14] Hisao Honda. Geometrical models for cells in tissues. volume 81 of *International Review of Cytology*, pages 191 – 248. Academic Press, 1983.
- [15] Atsushi Mochizuki, Naoyuki Wada, Hiroyuki Ide, and Yoh Iwasa. Cell-cell adhesion in limb formation, estimated from photographs of cell sorting experiments based on a spatial stochastic model. *Developmental Dynamics*, 211(3):204–214, 1998.
- [16] Payman Mosaffa, Nina Asadipour, Daniel Millán, Antonio Rodríguez-Ferran, and Jose J Muñoz. Cell-centred model for the simulation of curved cellular monolayers. *Computational Particle Mechanics*, 2(4):359–370, Dec 2015.
- [17] Makiko Nonomura. Study on multicellular systems using a phase field model. *PLOS ONE*, 7(4):1–9, 04 2012.
- [18] J. Jiang, S. Rudraraju, K. Garikipati, A diffuse interface framework for modelling the evolution of multi-cell aggregates as a soft packing problem due to growth and division of cells. *Bulletin of Mathematical Biology*, 2019, doi.org/10.1007

Sensitivity Analysis of Five-Link Suspension

Kimihiko Sugiura

Department of Mechanical System Engineering, Graduate School of Engineering, Nagoya University
sugiura.kimihiko@h.mbox.nagoya-u.ac.jp

Supervisor: Gregory M. Hulbert

Department of Mechanical System Engineering, College of Engineering, University of Michigan
hulbert@umich.edu

ABSTRACT

Multi-link suspensions are considered to be amongst the best and most functional independent suspension systems. One advantage of this suspension design is that it is capable of being optimized to meet both ride and handling objectives. In addition, this suspension allows a vehicle to flex more. However, disadvantages are their cost and complexity to design. To design or optimize Multi-link suspensions with lower cost, designers desire to understand which suspension links affects the particular wheel-kinematic characteristics but do not effect or have little effect on anything else. As such, a sensitivity study could show how to design or optimize into the geometry in the best possible way, so that wheel-kinematic characteristics such as camber angle, toe angle, wheel-travel angle, support angle, and roll center height can be tuned independently. In this paper, we present a general sensitivity analysis approach well suited to Multi-link suspensions and present examples of the results of such an analysis on a prototypic five-link suspension topology.

Undisclosed

REACTIVE DC MAGNETRON SPUTTERING OF MoS₂ AND MoS₂/HBN LAYERS

Koki HOJO

Department of Micro-Nano Mechanical Science and Engineering, Graduate School of Engineering, Nagoya University
hojo@ume.mech.nagoya-u.ac.jp

Supervisor: Suneel Kodambaka

Department of Materials Science and Engineering, University of California, Los Angeles
Kodambaka@ucla.edu

ABSTRACT

MoS₂ is one of two dimensional materials which show promising properties as electrical devices. In industry, most of MoS₂ films are prepared by Chemical Vapor Deposition (CVD) methods, which has limitation on the size of deposition area. In contrast, magnetron sputtering method enables large-scale MoS₂ film compared to CVD methods. However, this process has not been investigated because of the difficulty to grow highly crystalline MoS₂ films. In this research, we deposited MoS₂ film by using reactive direct current (dc) magnetron sputtering process with molybdenum target and H₂S gas. Moreover, we tried to grow MoS₂/hBN layer by exposing substrates into borazine gas before the deposition of MoS₂ film. We found that the X-ray diffraction (XRD) reflection changed from Mo-based peaks to MoS₂-based peaks by increasing H₂S partial pressure. We also observed that the intensity of MoS₂ peaks increased by exposing Al₂O₃(0001) substrate into borazine gas before the deposition of MoS₂.

Undisclosed

STABILIZE AND REPETITIVE CONTROLLER DESIGN FOR AN ACTIVE MAGNETIC BEARING

Hiroki Kogure

Department of Mechanical System Engineering, Graduate School of Engineering, Nagoya University
kogure.hiroki@a.mbox.nagoya-u.ac.jp

Supervisor: Tsu-Chin Tsao

Department of Mechanical and Aerospace Engineering, University of California, Los Angeles
ttsao@seas.ucla.edu

ABSTRACT

For suppression of the development cost and improvement of reliability, dynamic design of fuel turbopump rotor loaded on rocket engine is needed. In this motive, finite element model of LE-7A fuel turbopump which takes rotor dynamic fluid force concerned was built and simulation results can explain well the vibration characteristic which is collected from a ground firing test. To take a further step, some experimental result is required. To create that experimental device, a rotating shaft needs to track some desired circular orbit at various frequencies. Active magnetic bearing is chosen as a desirable device. Basic control strategy to track the circular orbit is learned in this project. A stabilizing controller is designed and installed because AMB system is open loop unstable but this is not sufficient for achieving the objective. Then a plug-in repetitive controller is installed to track some circular orbits.

1. MOTIVATION

1.1 MOTIVATION

For the purpose of suppression of rocket engine development cost and improvement of reliability, vibration analysis on fuel turbo pump rotor which is loaded on rocket engine has been conducted ^{[1]-[3]}. Rotor dynamic fluid force has been thought as one of the main causes of unstable vibration and leads to development failure or terrible accident. This force occurs when a rotor shaft revolves while it is rotating under a circumstance where the shaft is surrounded by fluid — fuel turbo pump rotor is surrounded by liquid hydrogen and rotates at high speed. And in some case, rotor dynamic fluid force caused by rotor revolution amplifies itself and results in an unstable vibration. This motivates more accurate analysis of rotor dynamic fluid force to predict vibration characteristic in certain design parameter or under the operational environment.

In my previous paper, rotational speed dependency of rotor dynamic fluid force is revealed in simulation using the parameters of LE-7A rocket engine. This rotational speed dependent rotor dynamic fluid force is applied to a finite

element model of the fuel turbo pump on LE-7A and eigen analysis is performed. Compared the data from ground firing test of LE-7A, this simulation result can explain well the vibration characteristic. To take a further step, not only a simulation result but also experimental one is required. In the simulation, the motion of revolution is assumed that travels a circular orbit at a speed of $-150\% \sim 150\%$ in the ratio to the rotational speed. This means that orbital trajectory and its revolving speed have to be controlled to gain an expected experimental result.

In this motive, Active Magnetic Bearing is chosen as a desirable device. The point of this research is to learn about MBC500 and control strategy and then to create a controller which enable to track circular trajectory at some expected frequencies.

1.2 HARD WEAR

Fig. 1 shows MBC500, which is developed by launch point ^[4]. Two active magnetic bearing are on both sides and hole effect sensors are equipped at each ends. Fig. 2 shows the experimental system. Controllers are designed on Mathworks Simulink Real-Time on the host PC and transferred to the Target PC.

Firstly, a boot disk of xPC Target is needed. To create DOS Loader files, kernel image and DOS Loader are written and copied to a flash drive. Target PC is booted from this target boot disk image.

Secondly, the host PC and Target PC should be connected. xPC Target supports two connection-and-communication protocols between the host PC and Target PC: serial and network. In this report, network connection is chosen and both PC are directly connected using a cross-over Ethernet cable. National Instruments PCI-6052e cards with 16-bit resolution were used for data acquisition and command.

Created controllers are compiled and transformed to the Target PC. Because of some malfunction, however, this report is limited to simulation.

2. SYSTEM IDENTIFICATION

2.1 MODELING

In this paper, black box model of MBC500 [5] is used to design controllers. The hole sensors output displacement in the X -plane and Y -plane at each ends — x_1, x_2, y_1 , and y_2 . This is apparently Multi-Input and Multi-Output (MIMO) system and inputs and outputs are coupled. This feature can complicate the control design. But, redefining inputs and outputs in a deferent way, it is possible to decouple the system and allow SISO control design. This handling translates the displacements at each ends into transformation and rotation in X and Y plane at the geometric centre of shaft. The following step of control design is based on this SISO system.

Decoupled frequency response data is collected and curve fitting is performed using Matlab command. Following is transfer functions for X -plane Transformation, X -plane Rotation, Y -plane Transformation, and Y -plane Rotation, respectively — X_T, X_R, Y_T , and Y_R :

$$\begin{aligned} X_T &= \frac{266.9(s^2 + 2126s + 5.47 \times 10^6)}{(s + 2479)(s + 442.8)(s - 460.9)} \\ X_R &= \frac{298.8(s^2 + 942.2s + 2.46 \times 10^6)}{(s + 2240)(s + 394.6)(s - 392.7)} \\ Y_T &= \frac{-632.6(s - 1720)(s + 1252)}{(s + 3602)(s + 401.6)(s - 396.2)} \\ Y_R &= \frac{-583.6(s - 2639)(s + 1694)}{(s + 4196)(s + 438.3)(s - 447.8)} \end{aligned} \quad (1)$$

Note that Y -plane transfer functions have non-minimum zero. This requires considerations when inversion model is desired.



Fig.1 MBC500 Turbo



Fig.2 Experimental System

2.2 MODEL UNCERTAINTY

Due to the safety concerns of Active Magnetic Bearing rotor operating at high speed, any controller developed must prove a measure stability. The robust stability criterion is a classic result. For the small gain theorem, if both \hat{T} and Δ are stable, the following is a sufficient condition for the overall system to be robust stable:

$$\hat{T} \times \Delta < 1 \quad (2)$$

where delta is the modeling error and \hat{T} is the complementary sensitivity function:

$$\Delta = \frac{\hat{P} - P}{P} \quad (3)$$

$$\hat{T} = \frac{C\hat{P}}{1 + C\hat{P}} \quad (4)$$

\hat{P} is the approximated system which will be used to design controllers and P is the nominal plant model [6]. C is the transfer function of a designed controller. Fig. 3 shows the model used for the robustness analysis of a controller C .

3. STABILIZE CONTROLLER

3.1 LQGi CONTROLLER

As well known, AMB systems are open loop unstable. To provide stability and robustness over the entire operating speed range, a Linear-Quadratic-Gaussian (LQG) servo controller with integral action is installed. Integral action is included to centre the rotor in relation to the stator housing to prevent collisions between the rotor and housing. Fig.4 shows the block diagram of LQGi controller. This controller is designed by Matlab command, `lqgtrack`.

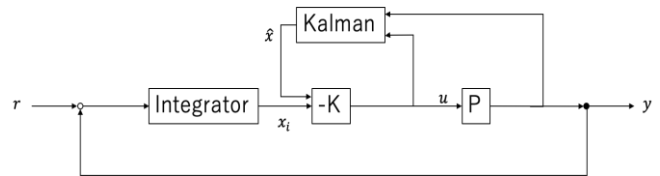
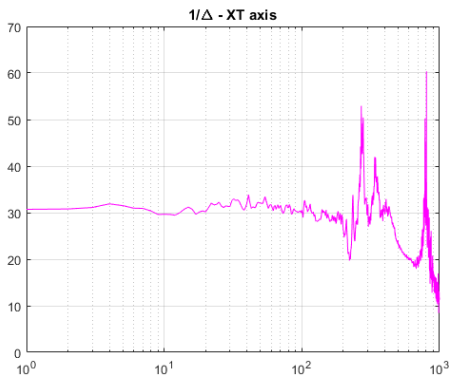
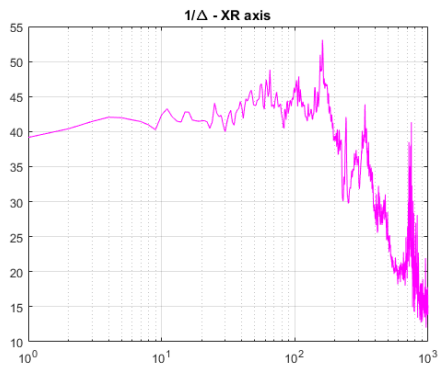


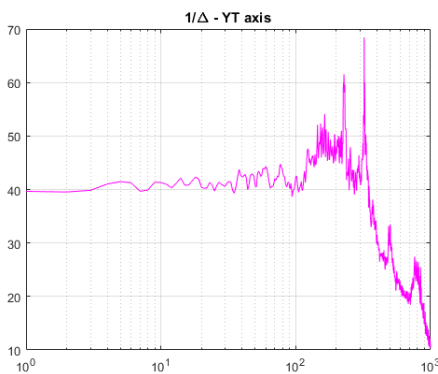
Fig.4 block diagram



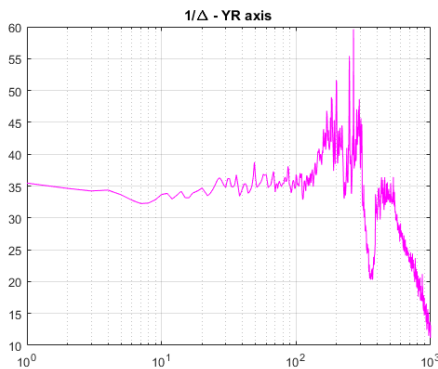
(a) X_T axis



(b) X_R axis

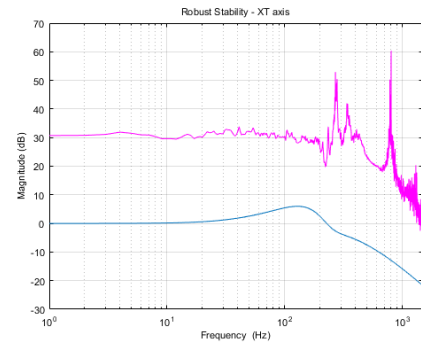


(c) Y_T axis

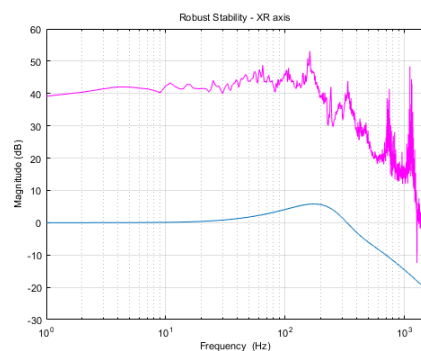


(d) Y_R axis

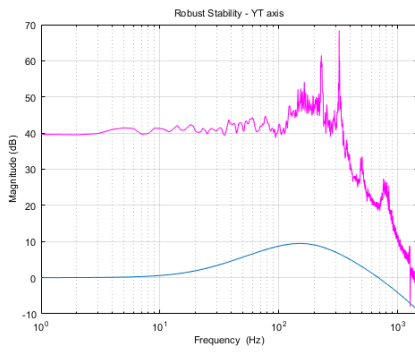
Fig.3 The Inversion of Model Uncertainty



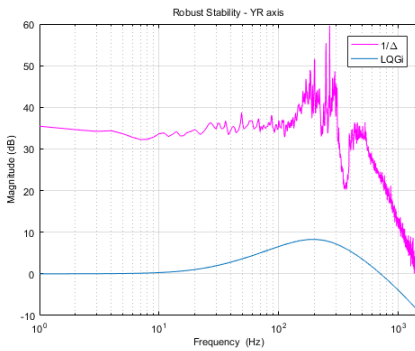
(a) X_T axis



(b) X_R axis

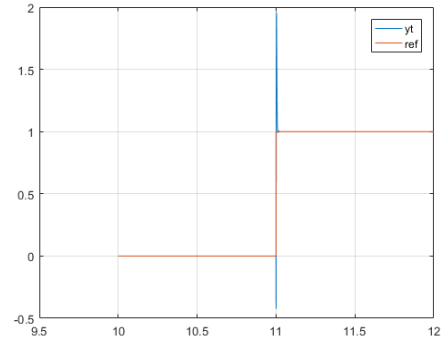


(c) Y_T axis

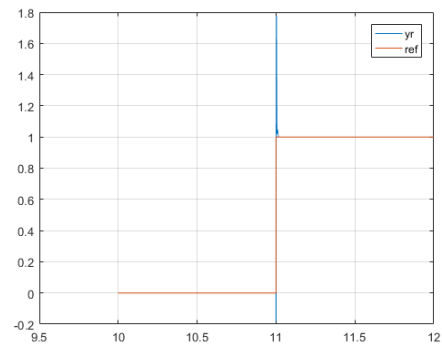


(d) Y_R axis

Fig.5 Robust Stability Analysis

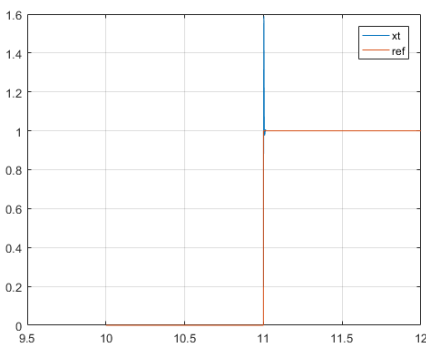


(c) Y_T axis

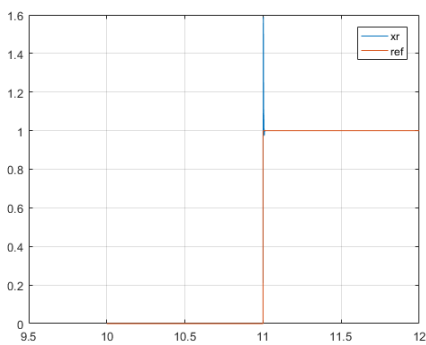


(d) Y_R axis

Fig.6 Step Response with LQGi



(a) X_T axis



(b) X_R axis

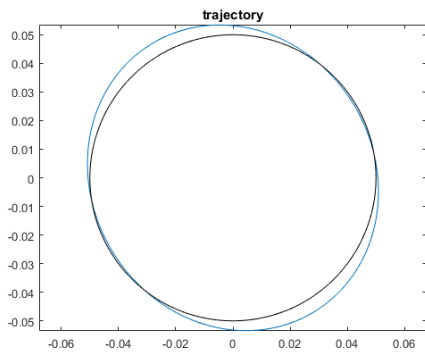
3.2 ROBUSTNESS ANALYSIS

Fig. 5 is plotted the condition for robust stability: $\hat{T} \times \Delta < 1$. This condition is respected by both axis, so that the system will be robust stable.

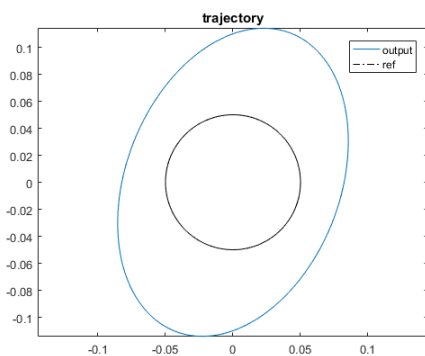
3.3 SIMULATION

Simulations which is performed here can be separated into two parts by the objective of control. Firstly, step response is simulated to see if this system is well stabilized. Secondly, sinusoidal references are input to track circular trajectory. The X -plane and Y -plane are $\pi/2$ radians out of phase. This produces the circular trajectory. In consideration of the desired condition, the frequencies of sinusoidal references vary $0Hz, 10Hz, 80Hz, 100Hz,$ and $125Hz$ that means $0\% \sim 125\%$ in the ratio to rotational speed of the shaft when it is spun up to $100Hz$.

The step response in Fig. 6 shows the system is well stabilized. On the other hand, it seems this controller cannot track circular orbit. This controller does not meet the expectation in both gain and phase responses at any frequency except for $0Hz$. LQGi controller can keep the shaft at centre position of housing and prevent collisions between the rotor and housing, but not appropriate for the primary objective of this report – to create circular orbit. These results mean other kinds of controller are necessary.



(a) 10Hz



(b) 80Hz

Fig.7 Tracking Circular Orbit with LQGi

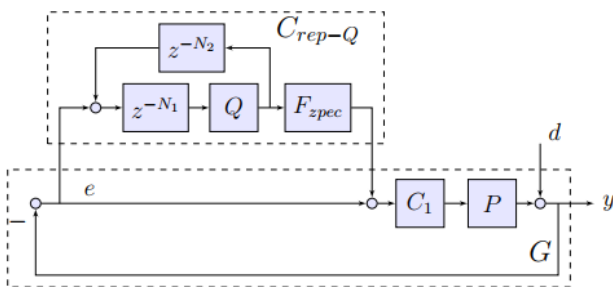


Fig.8 Block Diagram of Plug-in Repetitive Controller

4. PLUG-IN REPETITIVE CONTROLLER

4.1 PLUG-IN REPETITIVE CONTROLLER

To create a circular orbit, tracking sinusoidal reference in both axis is needed. To compensate a periodic disturbance or to track a particular periodic signal, repetitive controller is used. This type of controller is based on the internal model principle.

The internal model is generated by wrapping a positive feedback loop around an integer delay feedback. The delay length $N_p = \frac{1/T_s}{\omega}$ represents the primary period in multiple

of the sample time. This generates infinite control action at primary period. Control generated at higher harmonics can destabilize the system. To provide robustness, a zero-phase low-pass filter is typically included to attenuate control signals past the cut off frequency.

In previous chapter, this system is already stabilized by LQGi controller. To install a controller for tracking an input with minimal effect to the stability of the system, the plug-in structure is used. To accomplish the objective of this report, the overall transfer function should be 1, or very near to it. Giving that the plant G is already stabilized, the parameter to be adjusted is the controller F . If the requirement is $FG = 1$, the ideal condition becomes:

$$F = G^{-1} \quad (5)$$

But the exist of non-minimum phase zero in the Y -plane transfer functions requires some consideration to obtain the inversion of the pre-stabilized model G .

4.2 STABLE INVERSION

Because of non-minimum zero in each Y -plane transfer functions, a complete inversion for these systems can produce an unstable inversion. Thus, some approximate model inversion techniques are required. A popular method of performing the non-minimum phase system inversion is the Zero Phase Error Controller (ZPEC) which inverts the phase response at the expense of the magnitude [7]. For a factorization of the stable system:

$$G = \frac{z^{-d} B^+ B^-}{A} \quad (6)$$

d represents the relative system order, and A, B^+ , and B^- are the poles, stable zeros, and unstable zeros, respectively. The ZPEC inversion is defined as

$$F_{zpec} = \frac{A[B^-]^*}{\gamma z^{-d} B^+} \quad (7)$$

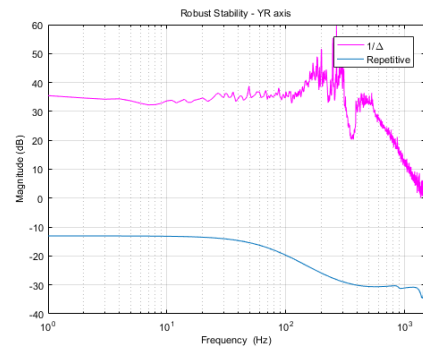
where $[B^-]^*$ is the complex conjugate of the unstable zeros. The accuracy of the inversion can be examined

through their product, $F_{zpec}G = \frac{B^- [B^-]^*}{\gamma}$ which has zero

phase since the zeros are complex conjugates of one another. Though the phase is compensated, the magnitude response is inherited from the position of the unstable zeros. To maintain stability, the constant $\gamma = [B^-(e^{j\omega})][B^-(e^{-j\omega})]$ is used to scale the magnitude of the filter output to unity at the prescribed frequency.

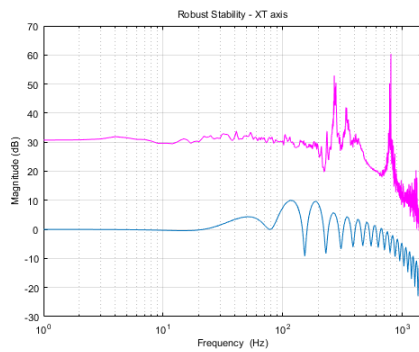
4.3 ROBUSTNESS ANALYSIS

Fig. 8 shows the result of robustness analysis. $\hat{T} \times \Delta < 1$ is satisfied so that this system is robust stable.

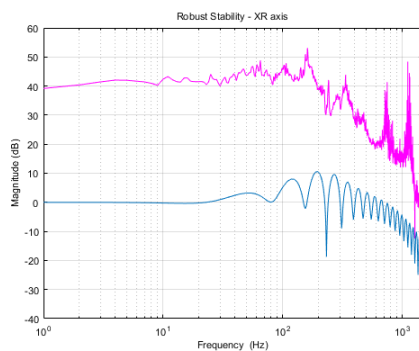


(d) Y_R axis

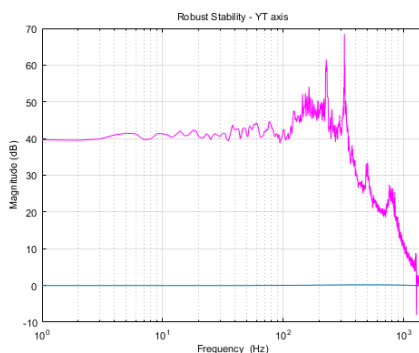
Fig.8 Robust Stability Analysis



(a) X_T axis



(b) X_R axis

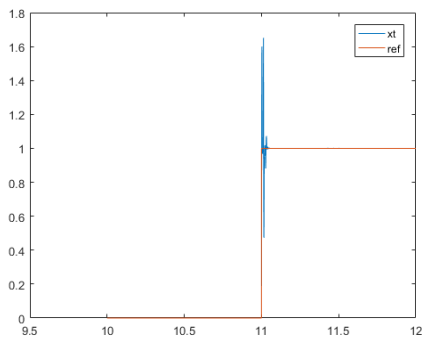


(c) Y_T axis

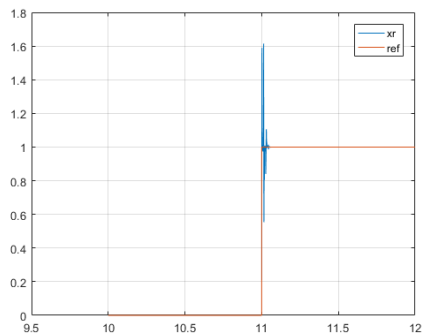
4.4 SIMULATION

Fig. 9 and Fig.10 is the result of simulations which are performed with the same condition as the section 3.3.

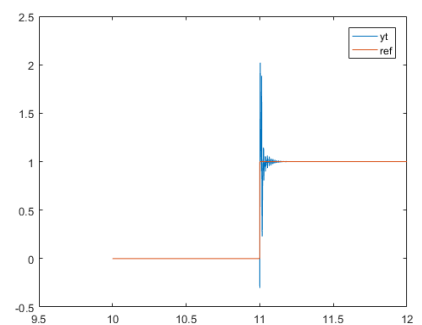
The step response in Fig.9 shows the controller is successfully installed without effects to already stabilized system. The primary concern is the results of tracking sinusoidal references. Comparing the results of LQGi controller, Fig.10 shows this controller accomplishes well creating circular orbit especially in lower frequencies. In higher frequencies, a little difference between input and output in Y -plane response is shown. But the performances are dramatically improved than the LQGi controller.



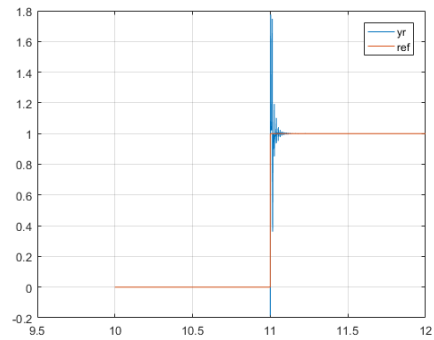
(a) X_T axis



(b) X_R axis

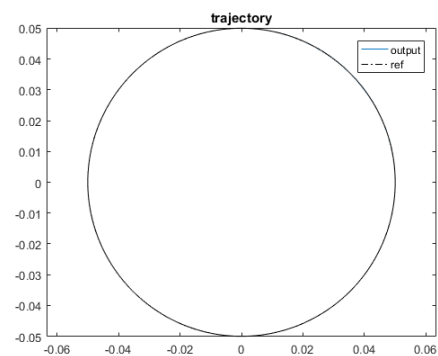


(c) Y_T axis

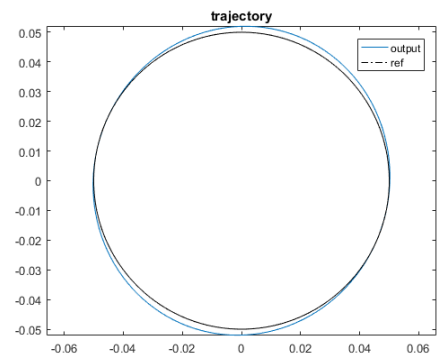


(d) Y_R axis

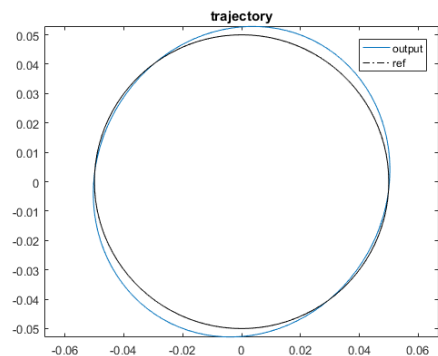
Fig.9 Step Response with LQGi + Plug-In Repetitive Controller



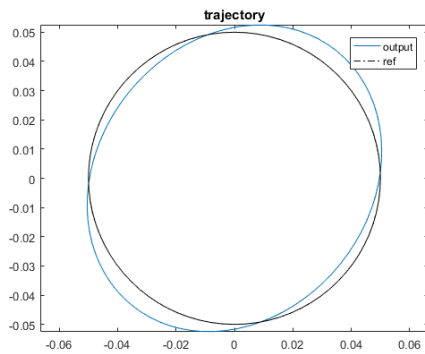
(a) 10Hz



(b) 80Hz

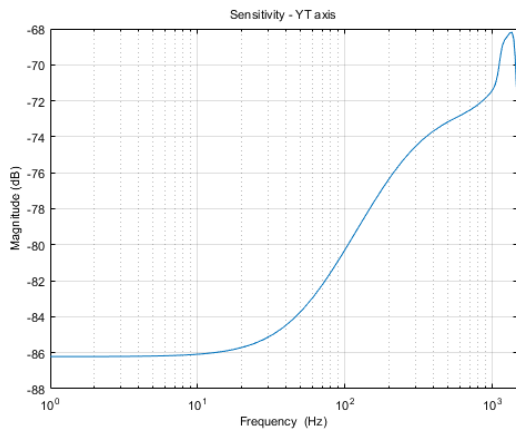


(c) 100Hz

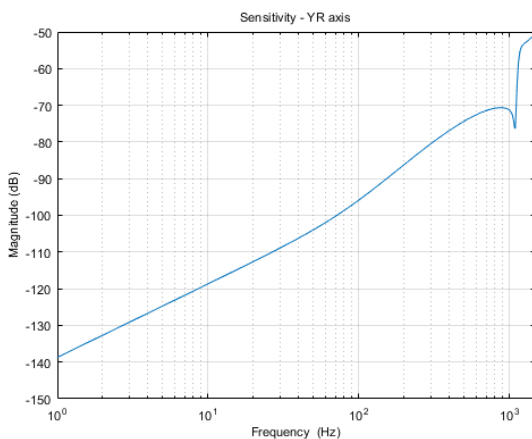


(d) 125Hz

Fig.10 Tracking Circular Orbit with LQGi + Plug-In Repetitive Controller



(a) Y_T axis



(b) Y_R axis

Fig.11 Sensitivity Function

4. CONCLUSION

A data of frequency response of MBC500 Turbo was collected and black box model to control was determined. A Linear-Quadratic-Gaussian (LQG) servo controller with integral action was installed. This controller could stabilize the shaft at centre but could not meet the expectation of this

report. To track accurately sinusoidal reference which has a certain frequency, a repetitive controller based on inner model principle was installed. Besides, to conserve the stability which had been provided by LQGi controller, a Plug-In module was adopted. This Plug-In Repetitive Controller performed well in tracking sinusoidal references and creating circular orbit particularly at low frequencies. A little difference between the input and output still remained at relatively high frequencies. This was indicated by the sensitivity function in Fig.11. To track more accurately, the low pass filter that this controller including can be improved. Furthermore, instead of low pass, other type of filter can be selected, a peak filter for example.

ACKNOWLEDGEMENTS

I am most grateful to professor Tsao for accepting me as a visiting scholar. I also must thank JUACEP office for giving such a valuable opportunity to young ambitious students for many years and in the year to come. Plus, I would like to express my gratitude to everyone I met in the US. Every guys made my visit unforgettable and it has definitely sentimental value for me.

REFERENCES

- [1] Childs, D.W., The Space Shuttle Main Engine High-Pressure Fuel Turbopump Rotordynamic Instability Problem, *ASME J. Eng. Power* 100(1) (Jan 01, 1978), 48-57, p.10.
- [2] Motoi,H., Kitamura,A., Sakazume,N.,Uchiumi,M., Uchida,M., Saiki,K., Nozaki,O., and Iwatubo,T., Sub-Synchronous Whirl In the LE-7A Rocket Engine Fuel Turbo-Pump, Second International Symposium on Stability Control of Rotating Machinery (ISCORMA-2) (2003), p.10.
- [3] Ikemoto,A., Inoue,T., Sakamoto,K., Uchiumi,M., Investigation on the Rotational Speed Dependence of the Rotordynamic Fluid Force, *IMECE2016-66688* (2016), p.7.
- [4] Brad Paden, Nancy Morse, and Roy Smith. Magnetic Bearing Experiment for Integrated Teaching and Research Laboratories." In *Control Applications, 1996., Proceedings of the 1996 IEEE International Conference on*, pp. 421~425, September 1996.
- [5] Kevin Chu, Yigang Wang, Jason Wilson, Chi Ying Lin, and Tsu Chin Tsao. Modeling and Control of a Magnetic Bearing System." In *American Control Conference, 2010. ACC '10.*, pp. 2206~2211, June 2010.
- [6] K. Zhou and J.C. Doyle. *Essentials of Robust Control*. Prentice-Hall, Inc., New Jersey, 1998.
- [7] M. Tomizuka. Zero Phase Error Tracking Algorithm for Digital Control." *Trans. of ASME, Journal of Dynamic Systems, Measurement, and Control*, 109(1):65~68, March 1987.

EVALUATION OF THE UCLA LOW-PROFILE DIRECT SHEAR SENSOR FOR AIR FLOWS IN WIND TUNNEL

Yuta Ujiie

Department of Mechanical System Engineering, Graduate School of Engineering, Nagoya University
Ujiie.yuta@f.mbox.nagoya-u.ac.jp

Chang-Jin Kim

Department of Mechanical and Aerospace Engineering, University of California, Los Angeles
ckim@ucla.edu

ABSTRACT

Measuring shear stress of flow is essential theme in fluid dynamics. This new direct shear stress sensor has simpler mechanism than usual one. The measuring mechanism of this sensor is measuring the displacement of floating plate moved by the shear stress sensor with optical linear sensor. Design and fabrication are described in this paper. After making it, it is tested in wind tunnel with from 5 m/s to 40 m/s airflow and evaluated. The result shows this sensor works well over 20m/s airflow. Under 20m/s, the displacement of the plate is too small. So, it is difficult to measure accurate. At another test in wind tunnel, changing the sample surface to riblet which has drag reduction effect and comparing with the smooth surface. The results shows this sensor is useful for research of riblet. This sensor can be used measuring the shear stress of airflow and many aerodynamics research.

Undisclosed

SYNTHETIC JET CHARACTERIZATION FOR DIFFERENCES IN NOZZLE SIZE AND THICKNESS OF GASKET

Kotaro Takamura

Department of Mechanical Science and Engineering, Nagoya University, Nagoya, Japan
takamura.kotaro@a.mbox.nagoya-u.ac.jp

Philippe Lavoie

Institute for Aerospace Studies, University of Toronto, Toronto, ON, M3H 5T6, Canada
lavoie@utias.utoronto.ca

ABSTRACT

The response of the exit-plane jet velocity to sinusoidal excitation was characterized in quiescent conditions in the present study. We performed the investigation of the characteristics by changing the thickness and the size of the jet slot of the gasket by the experiment. First, we investigate the influence of input voltage amplitude and it is clarified that the input voltage amplitude magnitude affects the averaged velocity but does not affect the turbulence intensity. Good responsiveness is obtained when we use the gasket of the jet slot of $l = 19.8$ mm and the $d = 3.18$ mm and 2.29 mm of gasket thickness.

1. INTRODUCTION

The formation of a wake behind a bluff body and the dynamics of their separated shear layers has been widely investigated [1-3] because of their significant effect on the aerodynamic forces and mixing in engineering applications. Synthetic jets are popular for flow control and are the common zero-net-mass flux fluidic actuator for flow control.

Synthetic jet actuator also have advantageous due to the fact that actuators can be designed such that no parasitic drag is introduced and, at the bare minimum, the control can be switched from on to off. The flow generated from these actuators directly contributes to turbulence. Therefore, if we try to control the flow, the characteristics of the jet should be accurately grasped as a prerequisite.

The synthetic actuator is composed of several elements, for example, top, bottom, and middle plates, neoprene gaskets, and piezoelectric actuators. The difference in these components affects the characteristics of the jet. If we want to control turbulence efficiently, jet responsiveness is important.

In this study, we performed measurements of the velocity at the synthetic jet exit. Here, synthetic jet slot employs driven by piezoelectric actuators. At this time, the characteristics of the jet were compared by changing the thickness and the size of the jet slot of the gasket. And finally, the optimum size of the gasket is proposed.

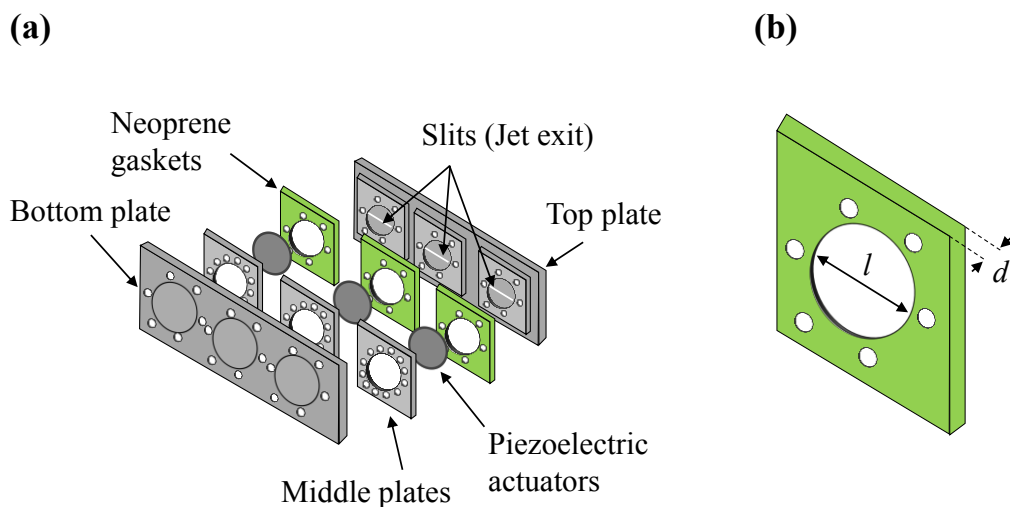


Fig. 1 Synthetic jet actuator details. (a) Solid model exploded view (b) Schematic of the Neoprene gaskets.

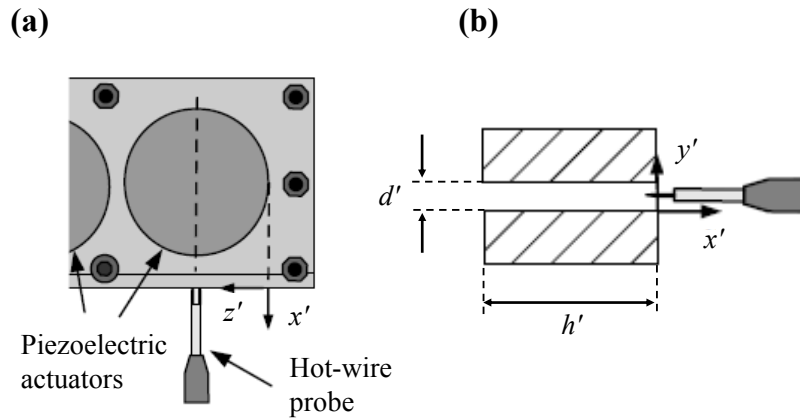


Fig. 2 Schematic showing the setup for the synthetic jet actuator characterization, including the coordinate system for the synthetic jet slot. (a) $x'-z'$ plane (b) $x'-y'$ plane.

2. EXPERIMENTAL SETUP

In Fig. 1(a), the structure of the synthetic jet actuator is composed of four parts: the top plate, middle plate, Neoprene gaskets, and bottom plate. Piezoelectric actuators are pinched between middle plates and Neoprene gaskets. The bottom plate mates with the middle plate in order to rigidly clamp the piezoelectric disks. In Fig. 1(a), three actuators can be accommodated, but in this experiment the actuator was installed only in the central slot. In the present study, four thickness ($d = 3.18, 2.29, 1.59, \text{ and } 0.79 \text{ mm}$) and two size of jet slot ($l = 20.6 \text{ and } 19.8 \text{ mm}$) are used for comparison (shown in Fig. 1(b)).

The actuators were driven at two voltage amplitudes, $V_{app} = 600 \text{ V}$ and 800 V , with frequencies ranging from 1000 Hz to 2000 Hz . Note that we use each piezoelectric actuators in this study because of the damaged actuator. Each actuator has different properties. However, the individuality of each actuator was judged to be sufficiently small to compare.

Measurements of the velocity at the synthetic jet exit were performed with the synthetic jet actuator clamped in a rigid stand. A schematic of the experimental setup is shown in Fig. 2(a). A hot-wire probe was positioned as close as possible to the center of the slot using a traverse with very fine resolution and manual adjustment. Measurements were performed with the probe positioned at the center of the piezoelectric actuators (shown in Fig. 2(b)).

3. RESULTS

First of all, we investigate the influence of an input voltage amplitude V_{app} . The response of U_{ave} to sinusoidal excitation is shown in Fig. 3(a). We use two cases of $l = 19.8 \text{ mm}$ and $l = 20.6 \text{ mm}$. In both cases, it can be seen that U_{ave} takes a larger value as V_{app} is larger. However, it is found that the turbulence intensity, u_{rms}/U_{ave} , takes the similar value in

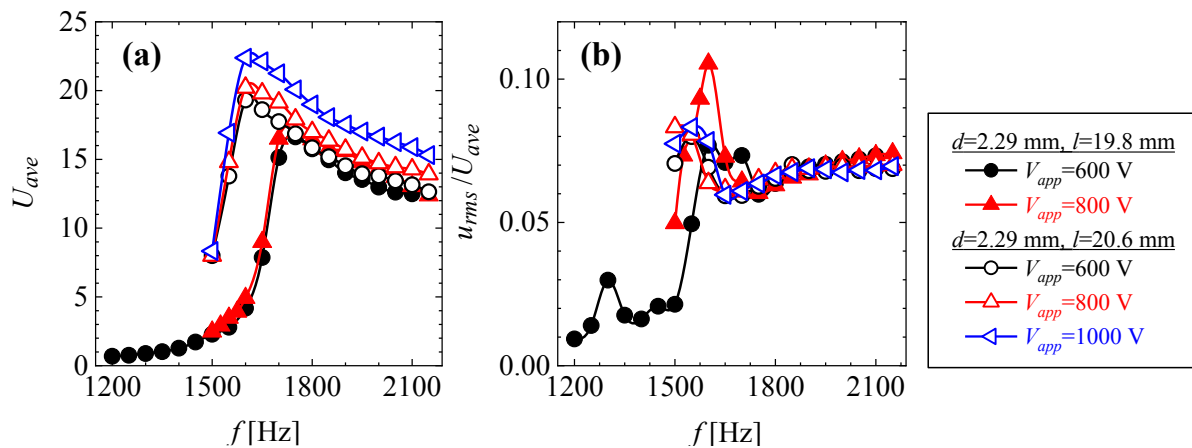


Fig. 3 Comparison of the input voltage amplitude. (a) U_{ave} (b) u_{rms}/U_{ave} .

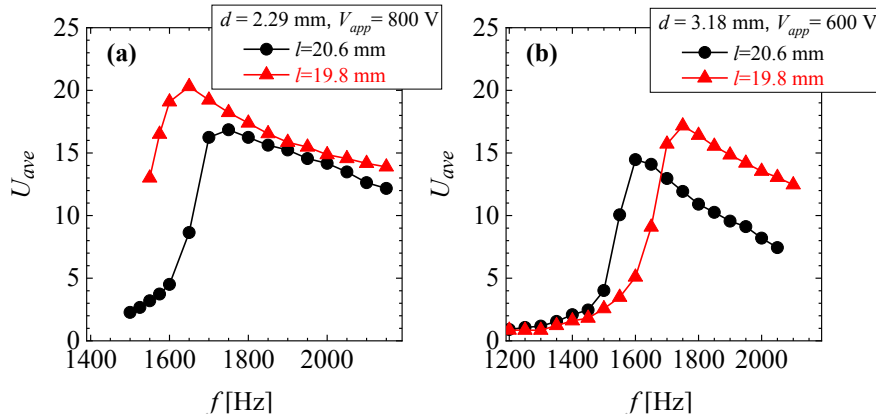


Fig. 4 Comparison of the size of the jet slot of the gasket. (a) $d=2.29$ mm, $V_{app}=800$ V (b) $d=3.18$ mm, $V_{app}=600$ V

all cases in the high frequency side than 1800 Hz (Fig. 3(b)). Also, u_{rms}/U_{ave} takes a constant value of $u_{rms}/U_{ave} = 0.07$ on the higher frequency side than 1800 Hz. From the results of Figs. 3, it is suggested that the difference in the magnitude of V_{app} affects the averaged velocity but does not affect the turbulence intensity.

The effect of the size of the jet slot of the gasket is shown in Figs. 4. The peak position of U_{ave} differs in each case. However, $l = 19.8$ mm has better response than $l = 20.6$ mm on higher frequency side. Therefore, it can be said that the case of $l = 19.8$ mm is better than $l = 20.6$ for investigating the characteristics. On the low-frequency side, in each case show completely different characteristics. Hence, it seems that the influence of individual gaskets is strongly received on the low-frequency side.

Finally, response characteristics due to the difference in thickness of the gasket, d , are shown in Fig. 5(a). In the case of $d = 0.79$ mm, it is understood that the response is most excellent at 1100 Hz. But, on the higher frequency side than 1500 Hz, it converges to low response value ($U_{ave}=3$). Conversely, the responsive in cases of $d = 2.29$ mm and 3.18

mm is high on the high-frequency side. The case of $d = 2.29$ mm is the most responsive on the higher frequency side than 1800 Hz. The turbulence intensity of these cases is shown in Fig. 5(b). When d is small ($d = 0.79$ mm and 1.59 mm), the turbulence intensity is not stable even on the high-frequency side. Cases of $d = 2.29$ mm and 3.18 mm take a constant value of $u_{rms}/U_{ave} = 0.7$ on the higher frequency side than 1800 Hz. This tendency was seen also in Fig. 3(b). From these results, it seems that the responsiveness on the high-frequency side stabilizes in the case of $d = 2.29$ mm and 3.18 mm.

4. CONCLUSIONS

We performed the investigation of the characteristics by changing the thickness and the size of the jet slot of the gasket by the experiment. First, we investigate the influence of input voltage amplitude and it is clarified that the input voltage amplitude magnitude affects the averaged velocity but does not affect the turbulence intensity. Good responsiveness is obtained when we use the gasket of the jet slot of $l = 19.8$ mm and the $d = 3.18$ mm and 2.29 mm of gasket thickness.

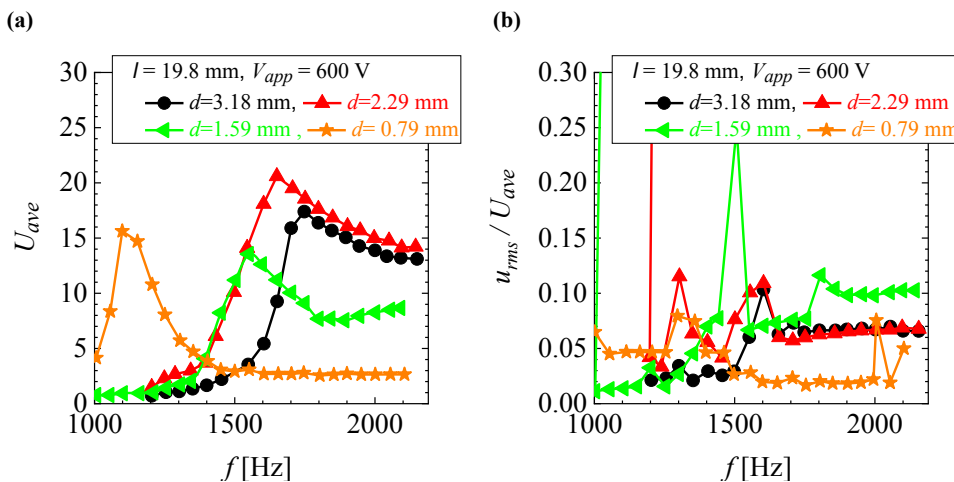


Fig. 5 Comparison of the thickness of the gasket. (a) U_{ave} (b) u_{rms}/U_{ave} .

ACKNOWLEDGEMENTS

I would like to thank my supervisor, Professor Philippe Lavoie, for providing this opportunity. Also I would like to thank my JUACP's supervisor, Professor Shaker A. Meguid who gave me various opportunities. Thank you for teaching the experiment by Mr. Cruikshank. I could have good times particularly through a discussion about how to use the experiment technics.

REFERENCES

- [1] R. Cruikshank, and P. Lavoie, Modulated High-Frequency Distributed Forcing of the Wake of a Blunt Trailing Edge Profiled Body, 2018 AIAA Aerospace Sciences Meeting, 16 pages (2018).
- [2] A. Naghib-Lahouti, H. Hangan, and P. Lavoie, Distributed forcing flow control in the wake of a blunt trailing edge profiled body using plasma actuators, *Physics of Fluids*, 27, 035110 (2015).
- [3] A. Naghib-Lahouti, P. Lavoie, and H. Hangan, Wake instabilities of a blunt trailing edge profiled body at intermediate Reynolds numbers, *Experiment in Fluids*, 55, 15 pages (2014).

ANALYTICAL AND NUMERICAL MODELING OF HIGH-TEMPERATURE PRESSURE TRANSDUCER

Shuichi Higaki

Department of Mechanical Systems Engineering, Graduate School of Engineering, Nagoya University
higaki.shuichi@g.mbox.nagoya-u.ac.jp

Supervisor: Pierre Sullivan

Department of Mechanical and Industrial Engineering, University of Toronto
sullivan@mie.utoronto.ca

ABSTRACT

The work aims to develop the transducer for high temperature and pressure. To do this, we made an analytical and a numerical model for the pressure transducer. In this paper, we report about the deriving procedure for analytical equation and the results of heat transfer model. This work is a continuation from the predecessor, and the predecessor simulated with the pressure transducer model not considering the fluid within the pressure transducer. Therefore, this time, we made the flow path and simulated heat transfer taking account fluid. The results show the temperature of the pressure transducer is raise 28.4K in probably case. Moreover, we considered fluid flow effect and we confirmed that the fluid flow homogenise the temperature of the pressure transducer. Finally, we noted what we have to do next.

1. INTRODUCTION

The purpose of the research is to design, manufacture and test high temperature and pressure transducers using MEMS and free of Mercury, oils, NaK, etc that can be used in melt applications. Typically, the sensing element is placed away from the process to avoid damage. The only part of the transducer that is in contact with the process is the membrane. The fill liquid is the responsible to transfer the pressure on to

the sensing element. The goal is to be able to measure temperatures up to 773.15K, and pressures up to 200 MPa.

An approach that has been explored by some researchers[1, 2] to help with the removal of force transfer medium is to use pushrods to transfer the strain from the diaphragm to the sensing element. In this approach, the force is applied by the pushrod. In this case, the push rod is responsible to transfer force only. In these cases, an SOI (Silicon on Insulator) sensor is used to measure pressure.

To do this, before we make the pressure transducer, we simulate the temperature of the pressure transducer using COMSOL Multiphysics™ (COMSOL). The predecessor made the 3D CAD model and simulated the heat transfer model. But that model only considered the solid component. In this paper, therefore, we present the model with the flow path and heat transfer results.

Moreover, to obtain more accurate results, we must consider the fluid flow within the transducer. When high pressure forces the pressure on the membrane, the membrane is vibrated by the pressure and, the flow in the flow path of the transducer is excited. To estimate the flow within the pressure transducer, we need an analytical model. Therefore, we derived LEM model for the pressure transducer and reported in this paper.

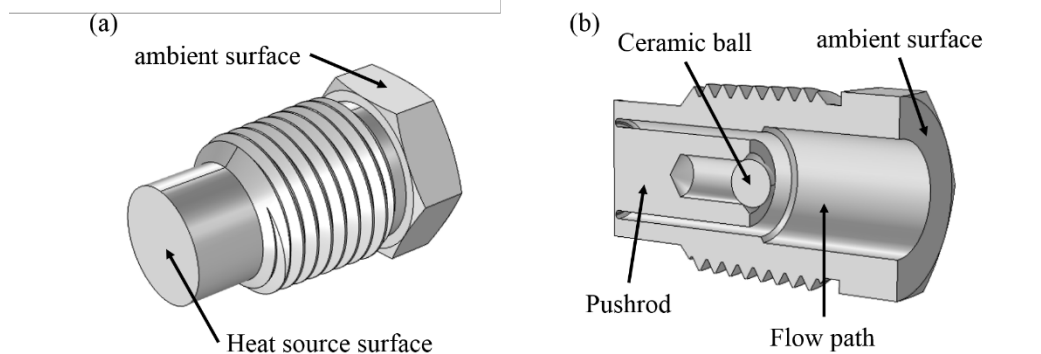


Fig. 1 the geometric pressure transducer model. (a) out line, (b) inside of transducer.

2. LUMPED ELEMENT METHODS

LEM models the behavior of a physical system through a finite number of components[3]. At present, the LEM model for synthetic jet actuator that has the similar structure with the pressure transducer is proposed[3, 4]. In order to create the LEM model for the pressure transducer, I considered the following three equations. First, the equation of motion of a one-degree-of-freedom forced-damped spring-mass system. Second, the equation of conservation of mass inside the cavity. Finally, the unsteady Bernoulli's equation between the cavity and just outside the cavity. The assumed model is shown in Fig. 1.

2.1 THE EQUATION OF MOTION OF A ONE-DEGREE-OF-FREEDOM FORCED-DAMPED SPRING-MASS SYSTEM

The equation is:

$$\ddot{x}_w + 2\zeta_w \omega_w \dot{x}_w + \omega_w^2 x_w = -\frac{p_i A_w}{m_{wt}} \quad (1)$$

where $x_w(t)$ is the membrane displacement at a generic time instant t , ζ_w is the actual damping ratio of the membrane, ω_w is natural frequency, p_i represents the cavity(internal) differential pressure, A_w is the diaphragm surface area and m_{wt} is the diaphragm total mass, including holder, SOI-chip, substrate and air added mass. Differentiating the equation respect to time, the following equation can be obtained.

$$\ddot{V}_w + 2\zeta_w \omega_w \dot{V}_w + \omega_w^2 V_w = -\frac{A_w}{m_{wt}} \frac{dp_i}{dt} \quad (2)$$

2.2 THE EQUATION OF CONSERVATION OF MASS

It is assumed that inside cavity pressure is uniform. The density of the bulk of the internal air can be expressed as follows:

$$\rho_i = \rho_a + \rho_i', \quad \rho_a \gg \rho_i'. \quad (3)$$

And the additional assumption that the magnitude of the volume variation due to the membrane motion is much smaller than cavity volume leads to the following equation.

$$V = V_c - A_w x_w, \quad V_c \gg A_w x_w \quad (4)$$

When this holds, application of the compressible form of the continuity equation to the air contained within yields,

$$\begin{aligned} \frac{dm_i}{dt} &= \frac{d(\rho_i V)}{dt} = \rho_i \frac{dV}{dt} + V \frac{d\rho_i}{dt} \\ &\approx \rho_a \frac{dV}{dt} + V_c \frac{d\rho_i}{dt} = -\rho_a A_w \dot{x}_w + V_c \frac{d\rho_i}{dt} \quad (5) \\ &= -\rho_a A_0 U \end{aligned}$$

where m_i is the mass of air in the cavity and U is the air velocity in the plane of orifice.

The bulk behavior can be considered isentropic compression/expansion. Therefore, the relation between density and pressure is as follow:

$$\frac{P_i}{\rho_i^\gamma} = \frac{P_a}{\rho_a^\gamma} \quad (6)$$

From this relation and above assumption, the differential of density is leaded as follow;

$$\begin{aligned} \frac{d\rho_i}{dt} &= \rho_a \frac{1}{P_a^\gamma} \frac{P_i^{1-\gamma}}{\gamma} \frac{dP_i}{dt} \\ &= \rho_a \left(\frac{P_i}{P_a} \right)^\gamma \frac{1}{\gamma P_i} \frac{dP_i}{dt} \approx \rho_a \frac{1}{\gamma P_a} \frac{dP_i}{dt} \quad (7) \end{aligned}$$

This result leads to the following mass conservation equation.

$$\frac{V_c}{\gamma P_a} \frac{dP_i}{dt} - A_w \dot{x}_w = -A_0 U \quad (8)$$

2.3 THE UNSTEADY BERNOULLI'S EQUATION

The Euler equation is

$$\frac{D\mathbf{v}}{Dt} = \frac{\partial \mathbf{v}}{\partial t} + (\mathbf{v} \cdot \nabla) \mathbf{v} = \mathbf{K} - \frac{1}{\rho} \nabla p \quad (9)$$

The second term, $(\mathbf{v} \cdot \nabla) \mathbf{v}$ can be rewritten as:

$$(\mathbf{v} \cdot \nabla) \mathbf{v} = \frac{1}{2} \nabla q^2 - \mathbf{v} \times \boldsymbol{\omega} \quad (10)$$

where $\boldsymbol{\omega} = \nabla \times \mathbf{v}$. Therefore, the equation can be expressed as

$$\frac{\partial \mathbf{v}}{\partial t} = \mathbf{K} - \frac{1}{\rho} \nabla p - \frac{1}{2} \nabla q^2 + \mathbf{v} \times \boldsymbol{\omega} \quad (11)$$

For no vortex flow, $\mathbf{v} = \nabla \phi$ can be assumed. Therefore, above equation becomes

$$\nabla \left(\frac{\partial \phi}{\partial t} + P + \frac{1}{2} q^2 \right) = \mathbf{K} \quad (12)$$

The external force can be expressed $\mathbf{K} = -\nabla F$ where F is the potential:

$$\nabla \left(\frac{\partial \phi}{\partial t} + P + \frac{1}{2} q^2 + F \right) = 0 \quad (13)$$

The left side is function of time only. Therefore unsteady Bernoulli's equation can be derived as follow:

$$\frac{\partial \phi}{\partial t} + P + \frac{1}{2} q^2 + F = f(t) \quad (14)$$

When the flow is unsteady, the velocity potential become function of time only. Thus ϕ can be rewritten $q(t)$ s using a length s .

$$\frac{\partial q}{\partial t} s + P + \frac{1}{2} q^2 + F = f(t) \quad (15)$$

When the equation (15) is applied to the region between inside cavity and just outside cavity, the following equation results

$$\dot{U} l_e + \frac{K}{2} |U|^2 + \frac{p_i + p_a}{\rho_a} = \frac{p_a}{\rho_a} \quad (16)$$

where l_e is the modified effective length of the orifice, K is the head loss coefficient. Differentiating equation (16) respect to time, the following equation can be obtained straightforwardly.

$$\ddot{U} l_e + K |U| \dot{U} + \frac{1}{\rho_a} \frac{dp_i}{dt} = 0 \quad (17)$$

Moreover, equation (8) is substituted in equation (17) and the following equation can be derived.

$$\ddot{U} + \frac{K}{l_e} |U| \dot{U} - \frac{\gamma p_a}{m_a V_c} U + \frac{\gamma p_a}{m_a V_c} \frac{A_w}{A_0} V = 0 \quad (18)$$

The LEM model for pressure transducer is constituted by equation (2), (8), (18) can be conveniently rewritten as

$$\begin{bmatrix} \ddot{V} \\ \ddot{U} \end{bmatrix} + \begin{bmatrix} 2\zeta_w \omega_w & 0 \\ 0 & \frac{K}{l_e} |U| \end{bmatrix} \begin{bmatrix} \dot{V} \\ \dot{U} \end{bmatrix} + \begin{bmatrix} \frac{1}{m_w} & 0 \\ 0 & \frac{1}{m_a} \end{bmatrix} \begin{bmatrix} \omega_w + \frac{\gamma p_a}{V_c} A_w^2 & -\frac{\gamma p_a}{V_c} A_0 A_w \\ -\frac{\gamma p_a}{V_c} A_0 A_w & \frac{\gamma p_a}{V_c} A_0^2 \end{bmatrix} \begin{bmatrix} V \\ U \end{bmatrix} = \begin{bmatrix} 0 \\ 0 \end{bmatrix} \quad (19)$$

3. SIMULATION SETUP

We use COMSOL for simulation. COMSOL can solve multiphysics simulation such as heat transfer via the fluid. I used the model shown in Fig. 1, and that was made by predecessor. The total length of the model is 2.54mm same as ordinarily industrial product, that aims to reduce cost. The model made by predecessor don't have flow path, therefore to simulate the fluid flow and heat transfer via the fluid within the pressure transducer, I made the flow path using detach function installed in COMSOL.

The simulation using COMSOL conduct with appropriately chosen physics. This time we considered only stationary condition. In this simulation, I chose "Heat Transfer in Solid" for the solid components, "Heat Transfer in Fluid" for the fluid components, and "Nonisothermal Flow" for Multiphysics simulation. The mesh is chosen "Finer" and "Physics-controlled mesh". The heat is transferred from the heat source surface to the ambient surface (Fig. 1(a)). The other surfaces have no heat transfer because we can assume no temperature difference between surroundings in practical condition. The heat source temperature is determined 773.15K and the ambient temperature is determined 303.15K. The heat transfer coefficients of the surface that contact with the heat source is named h_1 and the heat transfer coefficients of the surface that contact with ambient is named h_2 . We set three simulation case that heat transfer coefficient is as a parameter. In order to compare the simulation results of the predecessor, we use the previous condition. Each case is named probable case (case P), worse case (case W), ideal case (case I). These conditions are shown in Table 1. The material of the ball is assumed ceramic. The other components are assumed Steel AISI 4340.

Table 1. Simulation condition

	Case P	Case W	Case I
h_1 [W/m ²]	10	20	10
h_2 [W/m ²]	20	20	50

Table 2. Material properties

	Ceramic	AISI 4340
Heat capacity C_p [J/(kg·K)]	420	475
Thermal conductivity k [W/(m·K)]	2.7	44.5
Density ρ [kg/m ³]	5900	7850

4. RESULTS

First, I compared the result of the simulation with the flow, with fluid and without fluid. The case without fluid is conducted by predecessor. Fig 4 shows the temperature that is top of ceramic ball. Due to it contacts with SOI-chip in practical case, the temperature is important. The temperatures are rise with adding fluid. The temperature differences are 28.4K in case P, 50.K in case W and 7.84K in case I. In the previous model, inside temperature is fixed at a constant temperature (308.15K). Hence, solid components are chilled by the fluid. Due to that, when we consider fluid temperature within pressure transducer, the fluid temperature is changed by heated solid components. The more decrease the heat transfer coefficient differences ($h_1 - h_2$), the more increase the temperature of the ceramic ball. The relation has negative correlation (Fig. 3). Using this correlation, we can estimate the heat transfer coefficient when we conduct experiments and the results will contribute to improve simulation accuracy.

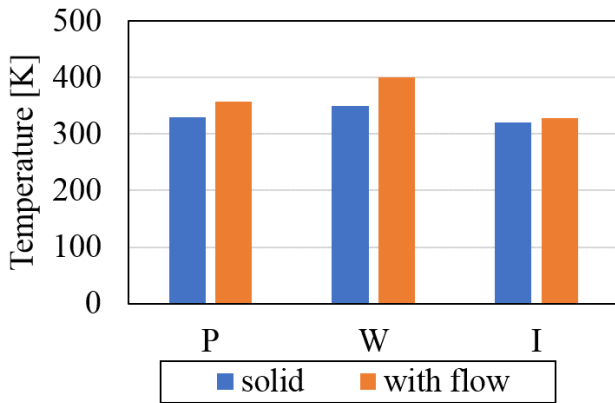


Fig. 2 The temperature of the top of ceramic ball

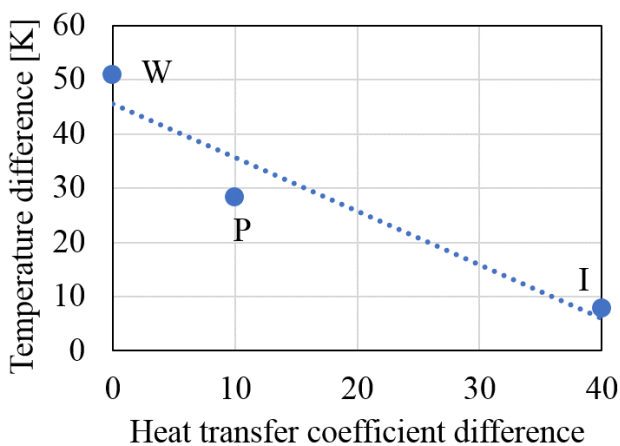


Fig. 3 The relation of between temperature difference and heat transfer coefficient difference

We investigated the effect of temperature homogenization with fluid flow. To do this, we compared the temperature of heat source surface and of the top of the

ceramic ball. The difference temperatures are shown in Fig. 4. In case W, the temperature difference is decreased 1.56K when the fluid flow is considered. other cases are confirmed also a decrease the temperature difference. It means that the heat from heat source became easy to be transported by the fluid. On the other hand, we have to focus that the temperature differences are small whether there is fluid or not. It means the structure and chosen material at each component does not work well and, we might have to improve the geometry.

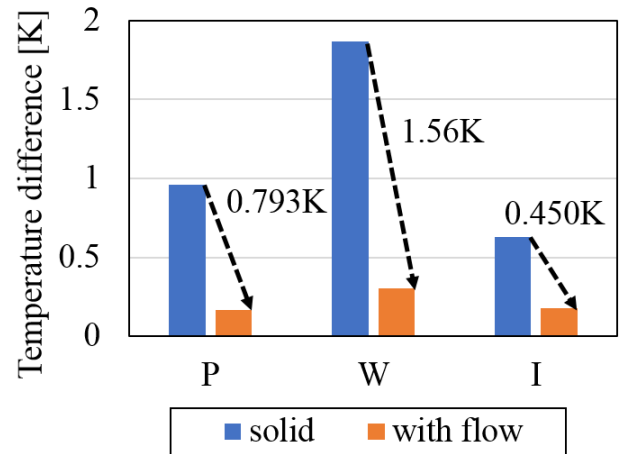


Fig. 4 The temperature difference between the heat source surface and the top of the ceramic ball

5. CONCLUSIONS

We led the LEM model for a pressure transducer. It can evaluate the flow within the pressure transducer. As previous stage to be that we can compare the predictions of the LEM model and the results of simulate, we made a numerical model using COMSOL to simulate heat transfer and flow caused by heat. According to using that, we obtain more realistic results of the temperature inside the pressure transducer. The results show that due to the heat is transported by the fluid from the heat source surface to other components, the ceramic ball temperature becomes almost the same temperature as the heat source surface. This result suggests that geometrical improvement is needed. In order to obtain more accurate results, the next step we have to do is to consider a membrane vibration. The vibration causes the flow within the pressure transducer. Hence, the temperature might be changed by the fluid flow. And then we will compare the results of the simulation with the prediction of the LEM model.

ACKNOWLEDGEMENTS

I appreciate my supervisor, Professor Pierre Sullivan to give me opportunity working in University of Toronto. Also, I appreciate Professor Shaker A. Meguid and Valerie Meguid who greatly supported me. Finally, I appreciate everyone in

the turbulence research laboratory who gave me various advice and helped life in laboratory.

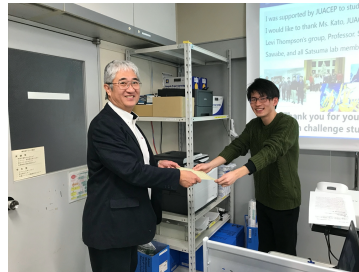
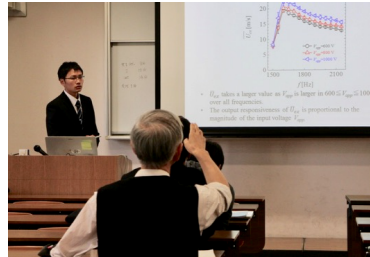
REFERENCES

- [1] Ngo H.-D., Mukhopadhyay B., Ehrmann O., Lang K.-D., Advanced Liquide-Free, Piezoresistive, SOI-Based Pressure Sensor for Measurements in Harsh Environments, *Sensors*, 15, 20305-20315 (2015).
- [2] Guo, Z., Lu, C., Wang, Y., Liu, D., Huang, M., and Li, X., Research of a Novel Ultra-High Pressure Sensor with High-Temperature Resistance, *Micromachine*, 9, 5 (2018).
- [3] Chiatto M., Capuano F., Coppola G., de Luca L., LEM Characterization of Synthetic Jet Actuators Driven by Piezoelectric Element: A Review, *Sensors*, 17, 1216 (2017).
- [4] Lin F., Ramkumar M. P. S. R. S. B., Modeling Acoustic/Structural Interaction of Synthetic Jet Actuators, *Journal of Vibration and Control*, 16(9), 1393-1414 (2010).

<3> Research Presentations

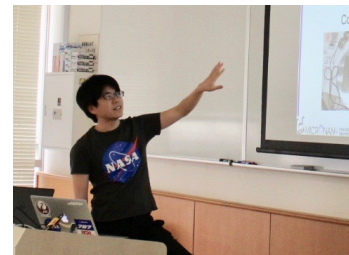
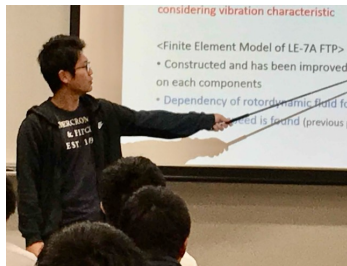
● For 2018 Short-term course ...54

Three presentations took place at the 23rd JUACEP Workshop at Lecture room 222 on October 9, 2018, and the other one did at his group seminar on January 22, 2019.



● For 2018 Medium- and Long-term course ...67

Five presentations took place at the 24th JUACEP Workshop at Lecture room IB 013 on March 28, 2019, and the other two did on February 19 and on October 8, 2019 respectively.





The 23rd JUACEP Workshop for 2018 short-term course students

Date: Tuesday, October 9, 2018
Venue: Lecture room 222, Eng-Bldg. 2

[Timetable]

- | | | |
|-------------|---|---------|
| 13:00 | Opening address: Prof. Ju, JUACEP Leader | |
| 13:05-13:20 | Shuichi Higaki , mentored by Prof. Pierre Sullivan,
<i>University of Toronto</i> | ...P.55 |
| | “Analytical and Numerical Modeling of High-Temperature Pressure Transducer” | |
| 13:20-13:35 | Kotaro Takamure , mentored by Prof. Philippe Lavoie,
<i>University of Toronto</i> | ...P.58 |
| | “Synthetic jet characterization for differences in nozzle size and thickness of gasket” | |
| 13:35-13:50 | Motoki Yamada , mentored by Prof. Richard Laine,
<i>University of Michigan</i> | ...P.61 |
| | “Synthesis of MZPFe nanopowders to thin films as solid electrolytes by Liquid-Feed Flame Spray Pyrolysis” | |
| 13:50-14:00 | Completion Ceremony | |

Date: Tuesday, January 22, 2019
Venue: Satsuma Laboratory, Eng-Bldg. 1

- | | | |
|-------------|--|---------|
| 11:00-11:15 | Keiichi Okubo , mentored by Prof. Levi Thompson,
<i>University of Michigan</i> | ...P.64 |
| | “Synthesis of Mo ₂ C Supported Metal Catalysts” | |

*10-minute presentation + 4-minute Q&A each

Analytical and Numerical Modeling of High-Temperature Pressure Transducer



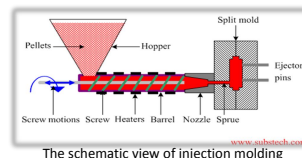
October 9th, 2018

Department of Mechanical Systems Engineering
Nagoya University
Shuichi HIGAKI

Mechanical and Industrial Engineering
University of Toronto
Professor Pierre Sullivan

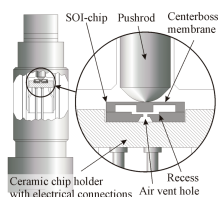
Introduction 1

- The high-temperature pressure transducer is needed for a various industrial scenes, for example, injection molding.
- Now, the liquid filled pressure transducer is used for high-temperature but the liquids, mercury, oils and etc., used for the transducer are problems in the view of environmental.



Introduction 2

- Some researchers proposed liquid-free transducer for high-temperature^{[1][2]}.
- The new concept for the pressure transducer is that the sensor is placed apart from heat source using pushrod.

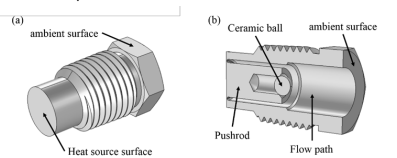


The schematic view of new concept pressure transducer^[1]

[1] Ngo H.-D., et al., Advanced Liquid-Free, Piezoresistive, SOI-Based Pressure Sensor for Measurements in Harsh Environments, Sensors, 15, 20305-20315 (2015).
[2] Guo Z., et al., Research of a Novel Ultra-High Pressure Sensor with High-Temperature Resistance, Micromachines, 9, 5 (2018).

Proposed design 3

- We propose a new shape liquid-free pressure transducer.
- The most important feature of our concept is using a ceramic ball as a component to push sensor.
 - Using a ceramic ball, the heat transferred the sensor is reduced because of the low heat conductivity.
 - The area touching the sensor is reduced because the component touching the sensor is a sphere.



Proposed design of pressure transducer

Previous work 4

- The predecessor made 3D CAD model of the pressure transducer.
- The heat transfer model without fluid is simulated.

➡ We need the heat transfer model **WITH** fluid and, we have to consider the flow within pressure transducer.

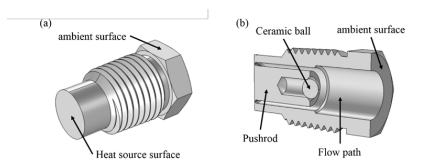


Fig. 3 Proposed design of pressure transducer

Purposes & Works 5

- Derive the equation expressing the flow within the pressure transducer.
 - A model equation named LEM equation is considered.
- Simulate the heat transfer model **WITH** fluid.
 - To compare the results of the temperature of top of the ceramic ball.

Deriving the equation 6

- Derive the equation expressing the flow within the pressure transducer.



Lumped Element Models (LEM) equation models the behavior of a physical system through a finite number of components.

- the equation of motion of a one-degree-of-freedom forced-damped spring-mass system
- the equation of conservation of mass inside the cavity
- the unsteady Bernoulli's equation between the cavity and just outside the cavity.

The equation of motion of a one-degree-of-freedom forced-damped spring-mass system 7

$$x_w'' + 2\zeta_w \omega_w x_w' + \omega_w x_w = -\frac{p_i A_w}{m_{wt}}$$

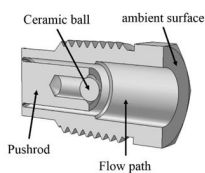
ζ_w : damping ratio
 ω_w : natural frequency
 A_w : membrane surface area
 p_i : fluctuating pressure

differentiate

$$\dot{V}_w + 2\zeta_w \omega_w \dot{V}_w + \omega_w V_w = -\frac{A_w}{m_{wt}} \frac{dp_i}{dt}$$

The equation of conservation of mass inside the cavity 8

- Assumption
 - Inside cavity pressure is uniform.
 - Fluctuating pressure is enough lower than ambient pressure.
 - The volume variation is much smaller than cavity volume.
 - The bulk behavior is isentropic compression/expansion.



$$\frac{V_c}{\gamma p_a} \frac{dp_i}{dt} - A_w x_w' = -A_0 U$$

V_c : cavity volume
 γ : heat capacity ratio
 p_a : ambient pressure
 A_0 : outlet area

Unsteady Bernoulli's equation 9

From Euler equation

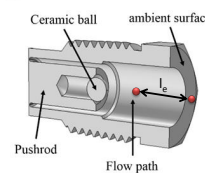
$$\frac{Dv}{Dt} = \frac{\partial v}{\partial t} + (v \cdot \nabla)v = K - \frac{1}{\rho} \nabla p$$

We can obtain unsteady Bernoulli's equation

$$\frac{\partial q}{\partial t} s + P + \frac{1}{2} q^2 + F = f(t)$$

Applying this equation to the region inside cavity and just outside cavity

$$\ddot{U} + \frac{K}{l_e} |U| \dot{U} - \frac{1}{\rho_a} \frac{dp_i}{dt} = 0$$

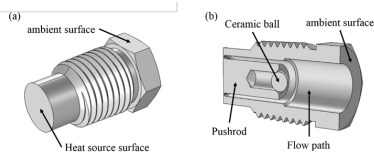


LEM equation 10

From these three equations, we can obtain following equation

$$\begin{bmatrix} \ddot{U} \\ \dot{U} \end{bmatrix} + \begin{bmatrix} 2\zeta_w \omega_w & 0 \\ 0 & \frac{K}{l_e} |U| \end{bmatrix} \begin{bmatrix} \dot{U} \\ U \end{bmatrix} + \begin{bmatrix} 1 \\ 0 \end{bmatrix} \frac{1}{m_{wt}} \begin{bmatrix} \omega_w + \frac{\gamma p_a}{V_c} A_w^2 & -\frac{\gamma p_a}{V_c} A_w A_0 \\ -\frac{\gamma p_a}{V_c} A_w A_0 & \frac{\gamma p_a}{V_c} A_0^2 \end{bmatrix} \begin{bmatrix} U \\ \dot{U} \end{bmatrix} = \begin{bmatrix} 0 \\ 0 \end{bmatrix}$$

➔ We can estimate the flow within the pressure transducer.



Simulation 11

- Simulate the heat transfer model **WITH** fluid.



COMSOL Multiphysics™ is used for simulation.

- The general purpose physics simulation software based on finite element method
- It can simulate multiphysics problem.

Simulation 12

- Simulate the heat transfer model **WITH** fluid.

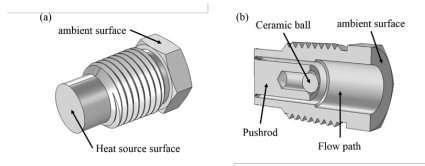


- The predecessor made 3D CAD model but it doesn't contain fluid.
- I made a flow path and conducted simulation with fluids.
- Finally, I compared the result between “only solid” and “with fluid”.

Simulation setup 13

- Model definition

Outer length	25.4 mm
Heat source surface diameter	10.4 mm
Ambient surface diagonal length	16.5 mm
Pushrod diameter	6.35 mm
Ceramic ball diameter	3.5 mm



Simulation setup 14

- Material property

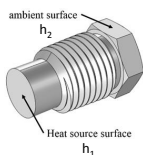
	Ceramic	AISI 4340
Heat capacity C_p [J/(kg·K)]	420	475
Thermal conductivity k [W/(m·K)]	2.7	44.5
Density ρ [kg/m ³]	5900	7850

- Heat transfer coefficient

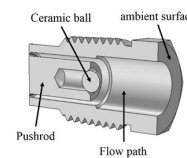
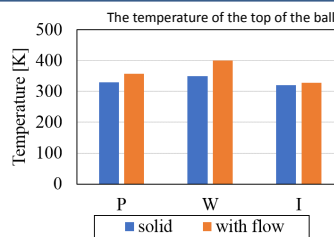
	Case P	Case W	Case I
h_1 [W/m ²]	10	20	10
h_2 [W/m ²]	20	20	50

- Environment temperature

Heat source temperature	773.15 [K]
Ambient temperature	303.15 [K]

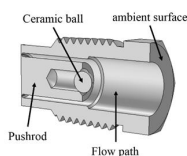
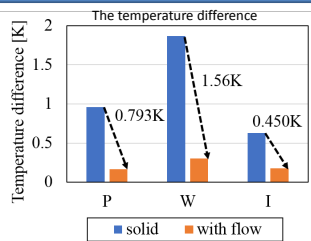


Results 15



- The temperature of the top of the ball is increased when we consider the fluid.
- The difference between “only solid” and “with fluid” is maximum at case W and minimum at case I.

Results 16



- Considering fluid, the difference between heat source surface and the top of the ball is decreased.
- It is not possible to separate sensor from heat source.

Conclusion & Future work 17

Conclusion

- We derived LEM equation for the pressure transducer.
- We simulated the heat transfer model for the pressure transducer with fluid and, we confirmed temperature increasing at the top of the ball.

Future work

- We have to make membrane vibrating model.
- We might reconsider the shape of the pressure transducer to separate from heat source.
- Calculate the flow within the pressure transducer using LEM equation and, compare it with simulation and experimental result.

Synthetic Jet Characterization for Differences in Nozzle Size and Thickness of gasket



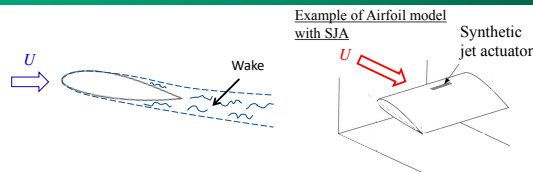
Kotaro Takamura
 Department of Mechanical Science and Engineering, Nagoya University

Prof. Philippe Lavoie
 Institute for Aerospace Studies, University of Toronto



Lecture room 222, Eng-Bldg. 2
 09/10/2018

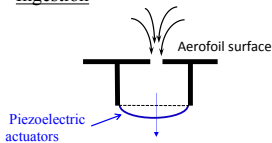
Background 1



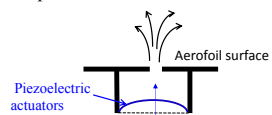
- Many researches about **wake** behind an airfoil have been done.
- The control of a wake is important because of their significant effect on the aerodynamic forces and mixing in engineering applications.
- **Synthetic jet actuator (SJA)** is often used to control the wake.
- SJA is extremely compact and can be easily implemented in wind tunnel models.

Background (Explain about SJA) 2

Ingestion



Expulsion



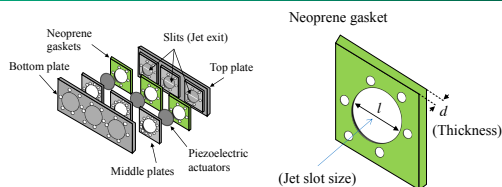
- Jet is generated by the vibration of the piezoelectric actuators
- When the piezoelectric actuators are distorted outward, the flow is ingestion, and when distorted inward, the flow is expulsion.
- The actuator can be designed such that no parasitic drag is introduced and, at the bare minimum, the control can be switched from on to off.

Purpose 3

- The characteristics of SJA vary with its elements and shape of it.
- The characteristics of the jet were investigated by changing the thickness and jet slot size of the gasket and changing the input voltage of SJA.

The purpose is to clarify the optimum condition such as the size of the gasket and input voltage amplitude.

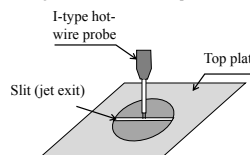
Synthetic Jet Actuator (SJA) 4



Condition of the SJA	
Thickness (d)	0.79, 1.59, 2.29, 3.18 [mm]
Jet slot size (l)	19.8, 20.6 [mm]
Voltage amplitude by function generator (V_{app})	200-1500 [V]
Modulated frequency of SJA (f)	1000-2000 [Hz]

Measurement of the velocity 5

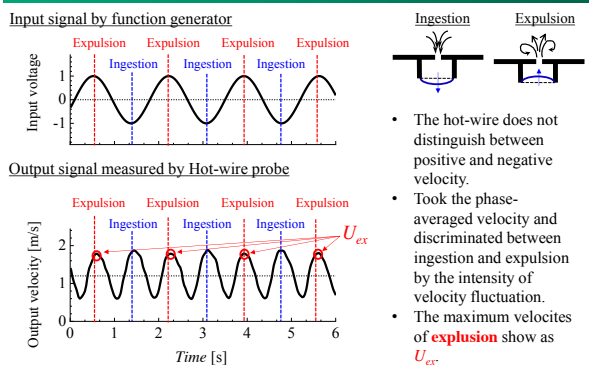
Arrangement of the hot-wire probe



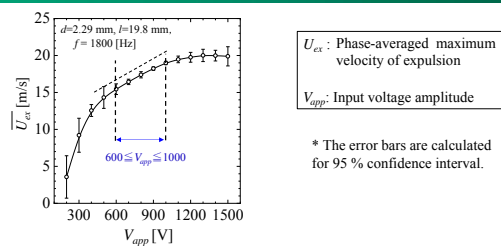
Condition of the hot-wire anemometer and probe	
Sampling number	262144
Sampling frequency	5 kHz
Thickness of the Tungsten wire	5 μ m
Sensing length	1 mm

- The measurements are accomplished using constant temperature hot-wire anemometer.
- A hot-wire probe is positioned where amplitudes of velocities between the ingestion and expulsion of jet are equal.

Input and Output Signals 6

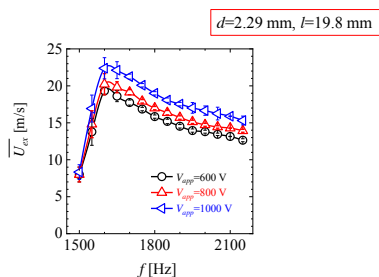


Comparison of the input voltage amplitude 7



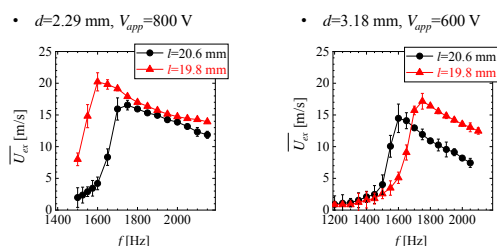
- If the flow of jet is correctly responding for the input signal, V_{app} should be in proportion to \bar{U}_{ex} .
- \bar{U}_{ex} increases linearly with V_{app} in $600 \leq V_{app} \leq 1000$ [V].
→ Good responsiveness!!
- Examine the frequency response characteristics in this input voltage.

Comparison of the input voltage amplitude 8



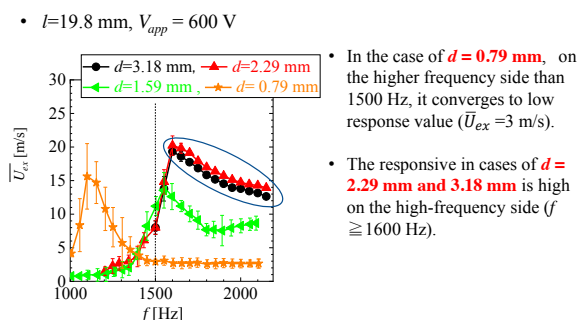
- \bar{U}_{ex} takes a larger value as V_{app} is larger in $600 \leq V_{app} \leq 1000$ over all frequencies.
- The output responsiveness of \bar{U}_{ex} is proportional to the magnitude of the input voltage V_{app} .

Comparison of the jet slot size of the gasket 9



We focused on the high frequency side ($f > 1500$) because the high-frequency forcing is often used to control the wake.
 $l = 19.8$ mm has better response than $l = 20.6$ mm on higher frequency side.
 (Same tendency was also confirmed in the another d and V_{app} .)

Comparison of the thickness of the gasket. 10



Conclusion 11

We performed the investigation of the characteristics by changing the thickness and the size of the jet slot of the gasket by the experiment.

The output responsiveness \bar{U}_{ex} is proportional to the magnitude of the input voltage V_{app} in $600 \leq V_{app} \leq 1000$.

Good responsiveness is obtained in high-frequency side ($f > 1600$ Hz) when we use the gasket of the jet slot of $l = 19.8$ mm and $d = 3.18$ mm and 2.29 mm of the gasket thickness.

ACKNOWLEDGEMENTS

I would like to thank my supervisor, Professor Philippe Lavote, for providing this opportunity. Also I would like to thank my JUACEP's supervisor, Professor Shaker A. Meguid who gave me various opportunities. Thank you for teaching the experiment by Mr. Cruikshank. I could have good times particularly through a discussion about how to use the experiment technics.

Thank you for your attention.

Synthesis of MZPFe nanopowders to thin films as solid electrolytes by Liquid-Feed Flame Spray Pyrolysis

Motoki Yamada
Goto Laboratory, Dept. Materials Science and Process Engineering,
Nagoya University

Eleni Temeche
Richard Laine Group, Dept. of Materials Science Engineering
University of Michigan

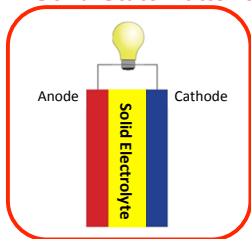
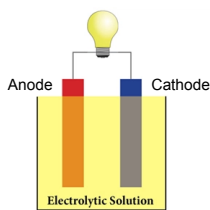
Outline

- Introduction
- Research Purpose
- Experimental
- Results & Discussion
- Conclusion

1

Introduction – Solid electrolyte -

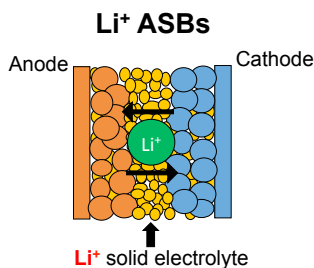
Conventional Batteries All-Solid-State Batteries



Merits of ASBs (All-Solid-State Batteries)

- High safety
- Flexible in design
- Wide operating temperature range

Introduction – Li⁺ ASBs -



Lithium
Most widely implemented metal for batteries

- High voltage
- High energy density

Problem
Low accessibility
↪ High cost

✓ Demand for development of non-lithium ASBs

Introduction – Mg²⁺ conducting electrolyte -

Magnesium ion based ASBs

Why Magnesium ??



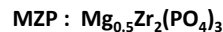
- High natural abundance (10⁴ times that of Li)
- High volumetric capacity (1.8 times that of Li)
- Higher atmospheric stability and melting point than Li

But..

Development of Mg²⁺ solid electrolyte

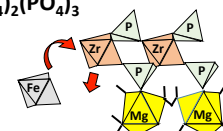
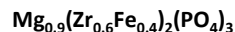
➔ So difficult .. Limited reports about Mg²⁺ ASBs

Introduction – MZP thin films -



One of limited reports about Mg²⁺-conducting solid electrolytes.

✓ To improve the performance of MZP, partially Fe³⁺ substitution for Zr⁴⁺ is expected



Research Purpose

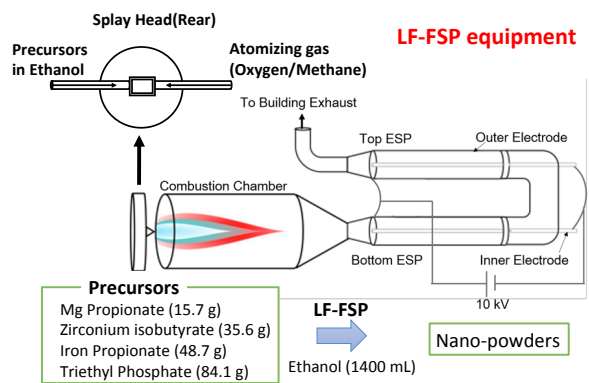
To develop conductive MZP thin films from nano-powders

Experimental – Procedure Flow -

Flow

- To synthesize nano-powders via Liquid Feed- Frame Spray Pyrolysis (LF-FSP)
- To make suspension (Liquid-state sample)
- To fabricate thin films by casting the suspension
- To sinter thin films by furnace heating
- To analyze sintered films (SEM, XRD, EDX)

Experimental – Nano-Powders Synthesis

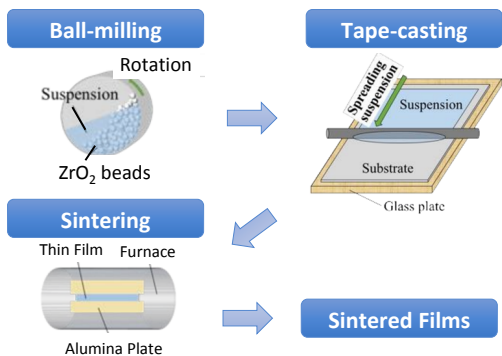


Experimental – Suspension Process -

Tab. Compositions of Suspension

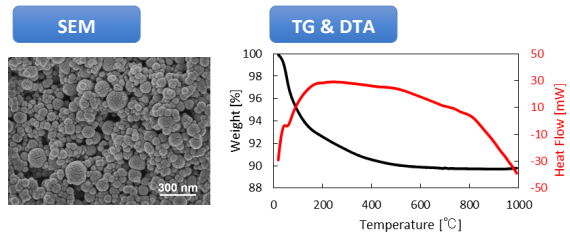
Components	Roles	Wt. g	Wt. %	Vol. %
Nano-powders	Powder	1.00	32	10
Polyvinyl butyral (PVB)	Binder	0.10	3	4
Benzyl butyl Phthalate(BBP)	Plasticizer	0.10	3	4
Acetone	Solvent	0.95	31	41
Ethanol	Solvent	0.95	31	41

Experimental – Film Processing -



Results & Discussion – NanoPowder -

As-produced nanopowder

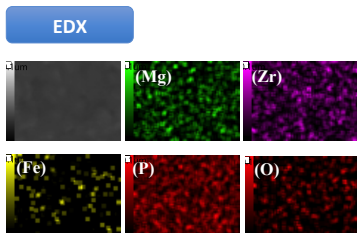


Results & Discussion – Sintered Film

Sintering Schedule: 750 °C/3h/air

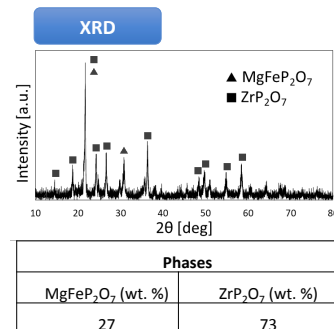
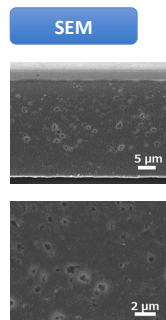


Thickness = 50 μm



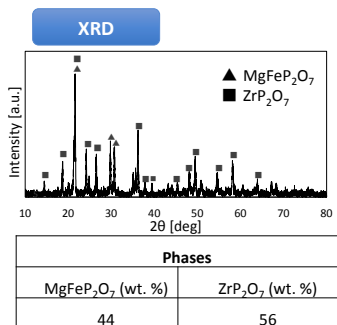
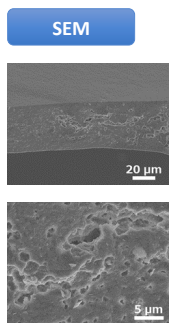
Results & Discussion -Films Morphology

Sintering Schedule: 750 °C/3h/air



Results & Discussion -Films Morphology

Sintering Schedule: 900 °C/3h/air



Conclusion

- ✓ MZP phase could not be seen in sintered films.
- ✓ Therefore, ionic conductivity could not be measured in this time.

Acknowledgement

This work was supported by Japan-US Advanced Collaborative Education Program. I would like to thank all office workers for processing my studying abroad.

Thank you for your attention 😊



 2019/01/22

SYNTHESIS OF MO_2C SUPPORTED METAL CATALYSTS

Keiichi Okubo
 Graduate School of Engineering, Nagoya University
 Chemical Engineering, Michigan University


Study abroad
2 / 17


 13 h



 Michigan University is located close to Detroit

Study abroad process


1. Find an **organization** that will fund you (if you need)
2. Find a **teacher** who will accept you
3. Do some **procedures** (Admission procedure, VISA)

You **Can** Go to Study Abroad

https://www.google.co.jp/maps/


What is JUACEP ?
3 / 17

JUACEP: Japan-**US-Canada** Advanced Collaborative Education Program


 I was supported by JUACEP to study in U.S.

Japan-US Advanced Collaborative Education Program
 Nagoya University, JAPAN

http://www.juacep.engg.nagoya-u.ac.jp/

JUACEP is an international student exchange program for graduate students at Nagoya University, University of Michigan, and UCLA and University of Toronto.

The primary purpose is to have the students gain research experience, knowledge, and skills at the visiting university, but we also expect them to be driven, flexible, cooperative, and tough in multi-cultural environment.


Money to study abroad
4 / 17

Studying abroad for people who have little money. (In my case)

INCOME = Scholarship

- 88,000 yen/month
- **80,000 yen/month via JUACEP**

Total **168,000 yen/month**

EXPENDITURE

- Rental fee for a house 600 dollars/month
- School insurance fee 170 dollars/month
- Visa application fee 400 dollars
- Airfare 1,510 dollars

Total 1,725 dollars/month = **190,000 yen/month**

You just need more **22,000 yen/month**


Michigan University
5 / 17

All school buildings are made of bricks




The University of Michigan is one of the most **historic, top-level** public high schools in the United States

University of Michigan is ranked **20th** in world university ranking (Tokyo University is ranked 42th)

It is the building which I used.





Introduction
6 / 17

Molybdenum carbides has been reported to be a useful catalysts for ammonia synthesis. It was said that the activity of ammonia synthesis depended on the crystal structure of molybdenum carbides.

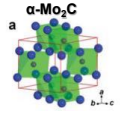
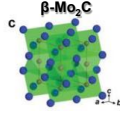



Fig. 1 Schematic of crystalline structure of $\alpha\text{-Mo}_2\text{C}$ and $\beta\text{-Mo}_2\text{C}$. (a, c) Unit cells of $\alpha\text{-Mo}_2\text{C}$ (a) and $\beta\text{-Mo}_2\text{C}$ (c).

Chai, J. F.; Zou, Q.; Song, W. Q. Adv. Mater. Res. 2013, 774-776, 1038.

Our project

Goal: To develop a high activity catalyst for ammonia synthesis.

Motivation: To investigate the unique properties of $\alpha\text{-Mo}_2\text{C}$ and $\beta\text{-Mo}_2\text{C}$.

Motivation: To improve the activity for ammonia synthesis by metal loading.

Purpose I was in charge of a part of a big project 7 /17

To prepare Mo₂C supported metal catalysts

Material synthesis → To elucidate the cause of high performance of Mo₂C → practical use for ammonia synthesis

My research theme: First step of a big project

- Synthesis of Mo₂C which has both α-phase and β-phase.
- Synthesis of M/Mo₂C (M: Co, Ni, Ru)

Step1

HSA-Mo₂C (High Surface Area)

→

Step2

Metal/Mo₂C

Metal: Co, Ni, Ru

Experiment Schedule for 2 months 8 /17

Schedule

11/5 ————— 12/21

Experiment practice (2 weeks) ← Experiment (5 weeks) →

- Synthesis of 3 materials × 3 = 9 samples
- 1 sample needs 3 days
 - Synthesis of Mo₂C
 - Metal loading
 - Reduction of the material

Typical Day

7AM	8AM	9AM		6PM	7PM
Get up	To school by bus	Start experiment		Finish experiment	Go home

Mo₂C preparation method 9 /17

Temperature programmed reaction technique

(NH₄)₆Mo₇O₂₄•4H₂O $\xrightarrow{\text{CH}_4/\text{H}_2 \text{ flow}}$ HSA-Mo₂C

Mo₂C preparation method 10 /17

(NH₄)₆Mo₇O₂₄•4H₂O (Sieved to 60-120 μm, Purchased by Alfa Aesar)

H₂ flow, 623 K, 12 h → CH₄/H₂ flow, 863 K, 2 h → Condition A → HSA-Mo₂C

(NH₄)₆Mo₇O₂₄•4H₂O $\xrightarrow{\text{CH}_4/\text{H}_2 \text{ flow}}$ HSA-Mo₂C

3 experimental conditions were tried. (Next slide)

Experiment Condition 11 /17

3 experimental conditions

Condition (Step)	Gas	T _{initial}	T _{final}	t _{temp}	t _{soak}	
A	A(1)	(H ₂)	298 K	623 K	70 min	12 hrs
	A(2)	(CH ₄ /H ₂)	623 K	863 K	90 min	2 hrs
B	B(1)	(H ₂)	373 K	623 K	70 min	12 hrs
	B(2)	(CH ₄ /H ₂)	623 K	863 K	90 min	2 hrs
C	The same program as condition B					
	Another reactor contaminated by slight oxygen					

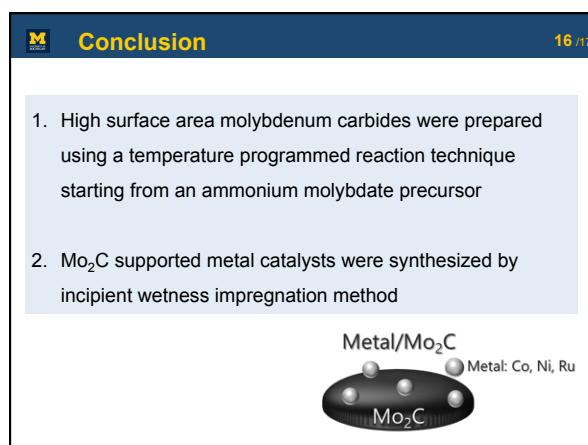
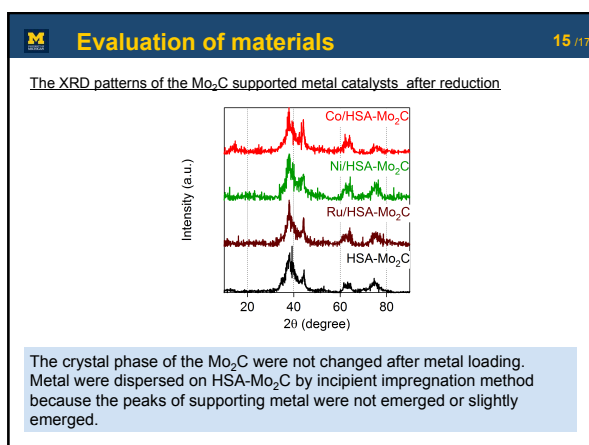
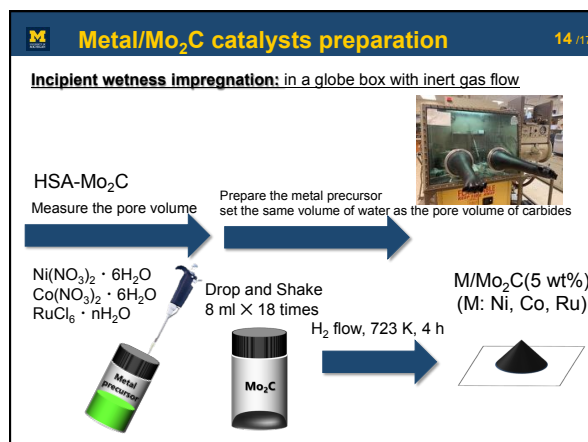
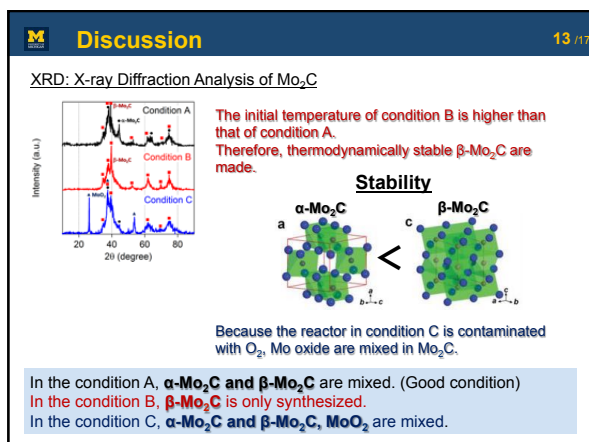
Evaluation of materials 12 /17

XRD: X-ray Diffraction Analysis of Mo₂C

In the condition A, α-Mo₂C and β-Mo₂C are mixed. (Good condition)

In the condition B, β-Mo₂C is only synthesized.

In the condition C, α-Mo₂C and β-Mo₂C, MoO₃ are mixed.



Acknowledgement 17 /17

I was supported by JUACEP to study abroad.
 I would like to thank Ms. Kato, JUACEP members,
 Levi Thompson's group, Professor. Satsuma, Senior Lecturer.
 Sawabe, and all Satsuma lab members.

**Thank you for your attention.
 You can challenge studying abroad.**

The 24th JUACEP Students Workshop

Research presentations and discussions of JUACEP
2018 medium/long-term course participants

Date... Thursday, March 28, 2019

Venue... IB 013

Timetable

*10 minute-presentation + 4 minute-Q&A for each

Time	Name Adviser at NU	Presentation title	Adviser at US/Canada
13:25	Opening address		
13:30	Takahiko Kosegaki Prof. Kazuo Shiokawa <i>Electrical Engineering</i>	Thermal Testing of the New Small Magnetic Sensor for SmallSAT ...P.68	Prof. Mark Moldwin <i>Climate and Space Science and Engineering, Univ. Mich.</i>
13:45	Yuta Ujiie Prof. Koji Nagata <i>Aerospace Engineering</i>	The New Directly Shear Stress Sensor for Aerodynamics Applications ...Undisclosed	Prof. Chang-Jin Kim <i>Mechanical and Aerospace Engineering, UCLA</i>
14:00	Ryo Tsunoda Prof. Takeo Matsumoto <i>Mechanical Systems Engineering</i>	A Computational Study of Cell Growth and Division as an Energy-Based Soft Packing Problem Using a Diffuse Interface Framework ...P.70	Prof. Krishna Garikipati <i>Mechanical Engineering, Univ. Mich.</i>
14:15	Koki Hojo Prof. Noritsugu Umehara <i>Miro-Nano Mechanical Science and Engineering</i>	Reactive Dc Magnetron Sputtering of MoS ₂ and MoS ₂ /hBN Layers ...Undisclosed	Prof. Suneel Kodambaka <i>Materials Science and Engineering, UCLA</i>
14:30	Kotaro Hotta Prof. Jiro Kasahara <i>Aerospace Engineering</i>	Experimental Investigation of Primary Breakup Induced by High Mach Number Shock Wave ...P.73	Prof. Mirko Gamba <i>Aerospace Engineering, Univ. Mich.</i>
14:45 15:00	Completion Ceremony Adjournment		

Inquiry... JUACEP Office 052-789-2799

Date... Tuesday, October 8, 2019

Venue... Lecture room 242

13:00	Kimihiko Sugiura Prof. Seiichi Hata <i>Miro-Nano Mechanical Science and Engineering</i>	Sensitive Analysis of Five-Link Suspension (Undisclosed)	Prof. Gregory M. Hulbert <i>Mechanical Engineering, Univ. Mich.</i>
-------	---	--	---

Thermal testing of the New Small Magnetic Sensor for smallSAT

Nagoya university
Dept. Electrical Engineering
M1 Takahiko Kosegaki

University of Michigan
Dept. Climate and Space Science and Engineering
Prof. Mark B Moldwin

1. Background –geomagnetic field-

Solid line : **geomagnetic field line**

From Moldwin 2008

From Miles et al. 2016

From Burch et al. 2016

2

2. Background -Magnetic sensor-

RM3100 Magnetic sensor

Figures from Leuzinger and Taylor, 2010

3

3. Previous study

L. Regoli et al 2018

Magnetic sensor: RM3100 by PNI corporation	
Resolution (40 Hz sampling)	8.73 nT
(1 Hz sampling)	2.2 nT
Stability (Kurtosis index)	3.0
Linearity (± 100000 nT)	< 3 %

Question
What kind of situation (temperature, pressure, radiation) can we use this sensor

Purpose of the research
To reveal the temperature dependence of this sensor

4

4. Experiment

- Using the dry ice (sublimation temperature: -78.5°C)
- The system was left running for 50 hours or more
- The sensors were controlled with the Arduino uno.

(a) shows the difference between the characters of sensors
(b) shows the difference between the inside and outside of the shield can
(c) shows the temperature dependency

5

5. Results and Discussion

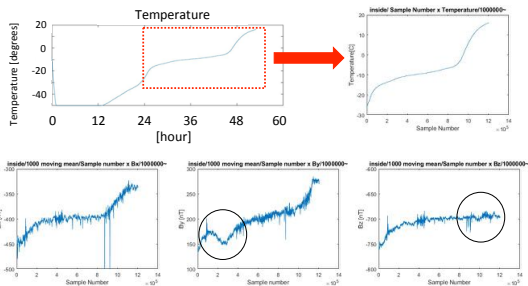
- The spike noises started to occur after the temperature went below -42°C
- Once the temperature going below -42°C , spike noises occurred when the temperature was changing

➤ The circuit was damaged due to excessive cooling

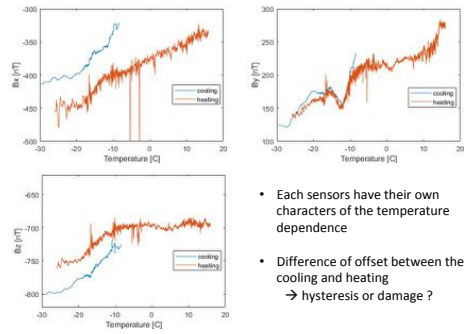
6

5. Results and Discussion

The measurements (spike noise was rejected and averaged)

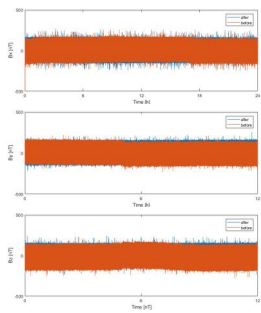


5. Results and Discussion



8

5. Results and Discussion



- Comparing with the measurements after and before thermal testing
- No permanent damage at least in term of resolution

9

6. Summary

- Understanding the global geomagnetic field is important for the space study
- RM3100 has ideally specification for small satellites
- RM3100 was tested the temperature dependence to reveal the versatility

Results

- RM3100 has temperature dependence

axis	Trend coefficients (nT/°C)
X	2.8
Y	3.1
Z	1.0

- RM3100 should not be operated below -42 °C or spike noises occurred
- RM3100 got no permanent damage due to excessive cooling at least in term of resolution

10

A computational study of cell growth and division as an energy-based soft packing problem using a diffuse interface framework

Ryo Tsunoda¹, J. Jiang², S. Rudraraju³ & K. Garikipati²

¹ Biomechanics, Mechanical Engineering, Nagoya University
² The Computational Physics Group, University of Michigan
³ Computational Mechanics and Multiphysics Group, University of Wisconsin-Madison

Background : Soft packing

cell aggregation
division, differentiation,
migration, packing...

mechanical interaction

chemical environment

BUT Affection according to spatial and temporal is primary

Application of computer simulation

lattice model

vertex model

¹ http://freshworld.souths.com/CellularAutomation.html
² Y. Zhang et al., PLoS ONE 4(10): e009996, doi:10.1371/journal.pone.0024996, 2011
³ GK. Xu et al., Journal of Biomechanics, 49, 2016

Theory of soft packing

Let $\Omega \in \mathbb{R}^2$ with a smooth boundary $\partial\Omega$ of Ω .
 Scalar fields $c_k, k = 1, \dots, N$ with $c_k \in [0, 1]$
 The interior of k^{th} cell, ω_k and the exterior of k^{th} cell, $\Omega \setminus \omega_k$.

The free energy density function :

$$\psi_1(c_k) = \frac{\alpha c_k}{2} (c_k - 1)^2 + \frac{\kappa}{2} | \nabla c_k |^2$$

$= f(c_k) + \kappa/2 | \nabla c_k |^2$

The total free energy of the multi-cell aggregate is a functional $\Pi[c]$, defined as

$$\Pi[c] = \int_{\Omega} \left(\sum_{k=1}^N f(c_k) + \sum_{k=1}^N \frac{\kappa}{2} | \nabla c_k |^2 + \sum_{k=1}^N \beta c_k \right) dV$$

keep the thickness of the boundary of cells
distinguish the interior and the exterior of cell

repel cells each other

penalize shape change

Theory of soft packing

Shape change of the cell is determined through the changes to the principal moment of the inertia (I^1, I^2) of the cell:

$$I^1 = \int_{\omega_k} x^2 dV, \quad I^2 = \int_{\omega_k} y^2 dV$$

The principal moment of the inertia is determined with following equation

$$I^1 = \int_{\omega_k} x^2 dV, \quad I^2 = \int_{\omega_k} y^2 dV$$

Then the total energy become

$$\Pi[c] = \int_{\Omega} \left(\sum_{k=1}^N f(c_k) + \sum_{k=1}^N \frac{\kappa}{2} | \nabla c_k |^2 + \sum_{k=1}^N \beta c_k \right) dV + \sum_{k=1}^N \left(\lambda (I^1 - I^1_{ref})^2 + \lambda (I^2 - I^2_{ref})^2 \right)$$

keep the thickness of the boundary of cells
separate the interior and the exterior of cell

repel cells each other

penalize shape change

Theory of soft packing

The variation of derivative with respect to c_k is following :

$$\frac{\delta \Pi}{\delta c_k} = \frac{d}{dt} \int_{\Omega} \left(\sum_{k=1}^N f(c_k + \epsilon \omega) + \frac{\kappa}{2} | \nabla (c_k + \epsilon \omega) |^2 + \sum_{k=1}^N \beta (c_k + \epsilon \omega) \right) dV + \frac{d}{dt} \int_{\Omega} \left(\sum_{k=1}^N \frac{\kappa}{2} | \nabla (c_k + \epsilon \omega) |^2 - \lambda (I^1 - I^1_{ref})^2 - \lambda (I^2 - I^2_{ref})^2 \right) dV$$

Then, chemical potential μ_k is defined as

$$\mu_k = \frac{\delta \Pi}{\delta c_k} = f'(c_k) - \kappa \Delta c_k + \beta + \frac{\kappa}{2} \Delta (c_k)^2 - \lambda (I^1 - I^1_{ref}) / I^1 - \lambda (I^2 - I^2_{ref}) / I^2$$

Kinetics : Cahn-Hilliard formulation

$$\frac{\partial c_k}{\partial t} = -\nabla \cdot (-M \nabla \mu_k) + s_k$$

Theory of soft packing

Time discretization

$$c_k^{t_{n+1}} = c_k^{t_n} + \Delta t (M \nabla \cdot \nabla \mu_k^{t_{n+1}} + s_k) \quad \left[\begin{matrix} \Delta t = t_{n+1} - t_n \\ t_{n+1} \end{matrix} \right]$$

$$\mu_k^{t_{n+1}} = f'(c_k) - \kappa \Delta c_k^{t_{n+1}} + \beta + \frac{\kappa}{2} \Delta (c_k^{t_{n+1}})^2 - \lambda (I^1 - I^1_{ref}) / I^1 - \lambda (I^2 - I^2_{ref}) / I^2$$

Weak form

$$\int_{\Omega} \omega_k c_k^{t_{n+1}} dV = \int_{\Omega} \omega_k c_k^{t_n} dV - \nabla \omega_k \cdot M \nabla \mu_k^{t_{n+1}} + \omega_k s_k dV$$

$$\int_{\Omega} \omega_k \mu_k^{t_{n+1}} dV = \int_{\Omega} \omega_k f'(c_k) dV - \nabla \omega_k \cdot \nabla (c_k^{t_{n+1}})^2 + \int_{\Omega} \omega_k \left(\sum_{k=1}^N \frac{\kappa}{2} \Delta (c_k^{t_{n+1}})^2 - \lambda (I^1 - I^1_{ref}) / I^1 - \lambda (I^2 - I^2_{ref}) / I^2 \right) dV$$

Basic formulation of finite elements methods determine dynamics of finite elements analysis
 Solved by standard finite element frame work

Algorithm of cell division

The cell mass of k^{th} cell at n^{th} time step is described as $m_k^n = \int_{\Omega} c_k^n dV$

initial single cell → become twice larger than initial volume → Then divided to two cells → initial condition of two cells → become twice larger than initial volume → Then divided to four cells → repeat expansion and division until cell filling the whole domain

The result of previous research

Achievements
Represented the cell division up to twelve-cell stage with considering mechanical property.

Parameter from numerical experiments

Parameters	α	κ	λ	M	s	Δt
Value	4	$1.0e-3$	100	1	$5.0e2$	$2.0e-4$

Limitations
Cells were not packed until divided to twelve cells.

Soft packing of real cells
Embryo of *Echinaster bradleyi* (A. E. Miguel, Universidade de São Paulo)
<https://www.cell.com/journal/embryogenesis>

initial single circular cell → Progression to four cells → Progression to eight cells → Progression to twelve cells

Full volume packing : Spatial treatment

Method

- If (cell mass < entire domain / the number of cells) source term = 1.0;
- If (cell mass > entire domain / the number of cells) source term = 0.0;

source term = 0 : no cell growing
source term > 0 : cell growing

- The cells fill the entire domain of the field at last.
- The thing is after the interface of the cells reach to the boundary, the cell skip the neighbor cell to expand.

Full volume packing : Temporal treatment

Method

- for $N=1-3$
- If (time for equilibrium $N < \text{current time} < \text{time for equilibrium } N+1$)
- If (cell mass < certain value) source term = 1.0;
- If (cell mass > certain value) source term = 0.0;
- If (cell mass > entire domain / the number of cells) source term = 0.0;

repeat three times

- Stop cell growing before the interface reach to the boundary
- Repel the each cells Then interface leave from the boundary

4 cells model and 8 cells model

- The cells fill the entire domain under static through all time steps.
- Have not considered mechanical character yet.

With the moment of the inertia term

$$\Pi(\mathbf{c}) = \int_{\Omega} \sum_k=1^N \frac{1}{2} \rho c_k^2 + \sum_k=1^N \frac{1}{2} \rho c_k^2 / r^2 + \sum_k=1^N \frac{1}{2} \rho c_k^2 / r^2 + \sum_k=1^N \frac{1}{2} \rho c_k^2 / r^2 dV + \sum_k=1^N \frac{1}{2} \rho c_k^2 =$$

Method

- The flame work of the model is same as the model without the moment of the inertia.
- We set the value of δ , $(\delta_1 k T_1, \delta_2 k T_2) = [0, 1.0 \times 10^{14} \text{ J}], [0, 1.0 \times 10^{15} \text{ J}], [0, 2.0 \times 10^{15} \text{ J}]$ where valid range of $\delta_1 k T_1$ is $\delta_1 k T_1 \in [1 \times 10^{14}, 2 \times 10^{15}]$.

$(\delta_1 k T_1, \delta_2 k T_2) = [0, 1] \times 10^{14} \text{ J}$

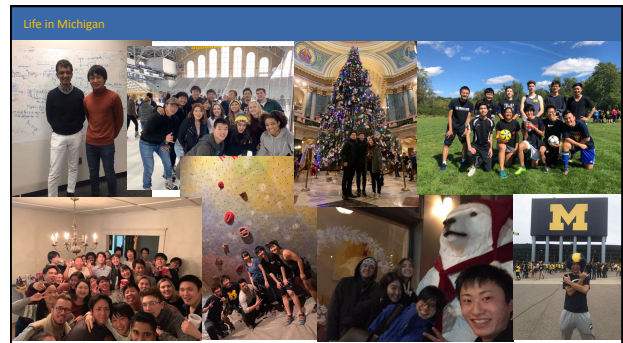
Summary and look ahead

Succeeded to represent the full packing model with certain number of cell

- ▷ Without the moment of the inertia term, described the model filled out with two, four and eight cells
 - The treatment of interface of cell is important to grow cells under stable. e put spatial and temporal treatments in this research.
- ▷ With the moment of the inertia term, described the only model filled out with two cells.
 - The model was calculated under stable only when mechanical modulus $(\delta k k T_1, \delta k k T_2) = [0, 1.0 \times 10^{-14}]$ though valid range of δ is $\delta k k T_i \in [1 \times 10^{-14}, 2 \times 10^{-15}]$.

As the next step of research

- ▷ The model filling the entire domain with cell at anytime on the way to growth.
- ▷ Finding the conditions where the cell grow under stable through the range of value of the moment of the inertia term.

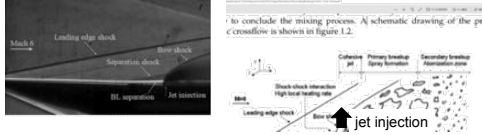


The 24th JUACEP Students Workshop
March 28, 2019
IB 013

Experimental Investigation of Primary Breakup Induced by High Mach Number Shock Wave


Kotaro Hotta
Supervisor: Mirko Gamba

Introduction

- **Scramjet engine**
A scramjet engine is an air-breathing jet engine that operates at speeds of 4 or more times the speed of sound.
Scramjets may one day have several applications: an air plane which has so much high speed.
Challenging : **The mixing process** between fuel and air
➡ It is important to understand the breakup process for Supersonic Crossflow
- **Primary Breakup Process for supersonic crossflow**
J. Beloki Perurena, et al.(2009) revealed the presence of the Bow shock in front of the liquid jet injection


Introduction

- **Primary Breakup Process for subsonic crossflow**
For **Subsonic** crossflow, there are various studies, and the important parameters, such as breakup mode and the breakup time, are arranged by Weber number and Ohnesorge number.
 $We = \rho u \infty \sqrt{2} d \sqrt{\sigma} / \mu = \text{aerodynamic force} / \text{surface tension}$
 $Oh = \mu \sqrt{2} / \sqrt{\rho \sigma} \sqrt{\sigma} / \mu = \text{viscous forces} / \text{surface tension and inertial forces}$
 For $We > 110$ and $Oh < 0.1$, shear breakup occurs.
 characteristic
 • disturbances on the windward side due to Rayleigh-Taylor instability
 Sallan et al.(2004) revealed characteristics of shear breakup.
 Breakup time, t_b An effective drag coefficient, C_D
 $t_b / t_b^* = \text{const.} = 2.5$ $C_D = m \theta a c / 1/2 \rho \infty (u \infty - u) \sqrt{2} d \sqrt{\sigma} = \text{const.} = 3$
 where, $t_b^* = (\rho d / \rho g) \sqrt{10.5 d \sqrt{\sigma} / u \infty}$ shear breakup[1]



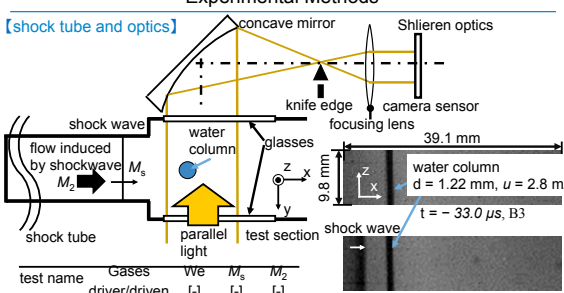
[1] Sallan et al.(2004)

Objective of this work

- Observe the entire breakup process for supersonic crossflow ($M_2 = 1.1 - 1.6$)
At the condition of $We > 110$ and $Oh < 0.1$, which is corresponding to the shear breakup for subsonic crossflow study.
- Investigate the effect of flow Mach number on the breakup time and an effective drag coefficient

Experimental Methods

[shock tube and optics]

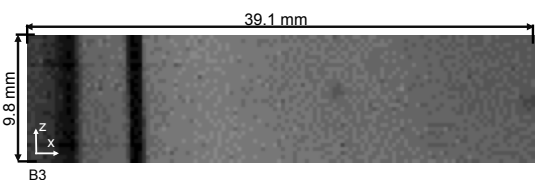


shock tube flow induced by shock wave M_2 shock wave water column parallel light test section shock wave concave mirror Shlieren optics knife edge camera sensor focusing lens 39.1 mm 9.8 mm water column $d = 1.22$ mm, $u = 2.8$ m/s $t = -33.0 \mu s, B3$ $t = -3.3 \mu s, B3$

test name	Gases driver/driven	We	M_s	M_2
A1	N ₂ /Air	3933	2.29	1.11
A2	He/Air	5071	4.18	1.58
B1	He/Air	9003	3.47	1.47
B2	He/Air	9238	3.86	1.53
B3	He/Air	8617	4.32	1.60

$Oh < 0.1$ at all cases

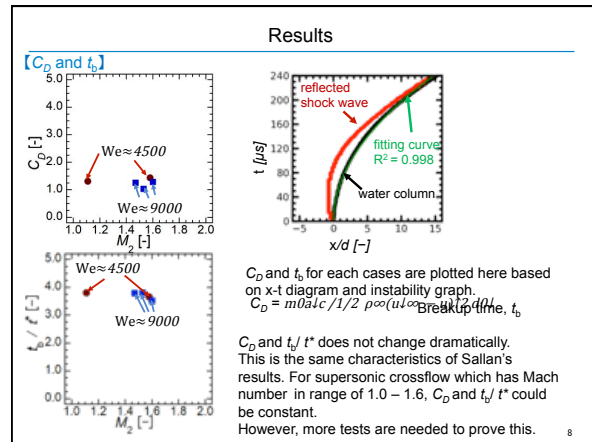
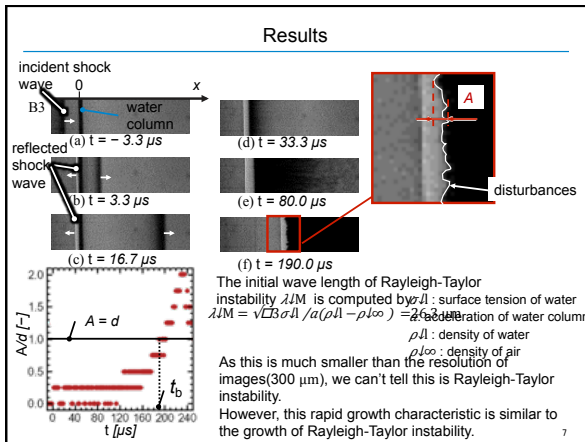
Results



39.1 mm
9.8 mm
B3

frame interval 3.33 μs
light source pulse duration 0.65 μs
resolution 0.31 mm/pixel

Because $q_{water} / q_{gas} = 0.02 \ll 1$, the water column move to the -Z direction by only 0.4 mm while this video.



Conclusion

- We observed entire process of primary breakup.
 - Shock impingement
 - a strip of ligaments and fine mist from water column
 - an expansion of the ligaments and fine mist area
 - an occurrence of the disturbance on the windward side
 - a growth of disturbance (could be Rayleigh-Taylor instability)
 - break up
- For supersonic crossflow which has Mach number in range of 1.0 – 1.6, C_D and t_b/t^* could be const.

<4> Findings through JUACEP

- Students' reviews ...76
- Questionnaires (in Japanese) ...87

My Life in Ann Arbor through JUACEP

Name: **Motoki Yamada**

Affiliation at Nagoya Univ.: **Materials Science and Process Engineering**

Participated program: **Short course 2018**

Research theme: **Synthesis of MZPFe nanopowders to thin films as solid electrolytes by Processing Liquid-Feed Flame Spray Pyrolysis**

Advisor at the visiting university: **Prof. Richard M. Laine**

Affiliation at visiting university: **Materials Science and Engineering
University of Michigan**



The life in Ann Arbor, Michigan, was spectacular to me. Before arrival, I was worried whether I could live here all by myself because everything would be inexperienced there in the house and laboratory, of course, the city itself. However, contrary to my prediction, they were so helpful to me, bringing me the relief. In the laboratory, one PhD student, probably assigned in charge of me, taught me a lot about the procedure of experimental and the way to use the equipment's in the lab. Therefore, although the research area was completely different from that in Japan, I could follow her directions, which led me the comprehension of the whole outlines of my experimental goal and lots about ceramics and its application. Regretfully, due to the short term of the stay, I found it difficult to take actions spontaneously in the laboratory.

As for the rental of the house to live in, I heard in advance that it would be difficult to contract the lease just for 2 months. So, I decided to use the application of Airbnb, a kind of private residential support service mainly functioning on the smartphone. As a result, it brought me the migration of the house in total 4 times. What I can say in common of those 4 houses is that the hosts welcomed me willingly, thus I could enjoy sharing the house space.

I also participated in some of the activities such as the pizza party, picnic, and boating held by international organizations, where I made some friends with foreigners. They are so curious about their research, so it impressed me a lot in terms of the motivation of work.

On the holidays, I went watching American football game with some JUACEP students, and baseball game with attendees of international circle. Needless to say, since these were the first experience for me to watch sports in other countries, I was so excited and mostly I can find them the most memorable events.

While living in Ann Arbor, I naturally learned to consider about my own countries compared to U.S. and found some meaningful differences between both countries. First, they in Ann Arbor frankly and willingly accepted foreigners. In Japan, I felt many Japanese hesitate to speak foreigners because possibly we are afraid of contacting with other cultures or speaking non-mother languages. When I faced some troubles and needed some helps, they in Ann Arbor gave me a hand even if they might feel difficult to understand what I was saying. I would not have lived without their helps in the scene of housing, living, and life in laboratory. I also found that most of the Asian people studying in University of Michigan are non-Japanese, most occupied by Chinese. Many of them I encountered are eagerly aiming to get the position such like PhD, rarely seen in Japan. Through these experiences, I should reconsider about my own future work.



To Enjoy Difficulties in U.S.

Name: Keiichi Okubo

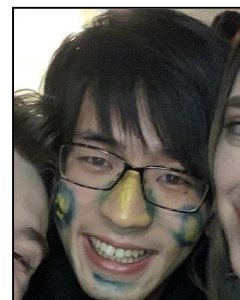
Affiliation at Nagoya University: Chemical Engineering

Participated program: Short course 2019 (From November to December)

Research theme: Synthesis of Mo₂C supported metal catalysts

Advisor at the visiting university: Prof. Saemin Choi

Affiliation at visiting university: Chemical Engineering, Michigan University



I came across many difficulties in U.S. But they all excited me and made me grow. Moreover they have transformed my life in U.S. into the enjoyable experience.

1. Sudden cancellation a month before going U.S. in searching for a teacher to accept me.

The teacher can't accept me because he had decided to move to other university.

2. Postponing the juacep program

Owing to 1, we had to postpone the juacep program. Thanks to many people's help, I could carry out the program. Thank you all.

3. Cancellation of Michigan University Sponsorship

Thanks to the mistakes in administrative procedures at the side of Michigan University, I could not enroll at the university.

4. Cold room

The room I stay in was too cold without an air conditioner, a suitable bed and a blanket. Therefore it was too cold to sleep enough.

5. Trouble with a rental car shop

I was told from the shop that we have no cars by overbooking. This incident will not happen in Japan.

6. Police!!!

We was involved in a small accident, and called the police.

7. Trouble at private accommodation (Airbnb)

The Chinese was using the room that we reserved and had locked the door, so we could not use the room.

Because I came across many difficulties, it was a happy two months.

Regular days do not remain in our memory. Engraving events into emotions, such as happiness, sadness, surprise, they will be a lifelong memory.

Courage is necessary to make a decision to study abroad. Please contact me if you need advice.

Lastly I will leave the sentence left in my impression. I was said that from a professor.

'Why DON'T Japanese study abroad?'



Findings through JUACEP

Name: Kotaro Takamure

Affiliation at Nagoya University:

Department of Mechanical Science and Engineering, Nagoya University

Participated program: Short course 2018

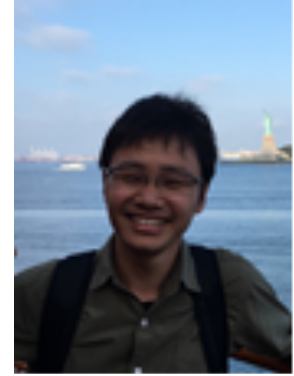
Research theme:

Synthetic jet characterization for differences in nozzle size and thickness of gasket

Advisor at the visiting university: Prof. Philippe Lavoie

Affiliation at visiting university:

Institute for Aerospace Studies, University of Toronto



First of all, I am very grateful to Professor Shaker Meguid who is a supervisor of JUACEP in UofT for much advice on Toronto's life and laboratory. I am also very grateful to Professor Philippe Lavoie for guiding me about research. He gave me an opportunity to conduct a very interesting and challenging research.

I visited University of Toronto for two months and worked at the Flow Control and Experimental Turbulence Laboratory in University of Toronto Institute for Aerospace Studies (UTIAS). I conducted a research on a synthetic jet characterization for differences in nozzle size and thickness of the gasket. I researched almost the same field as in Japan but the research theme was completely different. But, professor and students listened to my problems and they gave me some advice. , this research theme was very difficult for me, but I gained great confidence when I finished my research. I think it is a valuable experience for the future.

I stayed in Toronto by homestay. Homestay's owner gave me three meals a day. There were several people (Mexican, Turkish, and Korean) who came to learn languages, and they were all very kind. Sometimes, I enjoyed barbecuing and watching movies with homestay family. On holidays, I went to many places, for example, New York, Niagara Falls, and Rogers Center et al. Furthermore, I participated in language exchange and enjoyed exchanging information with Canadians. These times became valuable experiences that I could not experience in Japan.

Finally, I'd like to appreciate everyone who gave me the great opportunity to study in Toronto.



Findings through JUACEP

Name: Shuichi Higaki

Affiliation at Nagoya University: Mechanical Systems Engineering, Graduate School of Engineering

Participated program: Short course 2018

Research theme: Analytical and Numerical Modeling of High-Temperature Pressure Transducer

Advisor at the visiting university: Prof. Pierre Sullivan

Affiliation at visiting university (Dept & Univ):

Mechanical and Industrial Engineering, University of Toronto



The experience that I had in Toronto is extraordinarily valuable. I appreciate my supervisor Prof. Pierre Sullivan and JUACEP coordinator Professor Shaker A. Meguid. Also, I appreciate everyone who helped me. At first, I thought that it is hard to live in Toronto because of my English skill is poor. However, there was nothing to worry about it because the people who involved with me are so kindness; especially Professor Sullivan gave me enormous help. In such circumstances, I was helped by the many people and could live in Toronto. Thanks to that, I guess my English skill is a little bit improved.

In Toronto, I studied simulation using commercial software and modeling of the pressure transducer. My research in Japan is experiments not simulation. Therefore the study was new for me and I needed to study a lot about the theme. However, thanks to Prof. Sullivan and member of the laboratory, I could understand what the goal of the study is, what is needed and what I have to do. The duration was short to get great results. But the experience was good for me because I could learn the difference in the attitude to take research activities. I am sure of it lead me improving my research activities in Japan.

The life in Toronto except for research activities is also great. Toronto is so safety city and has good weather in summer. Also, Torontonians are tolerant about clumsy English because Toronto has many immigrants and, I think people who live in Toronto have the cooperative spirit, and the attitude trying to understand what someone wants to do. I went to many places during this program, for example, an amusement park, historical building and so on. I can't write it all of them, so I write some experience here. I love baseball and Toronto has an MLB team, Toronto Blue Jays. So I went to watch the game twice. It was so great. The atmosphere in Ball Park is different from Japan. Also, I played baseball in the local baseball club and so fun. The place where is deeply impressed is Niagara Falls. In there, I could see the spectacular nature that I can never see in Japan. Toronto is close by New York and I went there. NY is an exciting city and I had a great trip.

Finally, I would like to express appreciation again for Professor Sullivan, Professor Meguid, the member of the laboratory and JUACEP officer who gave me such excellent opportunity. Also, I appreciate the homestay family, agents, and friend I met in Toronto. They made me great experiences. Thank everyone very much.



Finding through JUACEP

Name: Takahiko Kosegaki

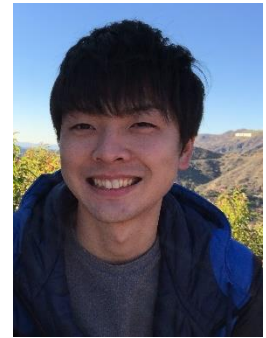
Affiliation at home country: Electric Engineering, Nagoya University

Participated program: Medium course: August 2018-January 2019

Research theme: Thermal Testing of the New Small Magnetic Sensor for SmallSAT

Advisor at the visiting university: Prof. Mark Moldwin

Affiliation at visiting university: Department of Climate and Space Science and Engineering, University of Michigan



The research in the US was basically tough because all resources, texts, papers and lessons, were written and spoken in English. However, the professor and the post doctor helped me whenever I was in some trouble. The research made me more interested in the space physics and the observatory. This is because the people in this department told about their research happily.

I visited a lot of states during the winter break. One of my recommendation is Florida because it was warm as we can get in the sea. I strongly recommend someone, who will stay in Ann Arbor, to visit a lot of states especially the eastern states where is far from Japan.

The college sports are also popular in Ann Arbor. People are excited to watch the game and send a cheer with waving the yellow and navy. You can enjoy to mimic to send a cheer, feel the passion of them and see the cheerleading performance even if you don't know well about the football.

I have a tip to live in the US. They use credit cards or debit cards every store and restaurant. I recommend you to have more than two credit cards or debit cards because they can be stopped due to the skimming. I had a credit card and a debit card but they both were stopped in six months. Also, you should check the receipt of cards frequently.

The life with many friends in the US was definitely exciting and interesting. I couldn't speak well in English, but some people in the US tried to understand that I meant and they told me something about the US, their country and something funny. This experience offered me some opportunities to make a lot of friends all over the world.



Great Time in Michigan

Name: Kotaro Hotta

Affiliation at Nagoya University:

Participated program: Medium course 2018

Research theme:

Experimental Investigation of Primary Breakup Induced by High Mach Number Shock Wave

Advisor at the visiting university: Prof. Mirko Gamba

Affiliation at visiting university: University of Michigan, Aerospace Engineering



I have great experience at the University of Michigan. First of all, I would like to thank the staffs at JUACEP. This program gave me a lot of helps, such as Funding, Introduction of Professor and advise for housing. Thanks to these helps, I was able to kick-start my life in US.

I studied about the breakup process of the water in the supersonic crossflow under Professor Gamba. We had weekly meetings, which helped me to think of the next step and to make right decision. When I faced difficulties, he spent long time to discuss the solution with me, and finally I could fix it. I conducted the experimental tests with a PhD student. He was so kind to me that he always answered a bunch of questions about the facilities and physics. It was helpful in understanding the manner of operations and the phenomenon in the facilities. He and other laboratory members frequently took me to many places to see, for example, a new ramen shop in Detroit, a famous Sandwich shop and Apple hunting. I spent great time with them. On the last day of my stay, they held the farewell party for me at a fancy American restaurant. I felt happy to see so kind friends in US.

Ann Arbor is famous for the football team. It has the second largest stadium in the world. I totally go to see football game three time in my stay. I didn't know that it was so popular that over 100,000 people get together in that stadium. I was so excited because when our team get points, the all audience stand up and make joyous scream. I watched superball at my friend's house. Because it was close to Chinese New Year, we made dumplings, which is traditional Chinese meal made on the New Year. Actually, the game was boring, but I spent a great time.

I found a lot of friends and cultures in US. I would never find them if there were not JUACEP program.



Findings through JUACEP

Name: Koki Hojo

Affiliation at Nagoya University: Department of Micro-Nano Mechanical Science and Engineering

Participated program: Medium 2018

Research theme: Reactive dc magnetron sputtering of MoS₂ and MoS₂/hBN layers

Advisor at the visiting university: Prof. Suneel Kodambaka

Affiliation at visiting university: Department of Materials Science and Engineering, University of California, Los Angeles



I have three achievements through this program. The first one is obtaining enough skills to do academic research in overseas. For the first few months, I spent a hard time to make myself understood to my laboratory members and learn knowledge of new science field. However, I got used to discussing difficult, specialized issues about my research and do experiments without any help from others. My discussion skill was improved enough to talk with my professor about my experimental plan individually. Finally, I could produce new data enough to publish more than two papers, though I have to continue writing the paper after finishing this project. Anyway, those experiences and new

skills should be my advantages to working on any research works after I come back to Japan.

The second achievement is joining a sports club in overseas. I participated in UCLA triathlon team until I left LA. They hold 11 practices, consisting of swim, bike, run, and mixed session, per week. I spent a very fun time with team members through the training, though I could join only a few sessions a week because I was lazy in the early morning and busy in the evening. My favorite training was biking around Malibu mountains. Ocean view from PCH (Pacific Coast Highway) was really awesome. Most of the time after the bike session, we stopped by local café and enjoyed a relaxing time with a cup of coffee. In November, we had “Teamsgiving” party, which derives from a traditional family holiday, Thanksgiving, in the U.S. We brought cooked foods to a team member’s house and enjoyed them with Sake, which I brought to the party. I thank them to hold the event because I didn’t have any family member to celebrate the holiday with in LA. The day before I leave LA, they gave me a team T-shirts and a message card. I cannot help but thank the team members.



The final accomplishment is participating some competitive races in LA. For the period I stayed in the U.S., I took part in two triathlon races and one trail running race. It was challenging for me to join those races without any help but had an exciting time. Sometimes I went a wrong route and lost time because the number of staffs was not enough to guide all of the participants. It reminds me that races in Japan were very hospitable, comparing to those in the U.S. Surprisingly, I won all of the races in my age division (U25). Through those races, I could receive many medals. Literally, it is a good memory.

As you can see, I could learn and experience so many things through this program. I would like to thank all of the people who supported me.

A good tip on happy life in the US

Name: Hiroki Kogure

Affiliation at Nagoya University: Mechanical system engineering

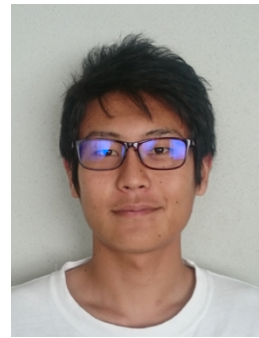
Participated program: Medium course 2018

Research theme:

Advisor at the visiting university: Prof. TC Tsao

Affiliation at visiting university:

Department of Mechanical and aerospace engineering,
University of California, Los Angeles



Many people believe, or try to believe the existence of difference between Japanese culture or personality of them and others' ones. And what is worse would be they really love to compare them. Through just 23 years of my life includes this foreign experience and discussion with foreign people, I temporary have following opinion, it totally depends on each individual. I have a cat, whose name is Leo, and there happen to have been two cats, whose names are Chuy and Gilby, in my second place to live in the US. Chuy has a more similar personality to Leo's one than Gilby's one. There is no way to tell if they speak Cat English or Cat Japanese, but it might be absolutely clear that it makes no sense to discuss about how different American cats and Japanese cats are. It must depend on each cat. At this point of view, when a Japanese man who is narrow-minded and arrogant and a American woman who kindly accepts me as a guest are compared, who on earth says Japanese people are polite and generous. You intelligent and thoughtful readers might want to think about your personality and self doctrine. One guy who serves obediently to those have more power would use those have less like a slave. One guy who has no confidence would act like a great leader once he is put in charge of. One guy seems to be nice would become an egoist in a tough situation. Personality varies with TPO and their mood. Hence, to generalize each people and define culture is like to grab the clouds because culture is just a collective body of individual. If you tried to understand foreign culture without recognition of colored spectacles, your prejudice would be stronger.

As described above, although the definition and recognition of personality are skeptical and vulnerable, it is really ignorant to determine who you are and to believe it is definitely right in just a limited environment and role. Getting out of that community might help. Let us say you have self esteem in some achievements on research or skill in your current lab with great help by many other people, it will be as useless as 100 dollars bill for washing machine because the way of coding, experimental devices, and even analytical approach must be different. Let us say you identify yourself as a generous person, it will be as painful as 10 dollars bill for Big Blue Bus because you would have less resources and you will get more treatment than you can give for other people. You will feel powerless. Let us say you think of yourself as a good listener, it will be as no use as penny and dime coins because you cannot convey your full empathy over the barrier of language — I deliberately avoid mentioning that the best listener talks nothing, just listens. The most acceptable coin and bill in daily life in the US are quarter coin and 1dollar bill by the way.

May I make a suggestion as useful as a Chase bank debit card. It is to get rid of prejudice on how you should be and how studying abroad should be. All you need is just to live like as if you have been living in the US and take a look around, you will find how beautiful sunrise, sunset, white beach, blue ocean, and green plants are. You will realize how warm your roommates, labmates, neighbors, and even people who live on street are. Get out of self-centered mindset or identity, which is not chronic but just temporal and to flow. This would help you with finding your new place or new role and living without social stress in a new environment. Furthermore, you will be stunned by how active and genius genuine yourself would be to find happiness. I heartily hope that many potential participants of JUACEP can think that they made a correct decision through their foreign experience. I am most grateful to JUACEP office for giving such a valuable opportunity to young ambitious students for many years and in the year to come.

Findings through JUACEP

Name: Ryo Tsunoda

Affiliation at Nagoya University: Biomechanics, Mechanical Engineering

Participated program: Long course 2019

Research theme: A computational study of cell growth and division as an energy-based soft packing problem using a diffuse interface framework

Advisor at the visiting university: Prof. Krishna Garikipati

Affiliation at visiting university: The computational physics group, UM



I got a lot of experiences through the JUACEP program at the University of Michigan. Especially I'm going to talk about these in researching and activities in some clubs.

I study a kind of the computer simulation, FEM (the Finite Elements Method) which is well-known if you are mechanical student although my specialized in Nagoya university is biomechanics. The reason why I decided to study FEM is to obtain the skills for my study in Japan. The purpose of my research is to find out the mechanism of embryo morphogenesis and I study it experimentally in Japan. But I am interested in the approach of the inverse problem, but since this is not my field of studies, I decided to join this laboratory. First of all, I needed to know the basic theories and examples of FEM so I had to take the classes with the other UM graduate students for a semester before I started the research. It greatly helped me to further understand my research and made me realize how hard the students study in the US. It was very unique for a Japanese student like me who has only studied in Japan and it was a great experience.

Life in the laboratory was similar to that in Japan. We usually have worked from 10am to 6pm every weekday and had the meetings for the reports twice a week. All of the students, staff members and professors were kind and helped me even if it was a slight thing.

With respect to my club activities, I had joined JSA (Japanese Students Association), Bridges (A Christian association that organizes events for international students), M-Run (Michigan Running club) and MMC (Michigan Muscle Club). I made a lot of friends in these associations and it is the best thing I got out of this exchange program and also helped to improve my English, although when I was with JSA friends, I talked to them in Japanese. I spent almost of my weekends drinking with JSA guys. Bridges invited me to a lot of events like Thanks giving party, Christmas party, the dinner for Christian and so on. I prefer speaking with them because they speak calmly and it was easier to understand. For my recreation, I had joined the running club during an entire fall semester and muscle club during a half of winter semester. The environment for recreation in Michigan is perfect. Basically, the campus is extremely large compared to Japanese universities but the recreation facilities is greater than I expected so I was satisfied with working out. Also, it improved my concentration for research. It means, in Michigan winter, the weather is cloudy almost every day and it made me sleepy during the day time and I couldn't proceed my research enough. But I joined MMC and it made my life better. We trained from 7am at the gym every day and it woke me up without sunshine. I want to recommend working out during the mornings in Michigan winter if you have plan to come to Michigan.

I'm sure that what I got in this program (research, English, friends and muscle) should help my career in my future. Finally, I appreciate everyone I met in the US. Thank you.



Findings through JUACEP

Name: Kimihiko Sugiura

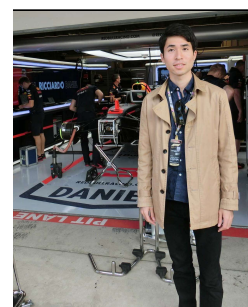
Affiliation at Nagoya University: Mechanical System Engineering

Participated program: Long course 2019

Research theme: Sensitivity Analysis of Five-Link Suspension

Advisor at the visiting university: Prof. Greg Hulbert

Affiliation at visiting university: Mechanical Engineering, University of Michigan



Academic life

I chose to come to the University of Michigan (UM) because I wanted to study more intensively in the field of automotive engineering research, and there are more research opportunities here. This is because there are many automobile companies near the university. My research was about automotive suspensions, which are important to certain basic functions of a vehicle: running, stopping, turning, etc.

When I first arrived at the UM, I was confused by how working with a research team was different in the U.S. in comparison to Japan. I was specifically confused about when it was appropriate for me to take initiative with a project and when I should wait for directions or permission from my professor. I was not sure how much initiative my professor wanted me to take. I determined the proper balance by observing other students around me, and I frequently met with the professor. By doing so, I learned to make suggestions for how to proceed in a certain project because I found that taking initiative is highly esteemed in my laboratory. At first, having to make my own decisions was difficult because I was accustomed to getting explicit instructions from my Japanese professors. However, I used several methods to overcome this challenge. For example, I would ask for advice from a researcher at another laboratory doing related research. As a result, I was able to determine an objective for my research with the aid of my professor and other researchers.

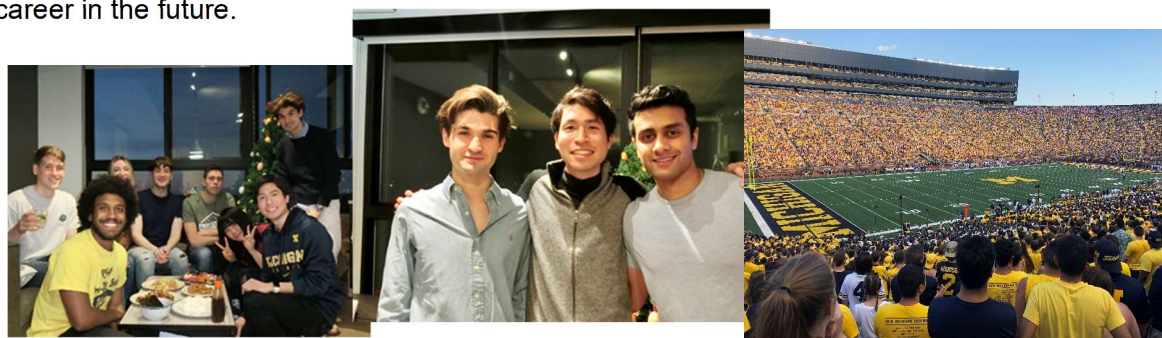
In addition, I have had many opportunities to learn about new things. For example, I experienced the difference in corporate culture between the U.S. and Japan through interacting with an automotive engineer. In February of 2019, the U.S.-Japan Automotive Conference was held here at the UM. I was also able to interact with a former member of the U.S. House of Representatives and with an executive from a Japanese automobile company.

I have made many new connections through my time studying abroad, and I am sure that the connections will be very helpful in the future.

Private life

I lived in an apartment with two roommates (American and German). We had never met before, but we became friends quickly because all of us were very outgoing. Being able to speak with them in an informal setting was also very helpful for me when my research was not going well. This study abroad experience would have been very different if I hadn't had such amazing roommates.

Finally, I had the chance to go to Texas for a weekend to watch a Formula 1 race. I was fortunate because I was able to interact with a Japanese staff member from the Honda F1 team who was a Nagoya University alumnus. I was so glad to meet someone from my same university who is leading a very successful life overseas. Meeting him encouraged me to pursue a similar, globally oriented career in the future.



Findings through JUACEP

Name: Yuta UJiie

Affiliation at Nagoya University: Mechanical Engineering

Participated program: Long course 2019

Research theme: evaluation of the UCLA Low-PRofile Direct shear sensor for air Flows in Wind Tunnel

Advisor at the visiting university: Prof. CJ.Kim

Affiliation at visiting university: Mechanical and Aerospace Engineering, UCLA



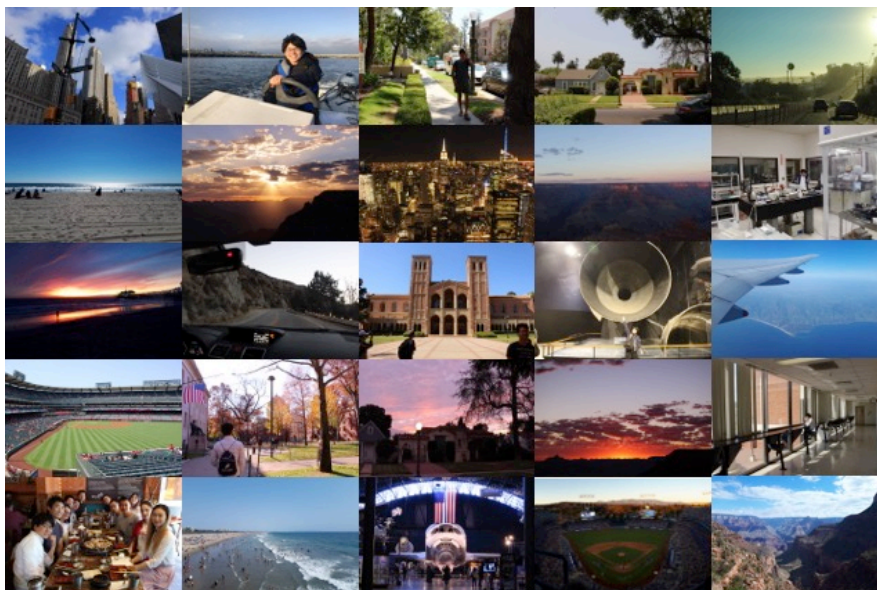
This is about my exiting days in LA.

I researched the shear stress sensor of airflow. I studied it in Japan too. But their mechanisms are different and have different disadvantages and advantage. Using and studying both sensors makes my studies better. This is the reason why I decided to research this theme in UCLA. In my research, there are many troubles and many things need to study. My professor and lab members help and advise me a lot. I appreciate their cooperation and kindness. I have eaten lunch with anyone in Lab everyday. It makes my English level improved and I learned a lot of things, for an examples culture of U.S. It is the exiting and enjoyable time.

The life in LA is livable and enjoyable. The weather is ideal, not hot in the summer, not cold in the winter and not humid like Japan. On the weekend, I usually go to Santa Monica beach which is about 30min by bus and surfing and swim in the summer, reading a book and listening music in the winter. The most beautiful scenery I think is the sunset of Santa Monica. I went there and see it, when I was tired and sad. But everything is not good in LA. The biggest program is that everything is very expensive. The rent is over \$1000, eating out is over \$10, medical expense is marvelous price. I think living in U.S. is harder than in Japan. I have been to many cities in U.S, Las Vegas, San Diego, New York, Boston, Washington D.C, Seattle. It is great experience and I feel the difference of the city ambience.

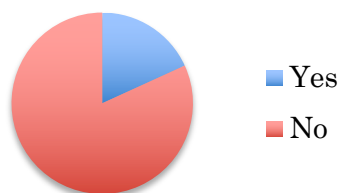
In this 8months, everything is not good. There are many painful and hard things and want to go back Japan many times. I can get over difficulties thanks to the kindness many people, friends and host family. They are my treasure. is the biggest challenge in my life. It is easy way that not changing and challenging anything. But changing and challenging make us grow. This experience makes me great grow.

To improve is to change -Winston Churchill

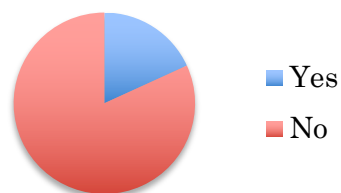


派遣プログラム参加者に行ったアンケート結果
 <博士課程進学に興味がある>

留学前

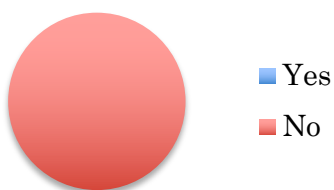


留学後

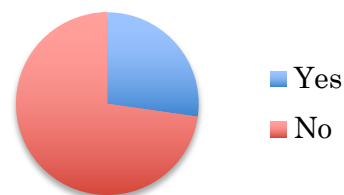


<外国の大学での博士課程進学に興味がある>

留学前

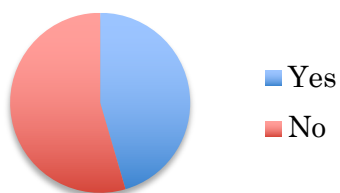


留学後

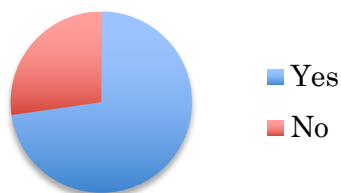


<日本での外資系企業への就職に興味がある>

留学前

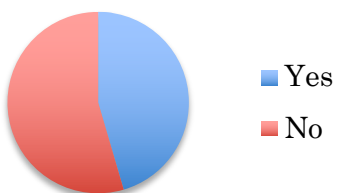


留学後



<外国での日系企業への就職（海外勤務）に興味がある>

留学前

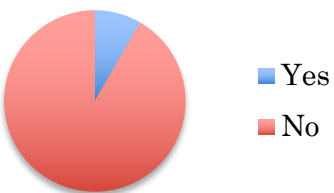


留学後

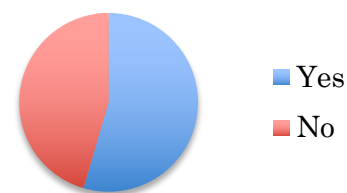


<外国での日系以外の企業への就職に興味がある>

留学前

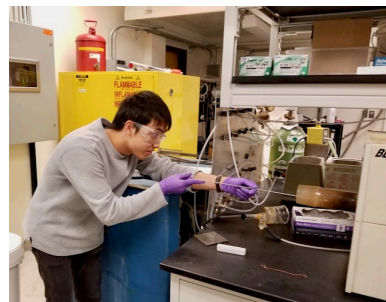


留学後



1. このプログラムの良かった点

- ・ 派遣先で授業を受ける必要がなく、研究に集中できる。その分野の先端に行く人たちと質の高い議論を日常的に体験できる。
- ・ 派遣先大学の質が高い。
- ・ 自分で英文履歴書やカバーレターを作って海外の教授にアプローチするという、ふつうは修士学生は単独ではやらないであろう経験ができた。
- ・ 受入先決定・航空券手配・宿舍手配…全て自分でやるので、留学終了時に自信となった。
- ・ 参加者同士の交流があり心強かった。
- ・ 奨学金がある。
- ・ 受入先を探す際に相手側から返事が滞ることがあったが、事務室の対応で解決した。
- ・ 過去の先輩の資料が充実しているので参考にしやすい。
- ・ ショートプログラムだと、研究室や家族の理解も得やすい。



2. このプログラムで改善してほしい点

- ・ 奨学金を月初めに入金して欲しい。定期的に入金して欲しい。入金連絡が欲しい。
- ・ 事前にざっくりとした必要予算を教えてくれるとありがたかった。ちなみに私のかかった費用（短期コース）は、準備金5万、渡航費20万、宿舍代22万、生活・娯楽・保険18万の計65万程度だった。
- ・ 名大渡航助成金を短期コースにも拡大して欲しい。
- ・ 宿舍探しは大きな不安要素の一つ。寮に入れると良い。
- ・ 物価が高くて、奨学金だけでは生活できない。
- ・ 英語のレベルをもっと高くしてから行くべき。派遣前の春学期に専用講座があるといい。
- ・ 機械系以外でのプログラム認知度が低くて残念。

3. 住居について

- ・ 宿舍の見つけ方：インターネットのエージェントを通じてホームステイ（3食付き）
感想：ステイ先の家族やステイメイトと交流を深めることができ、とても良かった。（CA\$800/月）
- ・ 宿舍の見つけ方：Airbnb
感想：短期コースでは賃貸物件に入居するのが困難なので民泊アプリは有効だと思う。2ヶ月間で4ヶ所の宿に泊まった。（US\$15～40/泊）
- ・ 宿舍の見つけ方：インターネットの掲示板（vivinavi）
感想：詐欺契約に気をつけよう。現地についてからでも見つけれられる。（US\$1,010/月）
- ・ 宿舍の見つけ方：最初は渡航前にFBで見つけた家具付きアパート。その後シェアハウスに引越し。
感想：静かで日本人街に近く、とても良い場所だった。（US\$700～860/月）
- ・ 宿舍の見つけ方：大学のホームページ
感想：新しくきれいで住みやすかった。（\$1,300/月）
- ・ 宿舍の見つけ方：知人を通じて6人用シェアハウスに入居。
感想：とても清潔で静かな家だった。逆のパターンもあるので運が良かったと思う。（US\$725/月）



- ・ 宿舎のを見つけ方：現地のエージェント
感想：ホームステイだったが門限もなく、3食付きで非常に良かった。(CA\$800/月)
- ・ 宿舎のを見つけ方：現地のエージェント
感想：相場は日本の感覚よりかなり高い。シェアが一般的で、個室はまず無理。(US\$899/月)
- ・ 宿舎のを見つけ方：最初に短期間住んだ Airbnb のオーナーの紹介
感想：短期間だと敬遠されるが、現地の業者とは知り合いになっておくと便利。(US\$700/月)
- ・ 宿舎のを見つけ方：Facebook, vivinavi
感想：学生とルームシェアをしていたがその後悪い勧誘から身を守るために引越した。(US\$1,350/月)
- ・ 宿舎のを見つけ方：知人
感想：ミシガン大周辺はアメリカの中でも有数の高物価地域。月 800-1000US\$が相場だと思う。(US\$600/月)

4. 滞在中の印象深いことなど

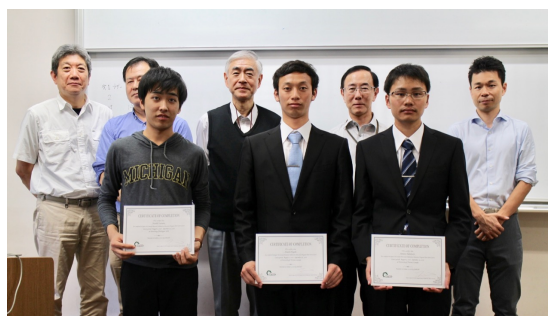
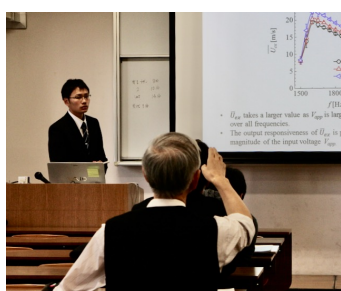
- ・ グランドキャニオンが最も印象深い。あの自然の雄大さは日本では感じることはできない。
- ・ ホストはいい人ばかりで週末には車で買い物に連れて行ってくれた。
- ・ 店員や初対面の人に対しても「Hi」や「How's it going?」などの挨拶をするのが印象的。カナダでは握手やハグも日常的で、日本よりもコミュニケーションを重視する文化だと感じた。
- ・ 国際交流団体のイベントで、多国籍の人達と話したり、無料の英会話レッスンに出たりと、研究室以外でもいろんな交流があった。
- ・ 2カ月かけて技術を習得した装置が壊れてそれ以降使えなくなった。
- ・ あまり先生とのディスカッションを好まない自分が、自分から PI のところに赴いて意見を仰ぐようになっていた。自分で調べる習慣も身についた。
- ・ 滞在中に現地の部活に所属し様々な大会に参加した。
- ・ この冬は歴史的な寒波で大学も休校になるほどだった。話によると、当初は予定はなかったが学生の署名により休校が実現したそうだ。日本では考えられない行動力だと思った。
- ・ 初日に見知らぬ人が研究室まで案内してくれた。
- ・ トロント大学は夏休み中毎日無料のツアーを実施している。大学構内が観光地としてガイドブックに乗っていることに驚いた。
- ・ 最初の宿が交通の便が悪くて困っていたところ、偶然使った Uber の運転手の女性が「うちに住みなさい」と言ってくれて助かった。車も貸してくれた。
- ・ NY では、見知らぬ人に写真を撮られ撮影料を請求される、突然 CD を手渡されて代金を請求される…などいろいろ要注意!
- ・ カリフォルニアでは薬物の使用率と勧誘が想像以上に多い。意識の引き締めと断り方を渡航前に身につけるべき。
- ・ Airbnb で予約したはずの部屋が他の人に使われていたり、契約したはずのレンタカーがオーバーブッキングで無いと言われたり。こんなことは日本では起こり得ない。



5. その他、自由コメント

- ・ 研究室のメンバーの多くが中国人でラボ内でも中国語を話していることが多かったため、何を言っているのかさっぱりわからないときが結構ありました。(笑)

- 日本人の留学生はかなり少ないと思いました。アジアの中でも中国人とインド人が多く、科学分野でこれらの国が伸びている理由がわかった気がしました。
- 留学前は治安が心配でしたが、アナーバーはとても過ごしやすく安全な場所でした。
- 研究留学という貴重な体験をさせていただき、ありがとうございました。
- トロントの9月はすでに寒く、上着必須。トロントでは公共の場所（一般人から見える場所）での飲酒は禁止だと前もって知っておく必要がある。研究室は日本と似ているようだが、基本的にポストとの接触は少ないように思う。気になることがあったら積極的に部屋に尋ねるべき。何も行動しなければ、先生は何も問題ないものと捉えられるので、最後の報告書を作るときに困ることになる。
- クレジットカードはまさかの時のために複数枚用意しておいた方がいい。
- 住環境や関わる人間によって留学は最高にも最悪にもなる。インターネットの情報は色がついていることを理解した上で、先輩たちの経験を参考に、自分がどのように生活したいのか確固としたプラットフォームを持つことが大切だと思う。
- 本プログラムの冠がなければ、このような有名大学での教授にアポを取り付けられる確率は低いと思う。長期にわたる大学間の関係構築に感謝している。
- 数々の問題に直面したがハッピーな期間だった。楽しいことも辛いことも、全て忘れ難い思い出である。



Copyright © JUACEP 2019 All Rights Reserved

Published in November 2019

Japan-US-Canada Advanced Collaborative Education Program (JUACEP)

Graduate School of Engineering

Nagoya University

Furo-cho, Chikusa-ku, Nagoya 464-8603, Japan

JUACEP@engg.nagoya-u.ac.jp

<http://www.juacep.engg.nagoya-u.ac.jp>